Universidade de Aveiro Departamento de Electrónica, Telecomunicações e Informática,
2019

Gonçalo Pereira Marques

Desenvolvimento de um Veículo Elétrico a Escala Reduzida para Testes de Sistemas de Apoio à Condução

Development of a Reduced-Scale Electric Vehicle for Testing Driving Aid Systems

Gonçalo Pereira Marques

Desenvolvimento de um Veículo Elétrico a Escala Reduzida para Testes de Sistemas de Apoio à Condução

Development of a Reduced-Scale Electric Vehicle for Testing Driving Aid Systems

Dissertação apresentada à Universidade de Aveiro para cumprimento dos requisitos necessários à obtenção do grau de Mestre em Engenharia de Eletrónica e Telecomunicações, realizada sob a orientação científica dos professores:
Professor Dr. Rui Manuel Escadas Ramos Martins, Professor Auxiliar do Departamento de Eletrónica, Telecomunicações e Informática da Universidade de Aveiro
Professor Dr. Alexandre Manuel Moutela Nunes da Mota, Professor Associado do Departamento de Eletrónica, Telecomunicações e Informática da Universidade de Aveiro

o júri / the jury

presidente / president	**Professor Doutor José Luis Costa Pinto de Azevedo** Professor Auxiliar da Universidade de Aveiro
vogais / examiners committee	**Professor Doutor José Paulo Oliveira Santos** Professor Auxiliar da Universidade de Aveiro (arguente)
	Professor Doutor Rui Manuel Escadas Ramos Martins Professor Auxiliar da Universidade de Aveiro (orientador)

agradecimentos / acknowledgements

Embora uma tese seja, pela sua finalidade académica, um trabalho individual, há contributos de natureza diversa que não podem e nem devem deixar de ser realçados. Quero por isso, expressar aqui os meus profundos agradecimentos a algumas pessoas sem as quais não seria possível o sucesso desta dissertação:

Ao Professor Rui Martins, por ter dado ouvidos aos meus interesses, tanto académicos como pessoais, e por me ter proposto o tema desta dissertação que tanto neles se enquadra. Por todo o apoio, pelo ambiente descontraído, rigoroso do ponto de vista científico e técnico e pela autonomia e liberdade que desde o início me proporcionou.

Aos meus pais e irmã, pela força e apoio incondicional que me transmitiram durante todo o percurso académico. Em especial pelas sugestões e ajudas que me foram prestando ao longo da realização deste projeto e por me terem proporcionado todas as condições e ferramentas para ser quem sou.

À Catarina, pelo constante acompanhamento e compreensão nas alturas mais exigentes deste percurso. Pelo enorme exemplo de força e motivação que me dá todos os dias. Por todas as horas de estudo que passámos juntos, sem as quais o prestígio deste trabalho não seria o mesmo. Por toda a estabilidade emocional que me transmite, por ser tão simples e por ter marcado esta caminhada da melhor forma possível.

Aos meus amigos, Marco Fernandes e Júlio Fontes, que mesmo não estando envolvidos neste projeto, se mostraram sempre diponíveis para debater ideias, partilhar conhecimento, companhia e sem os quais certamente não teria chegado tão longe.

Ao meu amigo Carlos Nicolau, por ter despendido uma tarde a explicar-me os conceitos básicos de *SolidWorks* e por ter estado sempre a uma chamada de distância para me esclarecer todas as dúvidas que foram surgindo durante a realização da parte de modelação deste trabalho.

Ao meu amigo Ricardo Silva, por todo o acompanhamento e motivação dada desde o primeiro dia do meu percurso académico, assim como pela disponibilidade para me ajudar a melhorar a parte estética dos veículos desenvolvidos.

Por fim, agradeço também a todos os meus colegas e amigos com quem, direta ou indiretamente, tive o privilégio de trocar ideias e partilhar conhecimento durante o meu percurso académico na Universidade de Aveiro.

Palavras-Chave

Veículos elétricos a escala reduzida, modelação de veículos, tração às quatro rodas, motor embutido na roda, segurança automóvel, sistemas de apoio à condução

Resumo

Esta dissertação tem como principal objetivo o desenho e a conceção física de um veículo a escala reduzida, caraterizado por ser elétrico e com um motor embutido em cada roda, permitindo que a tração seja feita às quatro rodas e de forma independente. O intuito da construção deste veículo resume-se a que sirva como plataforma de testes para sistemas de apoio à condução, sendo por isso dotado de eletrónica sensorial. É ainda um requisito que o protótipo desenvolvido inclua um sistema de suspensão para que o seu comportamento dinâmico se assemelhe o mais possível da realidade.

No decorrer do documento é mostrado em detalhe todo o processo de desenho e construção do modelo, servindo como um guia que pretende justificar todas as decisões e passos tomados.

No final deste projeto, foram realizadas rotinas de teste que permitem classificar como viável o uso deste modelo para futura implementação de sistemas de apoio à condução, tendo sido cumpridos todos os objetivos inicialmente estipulados.

Keywords

Small-scale electric vehicles, vehicle modelling, four-wheel drive, in-wheel motor, automobile safety, driving aid systems

Abstract

The main objective of this dissertation is the design and physical conception of a reduced-scale vehicle, characterised by being electric and with an in-wheel motor configuration, allowing All-Wheel Drive (AWD) traction configuration and independent control of each wheel. The purpose of this vehicle construction is to serve as a test platform for driving aid systems, therefore being endowed with sensorial electronics. A requirement set is that the developed prototype includes a suspension system, so that its dynamic behaviour resembles as much of reality as possible.

The entire process of design and construction of the model is shown in detail in the course of the document, serving as a guide that intends to justify all decisions and steps taken.

At the end of this project, several test routines were carried out, allowing to classify the use of this model for future implementation of driving aid systems as viable, and making it possible to set all the initially stipulated objectives as complete.

Contents

List of Figures

List of Tables

List of Acronyms

ABS	Anti-lock Braking System
ADAS	Advanced Driver Assistance Systems
AWD	All-Wheel Drive
BEV	Battery Electric Vehicle
CAD	Computer-Aided Design
DOF	Degrees Of Freedom
ECU	Engine Control Unit
ESC	Electronic Stability Control
EV	Electric Vehicle
FCEV	Fuel Cell Electric Vehicle
FWD	Front-Wheel Drive
GHG	Greenhouse Gases
HEV	Hybrid Electric Vehicle
ICEV	Internal Combustion Engine Vehicle
LSD	Limited Slip Differentials
NCAP	New Car Assessment Programme
PHEV	Plug-in Hybrid Electric Vehicle
RTC	Real-Time Clock
RWD	Rear-Wheel Drive
SIPS	Side Impact Protection System
SRS	Supplemental Restraint System
TCS	Traction Control System
TV	Torque Vectoring

Chapter 1

Introduction

1.1 Context and Motivation

It is fair to say that the automobile was one of, if not the greatest invention of the 18th century. The ability to transport either people or goods over short and long distances in an easy, fast, reliable and comfortable way has shaped the course the world as been developing.

The first automobile records date the year of 1769 [1], and as far as today it is known that the number of vehicles in our planet is over 1.2 billion, with an expectancy for this number to be crossing the 2 billion mark by 2035 [2]. Although the greatest percentage is still composed by Internal Combustion Engine Vehicles (ICEV), vehicle electrification is happening at an incredible rapid pace. As quoted from [3]: *"It took five years to sell the first million electric cars. In 2018, it took only six months"*.

The vehicle performance improvement has, among other things, translated into the capacity of the automobile to move at higher speeds. With higher speeds, comes a higher probability of accident occurrence with also increased intensities and greater personal and material damages. It is in this context that concerns with the safety of both passengers and pedestrians arise.

Automobile safety is divided into two main categories: passive and active systems. With passive being constituted by the security systems and measures aimed at reducing the consequences in the event of an accident (*e.g.* airbags, headrests, protective side bars, safety belts, pre-tensioners, child restraint systems, etc.), whereas the active systems (which are mostly based on micro-controllers and sensors) include the components and systems whose objective is to avoid the occurrence of accidents (of which are examples, the anti-lock braking system, the traction control system, the electronic stability control system, electronically controlled suspensions, assisted steering and visibility support equipments).

Developing better safety systems has been one of the most demanding tasks in the evolution of the automobile industry. The great challenge of this type of systems is to improve both stability and manoeuvrability of the vehicle under harsh driving conditions, without affecting the performance of the car, nor the driver's will (*i.e.*, acceleration, braking and steering control). In addition to being demanding, building up these systems can turn into a potently dangerous job and usually requires huge monetary investments and facilities for testing with

full-size cars. This is where the scale model vehicles come in handy.

Small-scale vehicles can be used to study vehicles on a real scale, if appropriate care is taken to ensure the dynamic similarity between the two systems. Testing with scaled vehicles has several advantages [4]:

- The developing process usually takes less costs and time;
- There is no need to put drivers or pedestrians at risk during testing;
- It is relatively simple to change testing conditions and environment (*e.g.* road surface);
- Testing is safer, faster, and repeatable.

The focus of this dissertation will be to build a prototype of these small-scale electric vehicles which are pretended to serve as platforms for studying kinematics, dynamics and for developing and testing active safety systems. In addition to being electric, the models to be developed will have the particularity of having a four-wheel drive traction system, with each wheel being controlled by an independent electric motor. This vehicle configuration deserves the attention of this research, taking into account its potential benefits regarding simplicity, level of control over the behaviour of the car and environmental protection.

Four-motor electric vehicles have several advantages: the electric motors torque generation is very quick and accurate, for both accelerating and decelerating. This characteristic enables the possibility of implementing systems like the Anti-lock Braking System (ABS) without additional mechanical components. Due to being compact, a motor can be easily built-in a wheel, which also from a mechanical point of view, translates into a simplification, not requiring transmission shafts nor other complex components. Consequently, the total weight of the vehicle and torque losses over transmissions can be reduced.

The number of studies about the vehicle configuration with four independently controlled electric motors is still reduced and although the first four-electric motor driven cars are emerging in the market, like the *Rimac C_Two* [5], this is still a pretty uncommon setup. Thus, this dissertation intends to evaluate the feasibility of this configuration, through the development and testing of scaled model car platforms, controlled by microprocessors and with modules capable of prospectively implementing the main active safety systems which will later be introduced.

1.2 Objectives and Methodology

Before introducing the objectives of this Master's thesis it is important to state that this work results from the combination of two previous dissertations produced by Electronics and Telecommunications Engineering *alumni* from the *Universidade de Aveiro*. The first, named *"Segurança automóvel: Sistemas de apoio à condução"* [6], written by Bruno Grego, is mostly focused on theoretical simulations around the dynamic behaviours of a four in-wheel electric motor vehicle, while the second, *"Desenvolvimento de um veículo elétrico em escala reduzida"* [7], by Sérgio Ferreira, is based on the development of a scale model car but with no suspension and, therefore, more distant from reality than the case to be analysed here.

The stipulated objectives to fulfil during the realisation of this dissertation include:

- Study the dynamic behaviour of a simple passive suspension system;
- Interpret and understand vehicle steering design kinematics criteria;
- Establish the main parameters and characteristics which dynamically relate a real-scale vehicle and the prototypes to be later built on a reduced scale;
- Draw and physical conception of two small-scale prototype vehicles, powered by four in-wheel independently controlled electric motors, including the effects of a suspension system;
- Develop algorithms capable of running on embedded hardware that wirelessly allow the control of the vehicles, and the interconnection between all the modules introduced in the prototypes for gathering informations regarding their behaviours;
- Submit the vehicles to several test routines, in order to validate their construction and comparison of the theoretical analysis with the experimental results.

Studying both the dynamics and kinematics of a vehicle is an important step when building a prototype. Not only because it helps understanding how the car will possible behave when excited by certain inputs, but also because there are rules and criteria that should be followed in an initial design stage to avoid undesired comportments, such as wheel slip that may result in control losses and potentially in fatal crashes. With this in mind, it is expected to be able to extrapolate the mathematical equations of motion of a passive suspension system and conduct studies that allow observing its step responses. Kinematically, it will be studied the Ackermann steering criteria. A motion analysis that searches for perfect geometries, able to deliver ideal turning angles for a car, while keeping its occupants safe.

Before starting the design and build stage of the model cars it is expected to choose a real automobile as reference, in order to establish a scale and perform a dimensional analysis to ensure a relation between the scaled and real car's dynamic behaviours, important for further validation of the studies conducted over the prototypes.

The following stage is to design and physical conceive the prototypes. Before going any further it is important to state that the necessary skills to perform this part of the project are not part of the Master in Electronics and Telecommunications course's program. Thus, and as another main objective of this dissertation, it will be necessary to investigate and learn how to work with Computer-Aided Design (CAD) tools, as well as to establish contacts, with individual people or companies, able to transform the designs into real tangible and functional material pieces.

The electronics will be controlled with an *Arduino Mega* development board. It is expected to implement sensors in the models capable of gathering information such as independent wheel speed, traveled distance and the overall car roll, pitch and yaw movements, as functions of time. A requisite for the vehicles is that they are controlled wirelessly, meaning that a suitable technology should be found, as well as an intuitive graphical user interface.

The final objective of this dissertation will be to validate the built prototypes by submitting both models to several tests, such as comparing how they do when performing a

selected path with different traction setups (*e.g.* All-Wheel Drive (AWD) versus Rear-Wheel Drive (RWD)), analysing the information gathered by the built-in modules, executing demanding turning tests to compare results with the ideal Ackermann criteria design and, finally, use all this information to approve the use of these models for future study and testing of innovative driving aid systems.

1.3 Dissertation Structure

This document is organised as follows:

- In **Chapter 1** it is introduced the theme of this document and its structure, the motivation for the work developed, the objectives to be achieved and the methodology adopted.
- In **Chapter 2** it is presented a review of the state of the art, focusing on the evolution of automobile safety systems, the evolution and importance of the suspension in a car, on the existing safety systems on the market, in electric vehicles, in-wheel electric motor configurations and in studies already carried out on this type of scaled vehicle test platforms.
- In **Chapter 3**, the importance of studying dynamics and kinematics is exposed. The nomenclature used in this document is shown, followed by the mathematical description of a quarter car suspension dynamics, its transfer function model and step response simulation for what is expected to be a working versus damaged damper behaviour. A steering motion analysis is presented, with reference to the Ackermann criteria and calculations. Finally, a short introduction to roll, pitch and yaw angles is made.
- In **Chapter 4**, the model's parameters are evidenced, such as scale and particular measurement comparisons between the real car and prototype. The used hardware is enumerated with justifications on why each component was chosen, followed by their assembly and connection diagrams. The 3D CAD modelling, prototype build and assembly are explained in detail, ending the chapter by showing how the vehicles are controlled, with an overview of the developed algorithms and user interface.
- In **Chapter 5**, a compilation of test routines performed over the prototypes and corresponding results are shown. This chapter is intended to serve as a validation of the studies and construction of the reduced-scale electric vehicles.
- In **Chapter 6**, the conclusions arising from the work performed are exposed. Suggestions for continuing the study of this theme are also given.
- In **Appendix A**, it is presented a detailed table with the costs of production of a single prototype, as well as information on the manufacturer, retailer and quantity of each specific part used in the building process.
- In **Appendix B**, the Arduino code developed for controlling the cars and retrieving data from its sensors is provided.

Chapter 2

State of the Art

As a starting point, and before further formulation and analysis on the built scale vehicle test beds, it is important to familiarize the reader with a few topics regarding the automobile, its electrification and safety systems. In this chapter it is shown how these safety systems have been improving over the last few decades and how they are implemented in conventional vehicles. It is also explained the way a car suspension operates and the importance of a good suspension system regarding an automobile and its occupants' safety. Taking into account that electric vehicles are the main focus of this dissertation, it will also be shown how they are evolving, pros and cons of using in-wheel electric motors, companies which are already exploring these technologies and, finally, studies concerning scale model vehicles in order to later compare and validate the work performed during this dissertation.

2.1 Evolution of Automobile Safety

August 31, 1869 represents the beginning of the car safety history. This was the day in which the first automobile fatality was recorded, resulting in the death of a woman in Ireland [8]. Since this date, the need for proper safety systems was eminent and, in 1922, Duesenberg Motors Company introduced what would be the first four-wheel hydraulic brake system, the birth of the active safety system's history. In the year of 1930 all Ford cars were being produced with a safety glass. And in 1949, Chrysler Crown Imperial became the first vehicle to be equipped with standard disc brakes.

When talking about automotive safety it is almost mandatory to make reference to the Swedish car manufacturer Volvo. This brand was responsible for the invention of the three-point seatbelt in 1959 [9] as we are still using today. Volvo Cars waived the patent rights to the three-point seatbelt so more people could benefit from this technology and it is believed that, since then, over one million lives have been saved. Just six years after its invention, in 1965, the first legislation regarding the mandatory inclusion of seatbelts anchorage points for the front outer seats in every new car sold in the United Kingdom was born. Later in 1987 the same legislation was applied to the rear seats [10]. In other countries this legislation took a few more years to come into practice.

By 1966 Jensen Motors' model Jensen FF made debut of the first mechanical Anti-lock Braking System (ABS) ever applied to a production car. Although this system was not the most reliable by the time, better and upgraded versions made it to today and this is a technology that is still highly studied by car manufacturers.

In 1978 Mercedes stepped up the game by introducing the first electronic ABS in its high-end S-Class model. This equipment was supplied by Bosch and represented a huge improvement compared with the first commercial version of Jensen Motors. Also Mercedes was the pioneer manufacturer of the driver's *airbag*, included in its Supplemental Restraint System (SRS). In 1987, Bosch began series production of the ABS-based Traction Control System (TCS) for passenger cars, which prevents wheel spin [11].

Volvo, once again, picked the vanguard of safety systems technology in 1991, producing a system that combines side-impact bars with seats on transverse rails to create what would be named as Side Impact Protection System (SIPS). Again in 1994 this system was improved with the addition of side-seat protection airbags.

In the following year, 1995, with the technology developed by Bosch, Mercedes introduces the first ever Electronic Stability Control (ESC), with its S-Class model again leading the way in the world of electronic safety systems.

The European New Car Assessment Programme, also known as Euro NCAP, a consumer information provider organisation on the safety of new cars, was created in 1996. This organisation, which still operates, is responsible for doing exhaustive crash tests to every new car that comes to the market. The first tests came one year after its foundation and rated the Volvo S40 model with a four-star score for Adult Occupant Protection. The first five-star car ever was the Renault Laguna in 2001, shortly followed by the five-star Volvo XC90 in 2002 which, by 2017, still had no recorded occupant fatalities in its three biggest markets - the UK, US and Sweden [12].

Citroen models C4, C5 and C6 introduced a lane departure system in 2015. This electronic aid warns the driver when the car is going out of the road lanes, improving, mainly, the driver's attention to the road. Another electronic aid, the blind spot monitoring, was introduced in the Volvo S80 saloon in 2007, letting the driver know of any vehicle activity in their driving blind spots. By 2008 the autonomous braking system was debuted in the Volvo XC60. This system tells the driver if a stationary frontal object is detected, automatically braking if there is no feedback from the driver, helping in an emergency stop situation. By 2015 Volvo innovates once again and introduces pedestrian detection in darkness, barrier detection and active cruise control with steering in the XC90 model.

By the time of this writing, in 2019, newer and safer systems are being produced. Some mid to high-end cars are already surrounded by cameras constantly analysing and detecting potential safety threats, as is the case of all Tesla models [13]. Autopilot and vehicular communications between cars are becoming, day by day, a thing from the present and a safer on-road future is not that far ahead of us.

2.2 Evolution and Importance of Car Suspension

Suspension systems are a topic that don't usually get much attention from the average vehicle drivers and passengers but they are probably one of the most important factors, not only providing a comfortable or sporty ride but also for driving safety reasons. The torque generated by an engine, or by motors in the case of electric driving, is useless if the driver can't handle it. In a perfect flat road situation, with no irregularities, a suspension wouldn't be necessary. But the truth is that the wheels of any vehicle have to constantly deal with bumpy imperfections on the pavement. As Newton's laws of motion say, any force is composed by both magnitude and direction, and when a wheel touches one of these bumps, a vertical acceleration is originated [14]. In a no suspension situation, the force originated by this acceleration would transfer all the wheel's vertical energy to the chassis' frame, causing it to move in the same direction and, with the downforce effect of gravity, causing the wheels to hardly slam back into the surface, potentially causing an accident. This is where the suspension system goes into action, absorbing the energy generated by the vertically accelerated wheel, allowing the vehicle itself to continue rolling without major perturbations, while the wheels follow bumps in the road.

Nowadays, a suspension is considered to be the combined work of tyres, the tyre's air itself, shock absorbers, springs and arms that connect the vehicle's chassis to the wheels, allowing motion between the pair. But it has not always been like this. The term *"suspension"*, in the context of this study, comes from the 16th century when wagons and carriages tried to solve the problem of feeling every bump in the road. The solution for this problem was found by attaching the carriage's body with leather straps to four posts of the chassis, creating what would look like an upturned table. As a result of the body being suspended from the chassis, the system came to be known as a *"suspension"*, a term that is still being used today [14]. Although not being a springing system, it did allow the vehicle's body and wheels to move independently.

In the 18th century, leaf spring suspensions, also know as semi-elliptical or cart springs quickly replaced the leather-strap approach by the French [15]. This system consisted in a simple stack of rectangular arc-shaped steel springs which would attach to both right and left side of the vehicle's body, with location for an axle in its centre. The damping action was provided by the interleaf friction originated in a bump. Leaf springs were very common in vehicles up to 1970 in Europe and Japan and late 70's in America, when front wheel drive cars started hitting the roads [16]. Since this approach has the advantage of spreading the load in a more widely way over the vehicle's chassis when compared to coil springs, it is still used in some heavy commercial vehicles such as trucks and vans.

Story says that, in a Summer day of 1904, William Brush originated what is known to be the modern vehicular suspension system. While driving his brother Alanson's Crestmobile he got into a curve at a rolling speed of 30 mph (48 km/h) and, by whamming the front right wheel of the car into a deep rut, made it start shimming violently. The undulations of the leaf spring conducted the shock waves across the axle to the left side of the vehicle, making Brush lose control of the car and crashing it through a barbed wire fence, hitting a ditch and overturning it in a cow pasture [15].

With the motivation to make a better automotive vehicle that would prevent this kind of accidents, in 1906, William and Alanson built a car dubbed *Brush Two-Seat Runabout*. This car featured a revolutionary vehicular suspension using front coil springs and shock absorbers at each wheel. That implementation allowed the vehicle's frame, body, engine and powertrain to be suspended by the springs in a position above the wheels [15]. The most common physical model of this system can be seen in Figure 2.1.

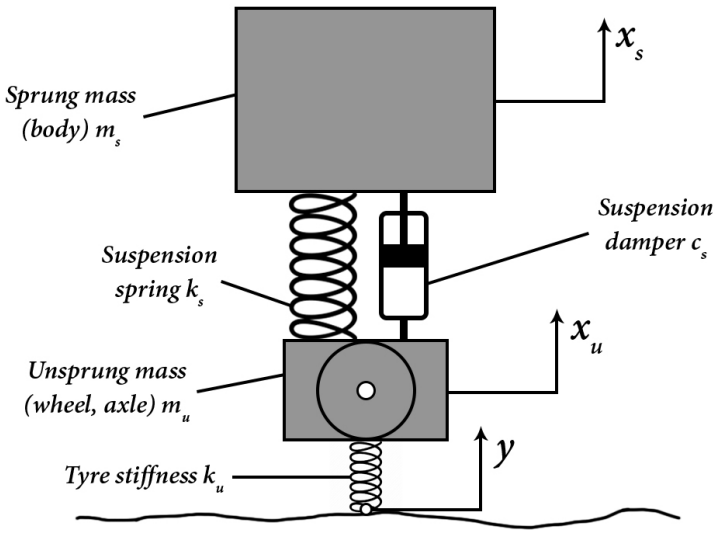

Figure 2.1: Physical model of the conventional passive suspension, adapted from [15].

Two key definitions to have in mind that will be important during the reading of this document are the concepts of *sprung* and *unsprung* masses. The *sprung* mass consists on the weight supported by the springs, like the chassis and the body. *Unsprung* mass is the weight of the components which move up and down with the wheel, such as the tyre, brake assemblies and other structural members [17].

Other kinds of suspension systems were tested and developed among the years, such as the torsion bar suspensions, used for the first time in the Leyland vehicle in the year of 1921 and shortly after introduced in the standard specifications of VW prototypes, in 1933, by Dr Ferdinand Porsche. While going through a road bump, the absorption of road vibrations are dealt by the twisting of the torsion bars, producing a smoother ride. This system was, and is still, used extensively on common vehicles, sometimes as an addiction to the spring setup introduced above [15].

Air suspension systems were firstly introduced by The Cowey Motor Works of Great Britain in the year of 1909, but did not success due to leaks. It was later in 1933 when Firestone released a working model for an experimental vehicle termed the *Stout-Scarab*. Air suspensions are optimised to cushion the ride and to keep the vehicle at constant height regardless the load. They typically consist of compressors responsible for maintaining a constant pressure in an air supply pneumatical tank. The air is piped in control pneumatical valves that feed this air to each spring as needed, increasing or decreasing automatically and keeping the vehicle's desired height from the road [15].

Another two key definitions to have in mind when going through the timeline of suspension systems' evolution are the concepts of *passive* and *active* suspensions. A suspension is said to be *passive* if the response it gives is only affected by external excitations and by the system parameters that have a direct action on the suspension. On the other hand, technology breakthroughs have created intelligent *active* suspensions. Unlike the previous concept, *active* systems are affected by indirect parameters, such as acceleration of the roll, pitch or vertical oscillations, and respond to these inputs with the use of variable damping and/or mechanisms capable of creating counter-forces, controlled by sensors and controllers typically connected to the vehicle's Engine Control Unit (ECU), improving the car's dynamic behaviour and riding experience [18].

With all the current and upcoming Advanced Driver Assistance Systems (ADAS) and connected cars, electronic devices are being added to *active* suspension systems, simplifying the complexity of its predecessors, operating with less moving parts and without fluids in the dampers. These implementations add shorter reaction times and may also be able to generate power from the damping, since they are using linear electric motors as dampers [19]. A partnership between Lexus and the speaker company Bose originated one of the most advanced innovations, a suspension fully controlled by linear electromagnetic motors [14], but it did not get much fame since they were heavy and highly expensive. Unfortunately not much has been made in this field besides that, so the air and hydraulic configurations are still considered as the base for the *active* systems [19].

In 2016, Audi presented their eROT prototype, a setup using electromechanical systems, said to be very responsive and needing less space when compared to a classic shock/spring layout. It does not use linear motors but rotational dampers instead, and is still able to recuperate energy [20].

Another example is the electronic suspension featured in the 2018 Volvo XC40, XC60 and XC90 produced by Monroe Intelligent Suspension, capable of constantly sensing the road and driving conditions and independently auto-adjusting the damping every 10 milliseconds [21].

Today's *active* systems have to react to the current vehicle state, however, due to the incorporation of more sensors like cameras or LiDAR systems with the capability of scanning the roads, road preview systems are being developed to actively prepare the suspension for what is ahead of the vehicle's drive, increasing both safety, comfort and performance [19].

Besides all these innovations, the classic spring plus damper configuration is still the most used due to its simplicity, cost and efficiency. As a result, this will be the system implemented in the scale model cars developed in this dissertation, and will be more in depth studied in the upcoming Chapter 3.

2.3 Driving Assistance Technologies

Emerging technologies are seen as a potential way of reducing the number of crashes and crash severity. Advanced Driver Assistance Systems (ADAS) are composed of a wide range of different devices and some will be introduced in the upcoming subsections.

2.3.1 Mechanical Differential and Electronic Differential

A mechanical differential is a component composed of multiple sprockets where, in most cars, the power makes its last stop before spinning the wheels. Especially when turning, the wheels of a car spin at different speeds. Each wheel travels a different distance through a turn and it is easily noticeable that the inside wheels cover a shorter distance than the outside ones. Since speed is the reason between the traveled distance and the time it takes to cover that distance, the wheels that travel a shorter distance travel at a lower speed [22].

For the non-driven wheels of a car (*i.e.*, the front wheels on a Rear-Wheel Drive (RWD) car, or the back-wheels on a Front-Wheel Drive (FWD) car) the differences between the wheels rotational speeds are not a problem since there is no connection between them, meaning that they can spin independently. On the other hand, the driven wheels are linked together for transmission purposes. If a mechanical differential did not exist, the wheels would be locked together and forced to spin at the same speed, compulsorily causing one of the traction tyres to slip when performing a turn, and potentially damaging other components of the car such as the transmission axles. Briefly, a differential has three functions [22]:

- Delivering the engine power to the driving wheels;
- To do a final gear reduction, slowing the rotational speed of the transmission before it hits the wheels;
- To enable both driving wheels to have different speeds when necessary, especially in a turning situation.

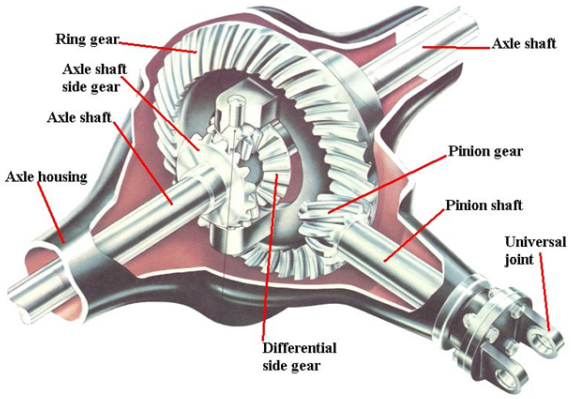

Figure 2.2: Mechanical differential representation [23].

In the case of an All-Wheel Drive (AWD) vehicle, besides the differentials between each set of drive wheels, an extra one is typically found between the front and the back as well, since each pair of wheels' travelled distances are also different when performing a turn.

The simple mechanical differential, as shown in Figure 2.2 does its job in a turn situation and evenly splits the engine's torque in a straight line. But it also have one major disadvantage: in a straight line situation, if one of the wheels from the same axle has less traction, almost all the supplied torque will be delivered to that particular wheel, while, in a perfect scenario, the opposite would have been expected [6].

In order to solve this mechanical problem Limited Slip Differentials (LSD) were created. This component has many different configurations but it is, commonly a high complexity mechanical device.

In the case of study, a vehicle with four electric motors, this problem is easily dealt with, since the control of each motor is independently made. All the electronic differential system is implemented in a *software* basis, which is highly advantageous when compared with the mechanical approach: there is no need for transmissions or gears; it has much faster response times; the torque is not limited by the wheel with the lowest traction and it enables regenerative breaking possibilities.

2.3.2 Anti-Lock Braking Systems

Anti-lock Braking System (ABS) consists of a mechanism capable of preventing brakes from locking when dealing with hard or slippery road braking situations. The ABS controls the brake line pressure independently of the force applied by the driver under the brake pedal, maintaining the wheel's optimum slip rotation and optimising breaking performance, not allowing full wheel lock [24].

During emergency braking, wheels do not get locked even if the driver hardly push the brake pedal and, hence, there is no skidding. This system was developed not to reduce the braking distance but to allow drivers to easily control and handle the car under slippery scenarios such as rain, snow and muddy roads.

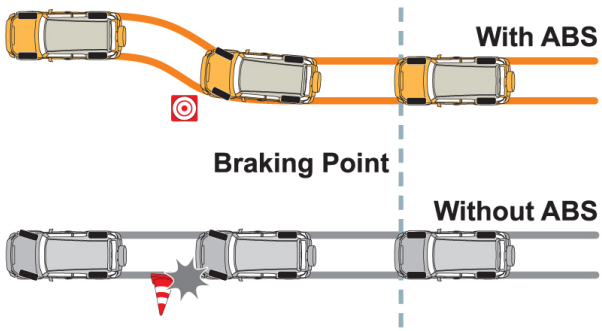

Figure 2.3: Steering control with ABS situation [24].

The ABS is composed by an Engine Control Unit (ECU), wheel speed sensors and hydraulic modulators, forming a closed circuit. Due to this reason, it is used a feedback control system that modulates the brake pressure according to the wheel's deceleration and angular velocity, preventing the controlled wheel from locking.

In a four in-wheel electric motor configuration, as the one being studied in this dissertation, the motors may be the only actuators necessary to perform the ABS, since the wheel's speed can be processed by a micro-controller and reduced according to deceleration, fulfilling the control objective. Another advantage of this implementation is the fact that the produced deceleration is able to act as a regenerative breaking system, producing energy to supply the vehicle's batteries.

One final note is that, in a pos-prototype situation, a mechanical brake system would have to be added to work in a parallel configuration with the motors to prevent a fail in the system, such as a power failure.

2.3.3 Traction Control Systems

The Traction Control System (TCS) has an identical behaviour and operating principle as the ABS. It is the key to maintain the vehicle tractive performance and stability, actively preventing the wheels from skidding while driving in a low grip situation.

In conventional combustion engine cars, the TCS applies braking impulses and reduces the power delivered to the drivetrain in order to keep the slip rate of the wheels within the desired range [25].

As represented in Figure 2.4, in a slippery situation with TCS activated, the wheel or wheels subjected to a skid will suffer a braking force that will prevent excessive spinning, while the opposite wheel will have its delivered torque being increased in order to maintain the handling.

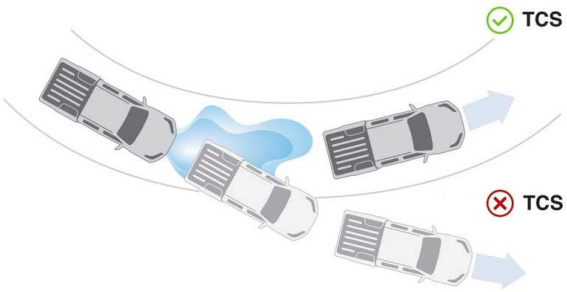

Figure 2.4: TCS ON and TCS OFF situations [26].

As for the ABS, the implementation of this safety feature in a four electric motor drive car is much more advantageous than the current approaches because the motors themselves, allied with *software* control, are able to implement this system.

2.3.4 Electronic Stability Control Systems

Electronic Stability Control (ESC) systems have become very popular since they were invented by Van Zanten and went into mass production by Bosch in the year of 1995, becoming mandatory in a number of countries and being considered as the second most important safety measure beyond the seatbelts in saving lives in car crashes [27].

The *World Health Organisation* states that, worldwide and each year, around 1.25 million people get killed in traffic accidents, a number heavily higher than the deaths caused by murders and military conflicts. Studies conducted by Bosch mention that the invention of the ESC prevents up to 80 % of automotive accidents related to skidding off the road, and that since its launch it has prevented 260 000 accidents and saved around 8 500 lives, just in Europe alone [27].

ESC systems were developed to act in situations where a car loses traction while performing a manoeuvre over an obstacle or drifting out of a corner. The ESC is able to prevent a vehicle from turning over itself while driving at high speeds. It acts by detecting the loss of traction and performing control upon this detection in order to stabilise the vehicle, allowing the driver to regain control of the car and preventing an accident [28]. This detection and control is done by a large number of sensors that give inputs to the control unit, which then decides where and when to act based on these values.

There are two main scenarios that may result in the loss of control of the car when performing a steep turn in a situation where the road is slippery or the vehicle's speed is very high for that turn: understeer and oversteer.

Figure 2.5: Understeer and oversteer situations where ESC is applied, adapted from [29].

Understeer occurs when the front wheels of the car lose grip through a corner, letting the extra momentum take control and pushing it straight on instead of turning. In an understeer situation, while performing a right turn, the ESC applies brake pressure to the right rear wheel of the vehicle generating a clockwise effect along its centre of gravity, bringing it back to its normal trajectory. On the other hand, in an oversteer situation it is the back of the car that tends to lose control and the main cause for this to happen is when a driver applies more power than the tyres can handle while performing a turn, making the car turn more than required along the vertical axis and consequently passing through its centre of gravity. Again, in a right turn situation, the ESC takes action by applying brake pressure to the left front wheel, generating a counter effect that helps bringing the car to its normal trajectory.

2.3.5 Torque Vectoring System

As it has been stated, the latest spread of electromobility in the vehicle industry carries lots of innovations, such as the possibility of having an independent electric motor powering each wheel, allowing its independent control and enabling the study and development of better control algorithms for vehicle stabilisation or intentional modification of the vehicle dynamics and behaviour. These were the reasons why Torque Vectoring (TV) systems were born.

TV systems were developed with the aim of controlling the vehicle stability and lateral dynamics, as well as to improve the car manoeuvrability and lower the driver's effort by electronically acting over the car's motors individually. This system is usually compared with the ESC due to the similarities of their purposes. The ESC mainly uses breaking over the desired wheel to control the vehicle stability, while, on other hand, the torque vectoring system uses the difference of torques being applied to each motor to fulfil this requirement. TV is also used in different situations, more specifically in less critical situations. If the ESC system starts controlling the car, the torque vectoring system should be turned off [30].

In order to stabilise or streamline the vehicle's yaw moment, the system adds more yaw moment, originated by the difference in the torque distribution. This yaw moment is then responsible for forcing the vehicle's dynamics to turn more, which results in incrementing the vehicle's yaw rate.

Figure 2.6 represents an understeer and an oversteer situation where TV is not in action, followed by examples of the system acting to correct the trajectories. The main difference when comparing to the ESC algorithm is the selected controlled wheel (see Figure 2.5). Here, the control system increases the torque on the red coloured wheel, generating additional yaw moment and stabilising the car.

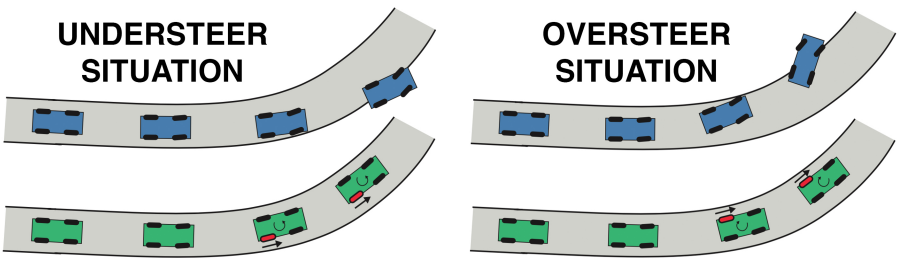

Figure 2.6: Under and oversteer situations without and with TV applied, adapted from [30].

As it is possible to state, the application of this type of system is an advantage of a four motor vehicle configuration as the one being studied, due to higher control over each independent wheel and the unnecessary use of complex mechanic differentials. In addiction to increasing the driver's safety, torque vectoring may also be used for perfomance purposes, making it possible to corner at higher speeds, and for fun, enabling a less experienced driver to intentionally drift the car without losing control.

2.4 Electric Vehicles

Despite some bibliographic divergences on this subject, it is believed that the history of the Electric Vehicle (EV) started in the United States in 1834, when the American Thomas Davenport built the first practical car with an electric motor [31]. It was over fifty years later that the first Internal Combustion Engine Vehicle (ICEV) was developed, in Germany, by Benz and Daimler. At the beginning of the 20th century, electric vehicles had a significant share of all engine-driven cars, becoming the top-selling road vehicle in the US by the year of 1900.

Until 1908, year in which Henry Ford started the first mass production of an internal combustion engined car in history, EVs and ICEVs were competing with each other for the title of the most used car. After this year, and caused by Ford's great success, ICEVs quickly replaced EVs, which became all but extinct by 1935.

Today, ICEVs' market penetration represents one of the biggest challenges against air quality and climate changes. Energy sourcing issues, cradle-to-grave considerations and other environmental concerns justify the need to rapidly decarbonise the transportation system. Also, the increased focus on public health impacts of transport emissions has resulted in a strong push to reduce the volume of pollutants generated by motor vehicles, being the EVs heralded as the obvious and most supported solution [31].

In 1997 the Kyoto protocol was created. Seen as one of the first conferences with the purpose of informing and creating awareness on populations and nations on climate change subjects, as well as to implement goals for the countries to lower Greenhouse Gases (GHG) emission levels. Since the transport sector has a large contribution in energetic and environmental problems, the need for EV solutions emerged [32]. 1997 also represents the year when the Toyota Prius model, the world's first mass-produced hybrid passenger vehicle, reached the market. Twenty years later, in 2017, Toyota's hybrid sales surpassed the 10 million mark and it is estimated that, when compared to gasoline-powered vehicles of the same size and performance, these numbers translate into 77 million tons of CO_2 emissions reduced, and approximately 29 million kiloliters of gasoline saved [33].

Worldwide governments considered the EV a good opportunity to tackle with the imposed limitations to GHG emissions and have been making considerable investments in this sector. In Portugal's case, there are a few financial incentives to the purchase and use of these vehicles, such as reductions in the acquisition taxes. Currently, according to Portugal's OE2019 (*Orçamento de Estado para 2019*), there is a 2 250 € incentive in the acquisition of EVs [34]. There is also a vehicle tax exemption (over the *ISV - Imposto Sobre Veículos*) and circulation tax exemption (*IUC - Imposto Único de Circulação*) when a 100% electric and emission free car is bought [35].

A report on electric vehicle sales and innovation by the Center of Automotive Management (CAM) states that the electric mobility market's trend has been positive in the last years [36], representing 4.6 % of the global marketshare in 2018, almost double of what it was in 2017.

China retains the leading position of the country with more EVs being sold, where registrations of new energy vehicles have almost crossed the one million unit mark, standing at 980 000 by the end of 2018. In addiction, due to China's protective policies, it is stated that 95 % of the electric cars sold in the country are being made locally. Also in China, strict rules to promote the car industry electrification are being applied since the beginning of 2019, with major manufacturers being punished unless they meet quotas for zero and low emission cars production [37]. In second place comes the United States' market, also exhibiting a strong growth and with the number of electric cars having grown by 84 %, to 365 000 units, from 2017 to 2018, representing a 2.1 % share of the total market. Leading this development is Tesla, more precisely the Model 3, accounting for 37 % of all EV registrations in the country. Considering Model S and X, Tesla's total sales also represent 50 percent of the market, with 159 000 units sold, according to CAM [36]. Last but not least, in the third place comes Europe, more precisely Norway. This tiny country represents the world's third largest market for plug-in vehicles, with 73 000 units sold throughout the year of 2018, and with an impressive market share of 47.9 %, meaning that, of all the vehicles being sold, almost half are electric.

Figure 2.7: Tesla Model 3 - The best selling EV in the U.S. [38].

When talking about electric vehicles it is important to know that there are available several different types of electrical implementations, classed by the degree electricity is used as their energy source, as it is explained in [31] and [39]:

- Hybrid Electric Vehicle (HEV) - This type of vehicles combine a petrol engine with electric motors. The electricity to power the motors is usually generated by the car's regenerative braking capability, a process where, by helping to slow down the car, the electric motors use the energy converted to heat by the breaks to recharge the vehicle's batteries. HEVs start off using the electric motors, then, as the speed increases, the internal combustion engine comes into action. The motors are controlled by an ECU responsible for ensuring the best economy for the driving conditions;
- Plug-in Hybrid Electric Vehicle (PHEV) - This is a variation of the HEV which offer the possibility to recharge the batteries while plugged-in to an electrical outlet, also including an internal combustion engine that predominantly generates additional electricity to extend the driving range offered by the batteries. The combustion engine may also self-propel the vehicle at higher speeds;

- Fuel Cell Electric Vehicle (FCEV) - Purely electric, FCEVs use hydrogen stored in on-board tanks in combination with a fuel cell stack to generate electricity, which in addition to a battery, are able to power an electric motor. These vehicles are not plugged-in to charge but refilled with hydrogen in a similar manner to convention ICEVs. This approach does not emit GHG, however, it does emit water in the form of vapour;

- Battery Electric Vehicle (BEV) - Fully electric vehicles, powered exclusively by one or more electric motors using electricity stored in their batteries. They need external electrical outlets or charging stations to charge their battery systems, not depending directly on fossil fuels to run. These are seen as the extreme end of vehicle electrification and are probably the most promising type of EV in the market. Although BEVs tend to take considerably longer times to recharge when compared to refuelling convention vehicles, quick-charging solutions are now being offered in modern EVs.

As well as any other innovation, the EV growth movement has its pros and cons. Some common drawbacks will be stated bellow, followed by the corresponding positive perspective [40].

To begin with, electric powered vehicles need charging stations to feed their batteries, and for someone to travel long distances, a network of strategically located stations need to be part of the journey's route stops. In addition, the recharging operation of batteries often takes about 3 hours, not being comparable with the time it takes to refuel a car with gas. Well, this is not exactly the truth anymore. Everyday, more and more gas stations and public car parks are offering charging station technologies, invalidating the old excuse about having nowhere to charge an EV. The vast majority of drivers use their cars to drive to and from work, and since it is possible to carry outlet chargers, it is possible to charge a vehicle while working. Also, taking Tesla's Model 3 as an example, a 30 minute charge is said to provide the batteries with efficiency for 270 km, when using a supercharger [38]. In March 2019, at the Geneva Motor Show, a German-Swiss car maker named Piëch Automotive debuted its first prototype, the Mark Zero, with an announced battery range of 500 km and capable of fast-charging up to 80 % in the impressive record of 4 minutes and 40 seconds [41].

Travelling range is another topic that usually comes into discussion. Most people tend to believe that an electric car can't travel more than a couple of kilometres. However, battery technology has been evolving at a quick pace and can now last longer and help the driver to go faster and further. A comparison between the ranges of several options in the market is shown in Figure 2.8. It is a fact that these ranges still don't match what most gasoline powered vehicles can offer, but higher travelling distances are emerging. Tesla has promised that its upcoming 2020 Roadster model will be able to travel up to 1000 km in a single charge [42].

Another disadvantage comes when talking about costs. It is a fact that the batteries needed to power these vehicles are expensive and may need maintenance or replacement. They are typically of lithium-ion, and since lithium is a rare metal that can only be mined in a few countries, it sets batteries' costs up to a few thousands each. But batteries are not the only expensive feature of an EV. However, and as stated above, governments are trying to encourage people to buy electric vehicles by offering attractive tax reductions, not offsetting the costs but certainly helping a lot.

Finally, pollution concerns are also associated with EVs. Although being seen by many as *"clean and green"*, this type of vehicles, indirectly, cause pollution too. Batteries contain toxic elements which can spew toxic fumes. Also, they are powered by electricity which unfortunately is still not completely generated from renewable energy sources. These environmental pros and cons do not mean that people should dismiss the electric option, as they are still more environmentally friendly than a regular car, and that is what is important.

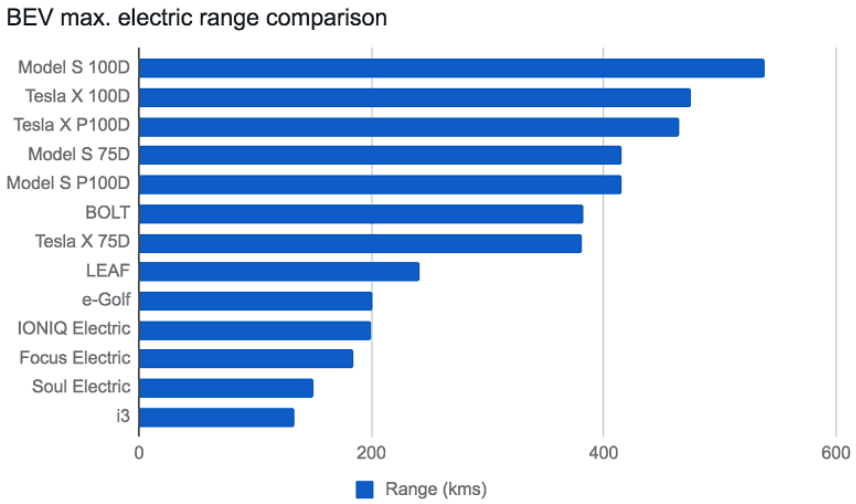

Figure 2.8: Available EV battery ranges comparison [40].

In terms of electric motors there are five main types used in EVs, exhibiting different characteristics and making it important to evaluate some basic parameters for choosing a particular type of motor, such as simple design, high specific power, low maintenance cost, and good control. Motors that are most commonly used by EV manufacturers are DC brushed motors, DC brushless motors, AC induction motors, synchronous motors and switched reluctance motors [43].

- DC Brushed Motor - Brushes along with commutators provide a nexus between an external supply circuit and the motor's armature. These brushes can be made of carbon, copper or metal graphite and are usually shaped in a rectangular format. One of the main drawbacks of DC brushed motors is the wearing of the commutators due to continuous cutting with the brushes, causing friction responsible for imposing limits to the maximum motor speed. DC brushed motors are able to achieve high torque at low speeds, making them suitable for traction systems. Another disadvantage associated with the use of this type of motors is their poor power density (felt when it is necessary a constant speed at a variable load situation), when compared to a BLDC motor.

- DC Brushless Motor - This type of motors, also known as BLDC motors, provide certain advantages over DC brushed ones, such as less maintenance and higher efficiency. The mechanical commutation, as seen in brushed DC motors, is replaced by an inverter circuit and a rotor-position sensing element, performing an equivalent electronic commutation. A BLDC motor provides higher torque at peak values of current and voltage

when compared to other motors, being able to deliver better operating characteristics at higher speeds.

- AC Induction Motor - High efficiency, good speed regulation and absence of commutators makes these three phase induction motors widely used in electric vehicles. The three phase AC supply is connected to a stator winding, establishing a revolving magnetic field which interacts with stationary rotor's conductors, making induced current flow through them. This induced current creates its own magnetic field, which in interaction with the revolving magnetic field, gives rise to unidirectional torque. Although DC batteries can supply these motors, a DC-AC inversor is needed. AC motors are usually able to deliver a better acceleration curve (identical to internal combustion engines) when compared to other motors.

- Synchronous Motor - In this approach, the rotor is excited from a DC supply, while the stator is connected to a three phase AC supply. This way, polarities of stator poles continuously change while rotor pole polarities stay constant, creating rotor rotation. Synchronous motors find its application in some electric vehicles due to their high efficiency and high torque density.

- Switched Reluctance Motor - These motors' torque is produced by a variable reluctance method. Energising stator's coils, variable reluctance is set up in the air gap between the stator and the rotor, causing it to move to the position of least reluctance and originating torque as consequence. High starting torque, wide speed range and good inherent fault-tolerance capability makes them suitable for electric vehicle applications.

Per car, each company differ in type and quantity of motors, depending on the purpose of the vehicle under development. Some variations of Tesla's Model S, Model X and Model 3 use one or two AC induction motors. Its future Roadster will feature a three motor setup (two in the back and one in the front), allowing an outstanding acceleration from 0 to 100 km/h in under 2.1 seconds and a top speed of over 400 km/h. A different setup example comes from the Nissan Leaf, powered by a single synchronous motor. The cars made by the Croatian electric car company Rimac Automobili, the Concept_One and C_two also offer powertrains composed by synchronous electric motors capable of spectacular performances.

Rimac was founded by Mate Rimac in 2009 and has been one of the most promising companies in the electric car sector. In addiction to producing electric supercars, about two-thirds of its work consists in developing and supplying solutions and components, like battery packs, drivetrains, Advanced Driver Assistance Systems (ADAS), infotainment and electronics in general to other car companies, enabling the automotive electrification to evolve at a greater pace. In June 2018, a 18.7 million euro investment was made by Porsche, taking a 10 percent stake of Rimac and enabling a transfer of technologies to the whole VW group, that contemplates carmakers like Audi, Bentley, Bugatti, Lamborghini and others [44].

An article published in Forbes' website with a vast list of some of the coolest 2019-2020 electric cars and its specifications can be found in [45].

Despite existing lots of different EV configurations, and more precisely even cars with four electric motors, the in-wheel motors approach discussed in this essay is still not available in the market as a conventional vehicle. The use of this alternative has some positive and negative points of view, which will be discussed in the following subsection.

2.5 In-Wheel Electric Motors

The in-wheel electric motor, also known as hub motor, is not exactly an innovation. In fact, at the end of the 19th century, Ferdinand Porsche in Vienna and Joseph Ledwinka and Fred Newman in Chicago attached an electric motor to each wheel of a horseless carriage with the aim of providing power simply, efficiently and controllably [46]. But withered by the ICEV expansion, this technology did not get much attention until a few years ago, with its interest raised by the recent need of vehicle electrification.

Figure 2.9: Schematic of Protean Electric's in-wheel motor configuration [47].

The current approaches to the in-wheel motor systems consist in modifying the hub of each wheel by adding a complete drivetrain responsible for providing torque to its associated tyre, braking components and the motor-drive electronics. There is no denying this technology is promising. However, based on some criticisms, there is a lot of reluctance to adopt it by some manufactures [48]. This hesitation is mostly originated by the inevitable unsprung mass increase. Unsprung mass, as previously explained, refers to the weight of the components which move up and down with the wheel, and should be minimised to improve ride quality, as well as to make it easier for the suspension to keep the tyres in contact with the road. As expected, a vehicle powered by in-wheel electric motors will have a significantly greater unsprung mass, caused by the weight of the motor carried in each powered wheel.

In order to try to prove the critics wrong, Protean Electric, one of the most promising companies specialised in in-wheel motor technologies, in partnership with Lotus Engineering and Dunamos, conducted a six-month study into the dynamic implications and opportunities of an unsprung-mounted drivetrain [49]. As stated, a 2007 Ford Focus was evaluated for ride, handling and performance around corners and over bumps. This Ford Focus was then modified with added static and rotational mass to the front and the rear, with the target of simulating the added weight of the wheel motors, and retested. Results showed a slight difference, but that difference, according to Protean Electric and Lotus Engineering, was minimal and recoverable with traditional ride and handling refinement, making the experts affirm that the issue of unsprung mass is a pure misconception and that there are lots of benefits to using in-wheel motors [49].

Other key challenges often seen as weaknesses in the development of in-wheel motors, such as the integration of friction braking, thermal management, ingress protection and vehicle control, were successfully tested by Protean Electric and can be seen more in depth in [50].

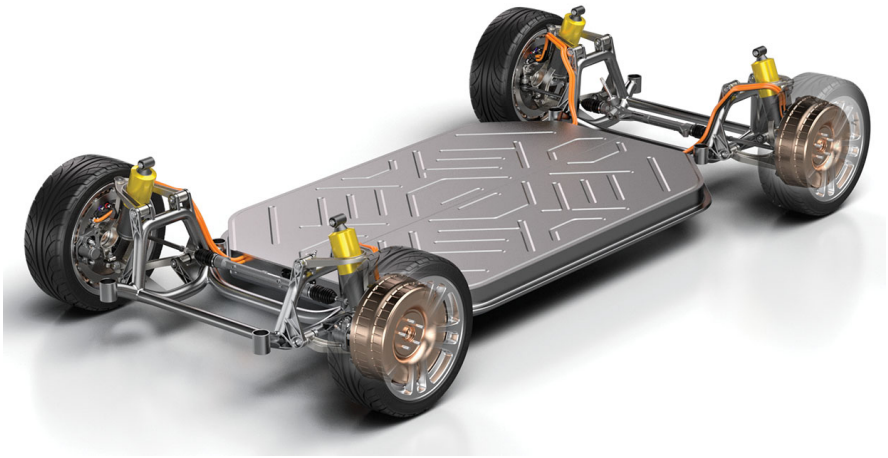

Figure 2.10: Mounting the motors in-wheel allows design freedom to accommodate more batteries, passengers or cargo [48].

Vehicles with hub motors are able to provide around 98 % mechanical power efficiency, while internal combustion engine cars achieve only around 30 %. This is possible since the electric motors are directly connected to the wheels, avoiding torque losses in the gearbox and differentials [49]. Other benefits are the greater ranges, which traduce in reduced running costs and in a lower charging frequency. Better handling and traction control, enhanced stability and shorter stopping distances are also other advantadges. No requirement for existing driveline components traduces into bigger freedom for car design, since there is more available space for passengers or batteries [51].

Along with Protean Electric, other manufacturers like Elaphe, Ziehl-Abegg and several Japanese suppliers and OEMs, including Mitsubishi and Nissan are working on the in-wheel technology. Commercial vehicles with this type of motors are not in the market yet, however lots of concept cars and experimental vehicles are being developed, such as LM Industries' autonomous passenger shuttle dubbed *Olli* and Fisker's 2019 upcoming Orbit autonomous bus. [46, 49].

2.6 Scale Model Vehicle Studies

At the introduction of this dissertation it was already mentioned the importance and benefits of conducting studies and essays over scale model vehicles. Every driving assistance technology and innovation would became expensive and potentially dangerous if tested in full-size vehicles at first. Also, few facilities where full-size testing of such systems can be performed are available and accessible to most researchers from universities and small companies, hindering the conception of new and safer technologies at a greater pace. As mentioned in [52], when examining the use of scale-models throughout history it is possible to conclude that they are technologically suitable alternatives to tests with full-size equipment. As examples,

let's take one of the most influential inventions of the 20th century, when Orville and Wilbur Wright conducted tests using scale wing designs in a wind tunnel before building what would became the first airplane. Likewise, during 1960's, tests performed over scale models allowed the design and experimental determination of the overall vehicle dynamics of the lunar rover, the vehicle that would later drive across the surface of the moon [53].

Undoubtedly, scale models have been providing the engineers with useful data that is used in the production of actual vehicles.

In [53] there is an important reference concerning modelling and control of scaled vehicles. This document reports the development of a physical testing platform called *IRS (Illinois Roadway Simulator)*, based on a treadmill. In addiction to reducing the area required for testing, the development of this component contributes to making tests safe, consistent and repeatable. Three different test vehicle setups are used: a Rear-Wheel Drive (RWD) with front steering model, a single motor All-Wheel Drive (AWD) with four wheel steering and finally another AWD with a four independent motors configuration and four wheel steering. The signals from the sensors and those that target the actuators are transmitted via radio frequency. However, the position of the vehicle is measured by a mechanical arm that is permanently connected to it. This is a conditioning factor for the possible manoeuvres to test, in addition to the fact that the vehicle is always moving forward, which, as an example, does not allow the test of circular trajectories.

Also in [54], the reader is presented with a test platform similar to the *IRS*, denominated as *PURRS (Pennsylvania University Rolling Roadway Simulator)*. This document presents some relevant procedures in detail, such as how to experimentally obtain fundamental parameters of a small-scale vehicle, such as the centre of mass. In addiction, benefits and tradeoffs of scaled vehicle usage for studying vehicle chassis dynamics and control are concluded.

The development of an innovative low-scale test vehicle is stated in [55]. Unlike in the previous studies, this is characterised by not using a treadmill as test surface and also because the scaled vehicle commands are remotely transmitted. Thus, the vehicle has greater freedom of movements, and a wider range of manoeuvres can be studied, with the drawback of needing a larger available area for testing. Empirically, it was verified that the small-scale vehicle correlates well with the mathematical models, as well as with those of a full-scale car. Also in [55], it is possible to find recommendations in order to avoid the limitations found in the course of the adaptation of the test vehicle and consequently in its study. Since an off-the-shelf 1:10 scale radio controlled car was adapted to perform the desired tests, instead of being built from scratch, difficulties related to packing all the required electronics have compromised the project. Advices regarding the advantages of using aluminium materials in the build of a custom vehicle chassis are shown as a way of fulfilling parameter requirements of a full scale vehicle. Finally, problems related to the close loop response of the used control system are presented, such as the involuntary nonlinearities introduced, causing conflicts between the wireless communications and the control of the motors and servo, concluding with recommendations on the use of a multipurpose development board like the Arduino kits.

Chapter 3

Dynamics and Kinematics

As "the machine that changed the world", the vehicle has been a subject of studies, at least, for the past two hundred years. When examining the development history of vehicle technologies it is instantly perceptible that a great part of this research and development has mainly relied on the improvement of mechanical structures and mechanisms, allowing better and safer rides.

The studies on the motion theories of vehicle systems and on the performance of the integration of these same systems with each other is known as vehicle dynamics. By dynamics it is meant the full consideration of time varying phenomena in the interaction between motions, forces and material properties. On the other hand, kinematics consists on the study of the motion of points, bodies and systems of bodies without considering the forces which caused the motion. Also known as the "geometry of motion", kinematic analysis is based on the study of the geometry of a given system, from which position, velocity and acceleration can be determined.

Nowadays, multiple requirements should be taken into account when designing the dynamic and kinematic performance of a vehicle, such as ride comfort, handling stability and safety. Due to the vehicle being a complex system composed of up to several thousands of parts and many times driven under various unpredictable working conditions, automotive researchers and engineers face great challenges trying to meet these requirements. Furthermore, the traditional design and research for meeting all these conditions has focused on primarily improving the mechanical parts and systems by finding solutions which are usually seen as compromises between conflicting performance requirements. Hence, sometimes it is difficult to come up with a result that simultaneously optimise all the requirements of the vehicle.

Formulating the mathematical model of a system is essential to predict its behaviour through simulation, to have a guide line in the design stage of the prototypes and to compare a theoretical study with the obtained experimental results. Any model, besides not being exact, has a relationship between simplicity and precision which is inversely proportional, that is, the simpler it is, the less precise and vice versa. Meaning that the studied models should not be too complex, but relevant information can't also be lost. Following next in this

chapter, the nomenclature of all the variables and parameters used in this dissertation will be presented. It will be shown a dynamic analysis over the quarter car suspension system with a comparison between a functional and a damaged damper, as well as a kinematic study over steering design criteria to be implemented in the model car design. Finally, the concepts of roll, pitch and yaw angles are introduced.

3.1 Nomenclature

The nomenclature adopted in this master's dissertation is presented in the following table:

Symbol	**Definition**	**Unit**
b	Axle track distance	m
l	Wheelbase distance	m
l_1,l_4	Length of the steering links of a four-bar linkage	m
l_2	Ackermann steering link length	m
$l_{2,0}$	Ackermann steering link length for zero turning angle	m
x_s	Sprung mass displacement	m
x_u	Unsprung mass displacement	m
y	Base excitation displacement	m
X_s	Steady-state amplitude of x_s	m
X_u	Steady-state amplitude of x_u	m
Y	Steady-state amplitude of y	m
θ_i	Inner wheel steer angle	°
θ_o	Outer wheel steer angle	°
ψ	Arm angle in trapezoidal steering mechanism	°
ψ_p	Prototype arm angle in trapezoidal steering mechanism	°
c_i	Ideal inner wheel Ackermann curvature radius	°
c_o	Ideal outer wheel Ackermann curvature radius	°
m_s	Sprung mass	kg
m_u	Unsprung mass	kg
k_s	Main suspension spring stiffness constant	N/m
k_u	Tyre stiffness constant	N/m
c_s	Main suspension viscous damping coefficient	N·s/m
X, Y, Z	Global coordinate axes	Dimensionless

Table 3.1: Nomenclature of vehicle model variables and parameters.

3.2 Quarter Car Suspension

The quarter car model is a very useful approach to study the vehicle suspension system. In this section, this model will be introduced and examined.

In this context, the suspension system consists in one-fourth of the body mass of the vehicle, suspension components and one wheel [56]. The assumptions of a quarter car modelling are as follows: the tyre is modelled as a linear spring without damping, there is no rotational motion in wheel and body, the behaviour of spring and damper are linear, the tyre is always in contact with the road surface and the friction effect is neglected so that the residual structural damping is not considered into the vehicle modelling [57].

3.2.1 Equations of Motion

The mathematical representation of a quarter car model vertical vibration may be composed by two solid masses, sprung mass m_s and unsprung mass m_u (Figure 3.1). In this specific scenario, the sprung mass m_s is composed by 1/4 of the body of the vehicle, while the unsprung mass m_u represents one single wheel and the components which move with it [58] (in the case of an in-wheel motor configuration, the mass of each motor should be considered as well).

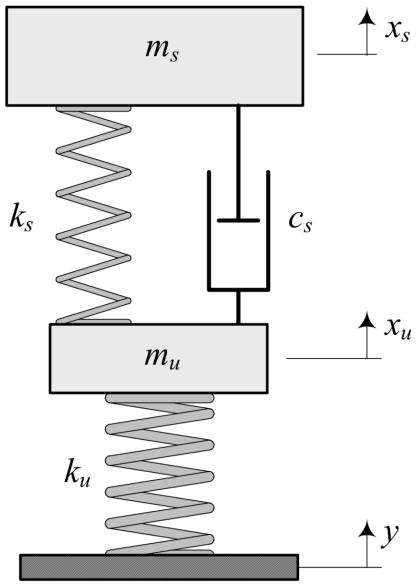

Figure 3.1: A quarter car model [58].

The main suspension is responsible for supporting the sprung mass and is composed by a spring of stiffness k_s and a shock absorber with viscous damping coefficient c_s. The unsprung mass is in direct contact with the ground through a spring k_u, representing the stiffness of the tyre [58].

The equations of motion for a quarter car model, as shown in Figure 3.1, are:

$$m_s \cdot \ddot{x}_s + c_s \cdot (\dot{x}_s - \dot{x}_u) + k_s \cdot (x_s - x_u) \;=\; 0 \tag{3.1}$$

$$m_u \cdot \ddot{x}_u + c_s \cdot (\dot{x}_u - \dot{x}_s) + (k_u + k_s) \cdot x_u - k_s \cdot x_s \;=\; k_u \cdot y \tag{3.2}$$

A damping coefficient c_u might have been added in parallel to k_u in order to model any damping in tyres. However, since c_u from the tyres is very small when compared with c_s, c_u is ignored to simplify the model [58].

3.2.2 Transfer Function Model

The transfer function describes the theoretical output behaviour of a function when prompted with a given input, allowing a mathematical analysis and prediction of how a system will work in practice.

In order to get the transfer functions from the equations of motion above let's assume that all of the initial conditions are zero, so that these equations represent the situation where the vehicle's wheel goes up a bump [59].

Applying the Laplace Transform over Equation 3.1 and 3.2, respectively:

$$(m_s \cdot s^2 + c_s \cdot s + k_s) \cdot X_s(s) - (c_s \cdot s + k_s) \cdot X_u(s) \;=\; 0 \tag{3.3}$$

$$-(c_s \cdot s + k_s) \cdot X_s(s) + (m_u \cdot s^2 + c_s \cdot s + k_u + ks) \cdot X_u(s) \;=\; k_u \cdot Y(s) \tag{3.4}$$

Transforming both equations into an $Ax = b$ matrix representation:

$$\begin{bmatrix} (m_s \cdot s^2 + c_s \cdot s + k_s) & -(c_s \cdot s + k_s) \\ -(c_s \cdot s + k_s) & (m_u \cdot s^2 + c_s \cdot s + k_u + k_s) \end{bmatrix} \cdot \begin{bmatrix} X_s(s) \\ X_u(s) \end{bmatrix} \;=\; \begin{bmatrix} 0 \\ k_u \cdot Y(s) \end{bmatrix} \tag{3.5}$$

The determinant Δ of the A matrix is given by:

$$\begin{aligned} \Delta \;&=\; \det \begin{bmatrix} (m_s \cdot s^2 + c_s \cdot s + k_s) & -(c_s \cdot s + k_s) \\ -(c_s \cdot s + k_s) & (m_u \cdot s^2 + c_s \cdot s + k_u + k_s) \end{bmatrix} \\ \Leftrightarrow \Delta \;&=\; (m_s \cdot s^2 + c_s \cdot s + k_s) \cdot (m_u \cdot s^2 + c_s \cdot s + k_u + k_s) - (c_s \cdot s + k_s) \cdot (c_s \cdot s + k_s) \end{aligned} \tag{3.6}$$

The last step before getting the transfer function $G(s)$ is to find the inverse of matrix A and then multiply by the inputs matrix on the righthand side as follows:

$$\begin{bmatrix} X_s(s) \\ X_u(s) \end{bmatrix} = \frac{1}{\Delta} \cdot \begin{bmatrix} (m_u \cdot s^2 + c_s \cdot s + k_u + k_s) & (c_s \cdot s + k_s) \\ (c_s \cdot s + k_s) & (m_s \cdot s^2 + c_s \cdot s + k_s) \end{bmatrix} \cdot \begin{bmatrix} 0 \\ k_u \cdot Y(s) \end{bmatrix}$$

$$\Leftrightarrow \begin{bmatrix} X_s(s) \\ X_u(s) \end{bmatrix} = \frac{1}{\Delta} \cdot \begin{bmatrix} (m_u \cdot s^2 + c_s \cdot s + k_u + k_s) & k_u \cdot (c_s \cdot s + k_s) \\ (c_s \cdot s + k_s) & k_u \cdot (m_s \cdot s^2 + c_s \cdot s + k_s) \end{bmatrix} \cdot \begin{bmatrix} 0 \\ Y(s) \end{bmatrix} \tag{3.7}$$

Since the suspension system in analysis is passive, *i.e.*, no control system is being used to ease the damping, and the only input being considered is $Y(s)$, $G(s)$ is expressed as:

$$G(s) = \frac{X_s(s) - X_u(s)}{Y(s)}$$

$$\Leftrightarrow G(s) = -\frac{K_u \cdot m_s \cdot s^2}{\Delta} \tag{3.8}$$

3.2.3 Step Response

A good suspension system is expected to deliver a satisfactory road holding ability, while still providing comfort when riding over holes, bumps and other disturbances on the road. When facing these undesired conditions, the vehicle body should not have large oscillations, and these oscillations should be quickly dissipated by the suspension system.

Since the distance $x_s - y$ is very difficult to measure, and the deformation of the tyre $(x_u - y)$ is also being neglected, the distance $x_s - x_u$ will be used as the output of the step response, instead of the total distance $x_s - y$.

The values used to simulate the step response were based on the following relations presented in Table 3.2 [58], for the average values of quarter car parameters.

Parameter	Average	Minimum	Maximum
$\frac{m_s}{m_u}$	3 - 8	2	20
$\sqrt{\frac{k_s}{m_s}}$	1	0.2	1
$\sqrt{\frac{k_u}{m_u}}$	10	2	20

Table 3.2: Average value of quarter car parameters, adapted from [58].

For simulation purposes, let's take as example a vehicle with a total sprung mass of 1000 kg. Having this defined, the quarter car m_s will be 250 kg. To anticipate further possible analysis with an in-wheel motor type of vehicle, since the mass of the motor is part of the unsprung mass, let's stipulate m_u as 50 kg. Consequently, k_s is set as 250 N/m and k_u as 5000

N/m. Regarding the damping coefficient c_s, two situations were simulated: one where the damper is expected to be working and a second scenario where the damper is considered to have a malfunction (and consequently a lower damping coefficient). At first, this parameter was set to 1200 N.s/m, an average value obtained in several experimental tests performed in [60]. For the damaged case, c_s was set to 120 N.s/m, being expected that the spring effect would take control over the system (keep in mind that the values assigned to each parameter are a mere example to simulate the behaviour of a hypothetical vehicle).

Using Matlab®, the response for a step disturbance input, $Y(s)$, with magnitude 0.1 m over the two presented systems is displayed in Figure 3.2.

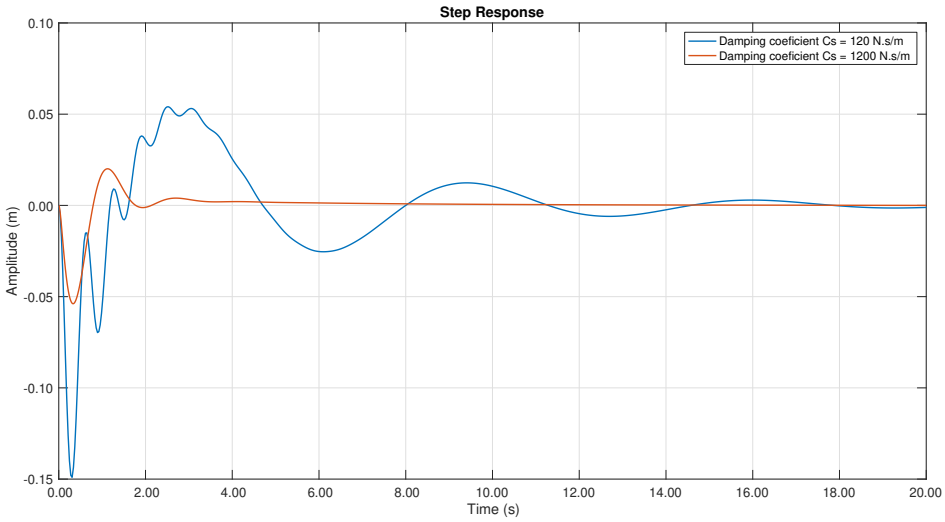

Figure 3.2: Step response for an input $Y(s)$ with magnitude 0.1 m.

From the analysis of the graphic it is possible to see that although this being an open-loop system (without any feedback control), a 10 cm disturbance on the road is well absorbed by the working suspension system of the car. Not oscillating too many times and showing an initial amplitude of around -0.054 m. On the other hand, and as expected, the damaged suspension does not absorb the impact well and takes too much time to settle down, not complying with the expected comfort standards for a car.

3.3 Steering Motion Analysis

In order to manoeuvre a vehicle a steering mechanism is needed to turn the wheels. Steering kinematics which we review in this section, introduces new requirements and challenges for the build of the model car prototypes that will be presented throughout this dissertation.

3.3.1 The Ackermann Criteria

The reason why Ackermann steering geometry exists is that so the tyres do not slip when a car is performing a corner, while searching for the ideal turning criteria [61]. In order to

understand the basics of this theory let's consider that a vehicle is performing a left corner and that all tyres are rotating around a central point, as seen in Figure 3.3. It is possible to see that the angle which the inner front tyre makes with respect to the central point (θ_i) will be greater than the angle made by the outer front tyre (θ_o). With that angle being greater it is possible to come up with this central point and all four tyres can rotate around it, meaning that the tyres will not have to slip as they perform the desired manoeuvre.

If the angles between the steering wheels were equal, the tyres would be forced to slip around some uncommon point and the behaviour of the car would not be as good, specially at higher speeds or on heavy load situations [62].

Looking at Figure 3.3 it is possible to see that each tyre's path has a different radius, meaning that each wheel is rotating at a different rate. Since the tyres on the outside of the curve need to travel a farther distance in the same amount of time when compared to the ones on the inside, it means that they are rotating with a higher angular velocity. In descending order, the rotating velocity goes from tyre 1 to 4 as labeled in the figure. This is also one of the reasons why differentials and torque vectoring systems are useful driving aids.

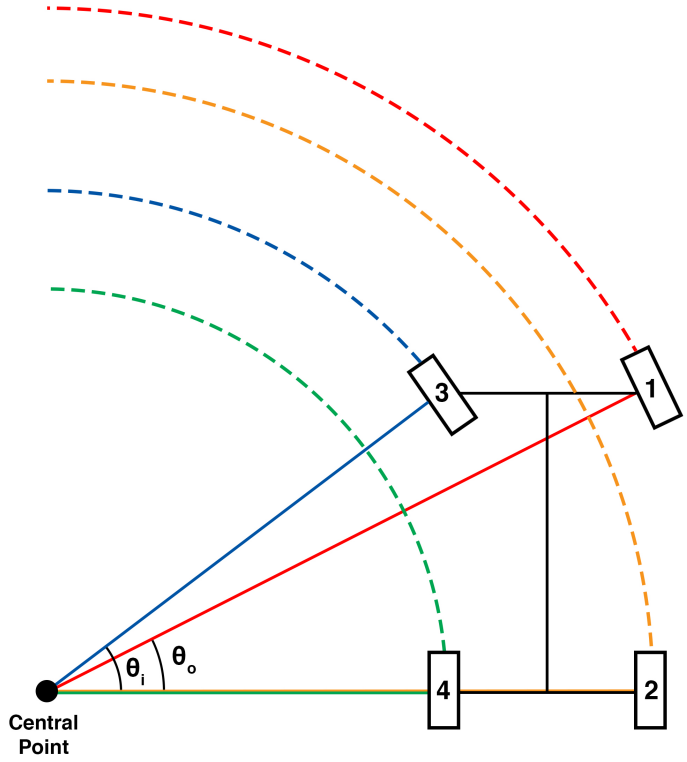

Figure 3.3: Wheel turning radius - Ackermann steering prevent tyres from slipping.

The Ackermann's geometry helps finding the right balance between both wheels and slip angles. By slip angle it is meant the angle made by the direction a wheel is pointing in and

the direction that the car is actually travelling [63]. This geometry is achieved by designing a steering system that ensures that if two imaginary lines are drawn from both left and right steering hubs (points in which the wheels turn around the Z axle), by crossing the hubs from the linkage they are attached to, these lines should meet exactly at the center of the rear axle as shown in Figure 3.4.

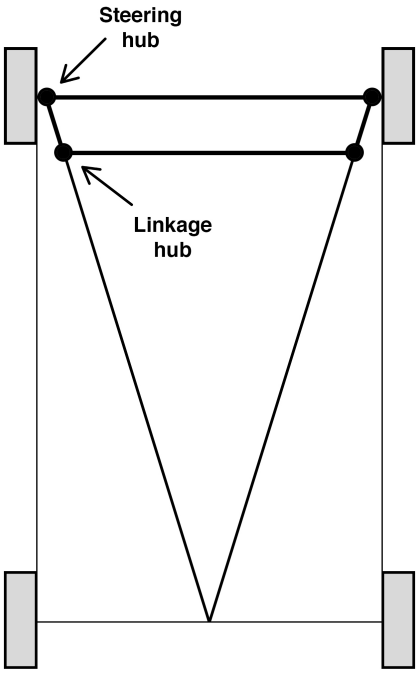

Figure 3.4: Perfect Ackermann geometry example.

There are several restrictions to engineer a steering linkage with the perfect Ackermann criteria. Figure 3.5 illustrates the ideal scenario for an automobile to perform a left turn when the four wheels only make pure rotations about a central point. This geometry requirements, as seen in Figure 3.5 can be expressed as [61]:

$$l \cdot \cot(\theta_i) - l \cdot \cot(\theta_o) = b \tag{3.9}$$

Where b represents the the wheels track, l the vehicle's wheelbase dimension, and θ_i and θ_o indicate the due angles of the front inner and outside wheels with respect to the center point of the curvature.

The Ackermann turning criteria is achieved by rearranging equation 3.9 as:

$$\cot(\theta_i) - \cot(\theta_o) = \frac{b}{l} \tag{3.10}$$

Ideally, the turning angles would behave in a way that both imaginary lines would always

meet while the central point moves from its origin up to infinity, in a straight horizontal way to the inner side of the curve, as in Figure 3.5. However, if this condition is not satisfied, the rotation centres of both left and right front wheels would not coincide with each other, causing unwanted sliding.

Paying attention to Figure 3.5, suppose that the bottom angle of a trapezoid linkage $ABCD$ is denoted by ψ. Then, when the turning angle is zero, the length of link BC is expressed as:

$$l_{2,0} \;=\; l_4 - 2 \cdot l_1 \cdot \cos(\psi) \tag{3.11}$$

It is also possible to calculate the length (l_2) of the steering linkage that meets the needs of this geometry. This linkage is a particular path tracing mechanism [61]. When turning to the left, considering that the inner wheel turned θ_i and the outer wheel turned θ_o, l_2 should be calculated as:

$$\begin{aligned} l_2 \;&=\; \sqrt{[l_4 - l_1 \cdot \cos(\psi - \theta_o) - l_1 \cdot \cos(\psi + \theta_i)]^2 + [l_1 \cdot \sin(\psi - \theta_o) - l_1 \cdot \sin(\psi + \theta_i)]^2} \\ &=\; \sqrt{2 \cdot l_1^2 + l_4^2 + 2 \cdot l_1^2 \cdot \cos(2 \cdot \psi + \theta_i - \theta_o) - 2 \cdot l_1 \cdot l_4 \cdot [\cos(\psi - \theta_o) + \cos(\psi + \theta_i)]} \end{aligned} \tag{3.12}$$

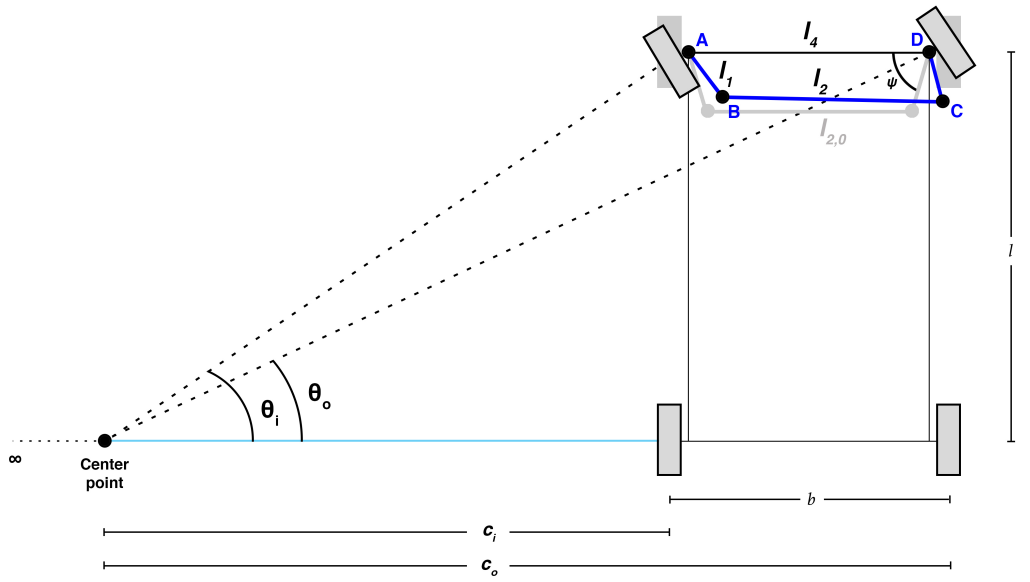

Figure 3.5: Restrictions for the steering linkage of a vehicle with Ackermann criteria.

From equation 3.10 we obtain:

$$\theta_o \;=\; \operatorname{arccot}\left(\cot\left(\theta_i\right) - \frac{b}{l}\right) \tag{3.13}$$

And finally substituting 3.13 into equation 3.12 yields:

$$\begin{aligned} l_2 \;=\; l_4 \cdot \Big[& 1 + 2\cdot\xi^2 + 2\cdot\xi^2 \cdot \cos\left[2\cdot\psi + \theta_i - \operatorname{arccot}\left(\cot\left(\theta_i\right) - \zeta\right)\right] \\ & - 2\cdot\xi\cdot\left\{\cos\left(\psi+\theta_i\right) + \cos\left[\psi - \operatorname{arccot}\left(\cot\left(\theta_i\right) - \zeta\right)\right]\right\}\Big]^{\frac{1}{2}} \end{aligned} \tag{3.14}$$

Where $\xi = \frac{l_1}{l_4}$, $\zeta = \frac{b}{l}$.

From a simple manipulation of these equations it is also possible to extrapolate the ideal Ackermann curvature radius for the inner wheel (c_i) and for the outer wheel (c_o), also represented in Figure 3.5:

$$c_i \;=\; \frac{l}{\tan\theta_i} \tag{3.15}$$

$$c_o \;=\; \frac{l}{\tan\theta_o} \tag{3.16}$$

3.4 Roll, Pitch and Yaw

It is also fundamental to mention three important attributes of the automobile physics: roll, pitch and yaw. A vehicle that is free to operate in three dimensions, can change its attitude and rotation about the three orthogonal axes centred on the vehicle's centre of gravity - the longitudinal, vertical, and horizontal axes [64], as represented in Figure 3.6.

Motion about the longitudinal axis is called roll. Roll defines how the car is able to distribute its weight while turning, either to the right or left side. Entering a corner is one such example as a car tends to lean in the opposite direction of the turn, consequently placing the load on the outer tyres.

Roll effects can either be positive or negative. If balanced, roll may help in dishing out more grip from the tyres, while, on the other hand, it can cause a vehicle to tip on two wheels and topple over, causing uneven wear to tyres and sometimes even damaging them.

Motion about the lateral axis is termed pitch. Pitch can occur either when a car is braking or accelerating. While under braking, the weight of the car is transferred forward onto the front wheels, consequently causing the body of the car to lean forward. In an acceleration scenario, the car leans back, transferring weight to the rear wheels.

Pitch effects are important since they can be translated into the level of grip being given to the tyres on straight line actions, such as the ones mentioned above. Let's imagine a RWD

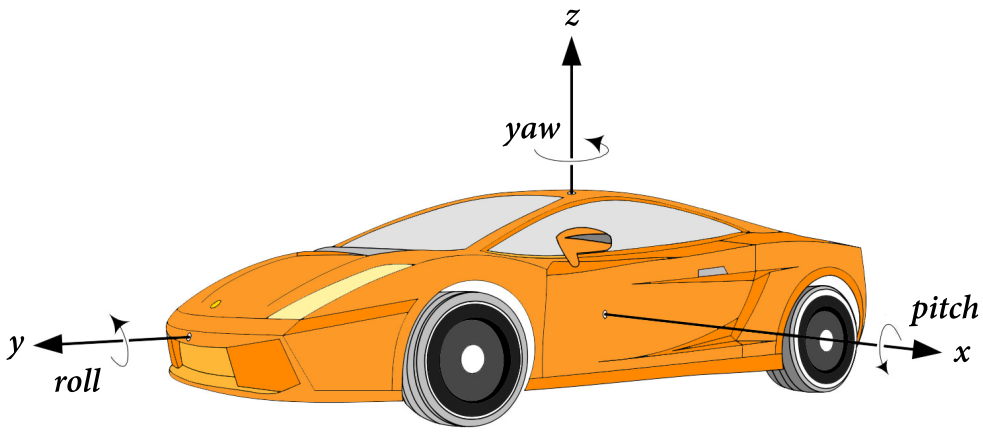

Figure 3.6: Roll, pitch and yaw angles, adapted from [58].

car that is not able to pitch. That would mean all four wheels would get equal brake power and acceleration, which would translate into safety problems. Since there is no pitch, when braking, the front wheels would not get the necessary weight transfer and less grip would be applied to the tyres, resulting in a longer braking distance or even a skid. The same thing happens when accelerating. Since no weight falls on the rear of the vehicle, the tyres would not have the necessary grip and an undesired burnout would most certainly happen.

Finally, motion about the perpendicular axis is called yaw. Yaw determines which way the front of the car is pointing. It is nothing more than a value and, therefore, it has no force upon a car. As seen in the section above, while performing a turn all the wheels of a car rotate at different speeds and consequently cover different distances. Knowing the yaw angle and the distance covered by each of the wheels, it is possible to validate theoretical analysis such as the Ackermann criteria presented above.

Roll, pitch and yaw concepts are important when studying the behaviour of a vehicle, especially such as the one being developed here, mainly since their values are usually a result of the suspension reacting to turns, accelerations, and road conditions.

Chapter 4

Scale Model Car

In order to validate the theoretical dynamics and kinematics presented in chapter 3, as well as to implement active safety systems in the future, the development of a scale model was proposed in the objectives of this dissertation. Not only one but two models ended up to be built. The main reasons why two vehicles were constructed were to allow the possibility of simultaneously testing different setups (as happened with the steering system and as will be mentioned bellow), to have an extra model (not slowing the development process if something happens to one of them, such as crashing or having problems in the electronics) and to possibly perform and compare simultaneous manoeuvres with control algorithms turned on and off.

This chapter is intended to report all the studies and work performed while developing the scale model vehicles. It starts by stating the reasons for the establishment of the model's characteristics, such as scale, used materials and all the necessary steps in order to build the prototypes.

An approach to every used hardware component with explanations on the choices made, details on how they work and on the interconnection between every element will be found in the next few sections. Other important aspects to mention are related to the use of Computer-Aided Design (CAD), followed by the processes of 3D printing and water-jet cutting, turning the designed structures into real and tangible objects, as well as the assembly of every part. The development and design of the mobile application used to control the cars, via Bluetooth, as well as a guide on how to use it and how to interpret the data provided by the included sensorial modules, concludes Chapter 4.

Before going any further, it is important to recall, as mentioned in the introduction chapter, that this work results from the combination of two previous dissertations produced by former Electronics and Telecommunications Engineering students from the *Universidade de Aveiro*. The first, named *"Segurança automóvel: Sistemas de apoio à condução"* [6], written by Bruno Grego, is mostly focused on theoretical simulations around the dynamic behaviours of a four in-wheel electric motor vehicle, while the second, *"Desenvolvimento de um veículo elétrico em escala reduzida"* [7], by Sérgio Ferreira, is based on the development of a scale model but with no suspension and, therefore, more distant from reality than the case to be analysed here.

4.1 Establishment of the Model Characteristics

Scale models are a cheap and more secure way of testing new systems. Studies show that these are technologically suitable alternatives to tests with full-size equipment [65]. Besides that, the simplicity of working on low scale cars makes it possible to perform all the necessary testing in a small closed environment.

Since a vehicle with four independent in-wheel electric motors is not commonly found in the market, the need to produce a prototype for testing purposes was inevitable.

To start with a solid base and in order to have a comparison term, it was decided to stick with the same real scale car used in [7], a 1999 Renault Megane Coupe (as shown in Figure 4.1). Meaning that the same real vehicle measurements were taken in consideration, as seen in Table 4.1.

Figure 4.1: 1999 Renault Megane Coupe Maxi [66].

In [7], Sérgio Ferreira opted for choosing a 1:14 scale to develop his prototype. In order to add the suspension system to a new model, and due to the increased design complexity and large variety of extra componentes needed, it was decided to go for a 1:10 scale. This decision made it possible to work with better materials, as well as to make use of a comercial suspension with the approximate desired characteristics, originated from a 1:10 radio control car.

Measurements	**Full Scale Vehicle 1:1 ($\pm$ 10.00 mm)**	**Small Scale Vehicle 1:10 ($\pm$ 1.00 mm)**	**Prototype vehicle ($\pm$ 1.00 mm)**	**Percent Deviation ($\pm$ 0.01 %)**
Length	3 970.00	397.00	397.00	0.00
Width	1 699.00	169.90	169.90	0.00
Wheelbase (l)	2 469.00	246.90	270.00	9.36
Front/Rear track (b)	1 430.00	143.00	161.90	13.22
Ground clearance	119.00	11.90	14.71	23.61
Wheel dimension	632.00	63.20	60.00	-5.06
Spring length	360.00	36.00	22.00	-38.89

Table 4.1: Real vehicle *versus* scale model and comparison with the developed prototype dimensions.

When looking at Table 4.1, it is important to clarify that the *wheelbase* represents the distance between centres of both front and rear wheels. The *front/rear track* is the distance between the centreline of two wheels of the same axle. *Ground clearance* stands for the height from the ground up to the base of the chassis and *spring length* represents the size of the suspensions springs with no load or compression applied.

Percent deviation measures how much the achieved values differ from the known theoretical data [67]. In this case, it gives us a relation between the different dimensions of the exact 1:10 scaled car and the developed prototype (Equation 4.1).

$$Percent\ deviation = \frac{Practical\ value - Theoretical\ value}{Theoretical\ value} * 100 \tag{4.1}$$

As seen in the equation, it is calculated by subtracting the known from the measured parameter, dividing the result by the known (theoretical) value and multiplying everything by 100, in order to obtain a percentage. If the result is a negative value it signifies that the prototype is smaller than expected in this certain parameter. Otherwise, if the percent deviation is positive, the model is bigger than it would be expected.

A perfect scale model would have zero percent deviation from reality, meaning that the real-scale car and model would be dynamically identical. As seen in Table 4.1 this was not achieved for every parameter other than for length and width, due to the increment of complexity carried at the design stage of the chassis, specially for fitting all the steering and suspension components.

4.2 Hardware Specifications

Before going any further, it is important to specify the hardware used to perform the desired actions such as control, data acquiring and processing.

In the next few subsections it will be discussed the components chosen to constitute the three main systems of the developed model: tractive, suspension and steering systems. It will also be introduced the micro-controller used to connect every system, as well as the communication devices and protocols which enable the user to control the car.

4.2.1 Wheels, Motors and Speed Sensors

Choosing the right tractive system for a vehicle is one of the key ingredients to achieve a prototype capable of acquiring results that go towards the goals of this investigation. One of these objectives was to build a vehicle with independent traction within its four wheels. In other words, this translates into the need of having four in-wheel motors assembled to moving parts of the chassis, capable of performing the necessary Degrees Of Freedom (DOF) imposed by both steering and suspension systems.

A great set of wheels, motors and speed sensors was the one used in [7]. All these components are manufactured by *Pololu*, an electronics manufacturer and online retailer focused on several robotic areas from sensors and motion control electronics to motors and wheels to complete robots [68].

Starting with the wheels, they are made out of plastic press fit onto 3 mm D shafts prepared to directly attach the micro metal gearmotors, making it easy to have an in-wheel motor solution (Figure 4.2). Their size represents a good compromise between the real vehicle and the scale model, with an absolute percent deviation of 5.06 %. The tyres are composed of silicone and have a width of only 11 mm, allowing the prototype to have a good grip level and agility.

As stated, the propulsion system is composed by four independent tiny brushed DC gearmotors. Due to the high angular speed these motors are able to provide, a metal gearbox with a gear ratio of 30:1 is attached to their bodies, making it possible to deal with the common operation speeds and increasing the available torque in a start from zero or low speed situation.

Figure 4.2: *Pololu* micro metal gearmotor and wheel representation.

The chosen motors are the *HP - High Power 6V* version with a no-load performance of 1000 RPM at 70 mA, a stall current of 1.6 A, stall torque of 0.57 kg-cm and a maximum output power of 1.5 W at 6 V conditions. At maximum efficiency, the manufacturer says these motors are capable of achieving 830 RPM, 0.10 kg-cm of torque, 0.36 A of current and an output power of 0.89 W. A more in depth performance graphic, with details on efficiency, power and speed as a function of the generated torque can be seen in Figure 4.3.

Based on the motor and wheel specifications above, the maximum longitudinal speed of the vehicle was calculated. For each complete rotation of the wheel, the car will travel approximately 0.188 meters. Meaning that at 1000 RPM the prototype is supposed to travel at around 11.28 km/h, and at 9.36 km/h when producing 830 RPM. Directly applying the scale factor of 1:10, 112.80 and 93.60 km/h would be achieved in a real car. Speed enough to test all the required control systems. This was another key factor taken into consideration when choosing the right gearmotors.

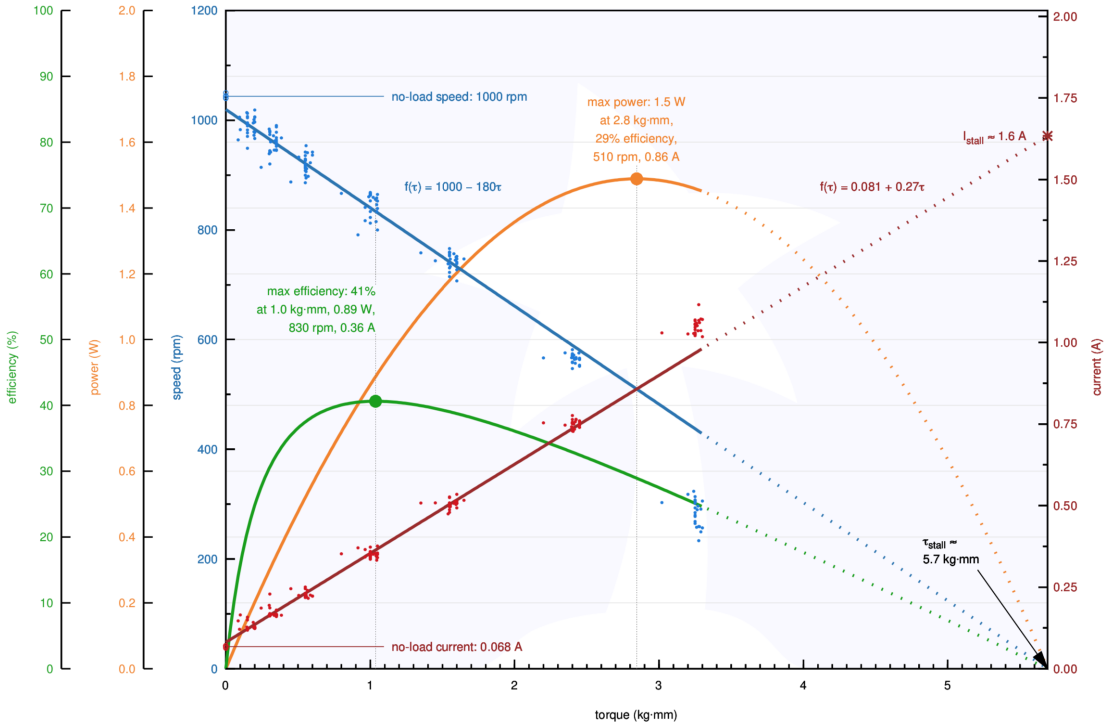

Figure 4.3: *Pololu 30:1 Micro Metal Gearmotor HP 6V* - Performance at 6 V [69].

Another characteristic of this motor model is having an extended back shaft, allowing the attachment of a magnetic encoder, as in Figure 4.4. These magnetic encoders, also from *Pololu*, use a magnetic disc and Hall effect sensors to provide 12 counts per revolution of the motor shaft. More specifically, each encoder includes a dual-channel Hall effect sensor board and a 6-pole magnetic disc that can be used to add quadrature encoding to the micro metal gearmotors (information on how Hall effect sensors work can be found in [70]). Knowing that each wheel travels approximately 0.188 m per revolution, and that the motor shaft is connected to a 30:1 gearbox, this means that these encoders are able to provide information, approximately, every 0.52 millimetres traveled, providing 360 reads per revolution of the wheel. Translated in time, at 1000 RPM, a signal can be sent every 0.17 ms or, in the frequency domain, at approximately 6 kHz.

The encoder board is directly soldered to the back of the motor, with the back shaft of the motor protruding through a hole located in the middle of the circuit board. A VCC and a GND pin power the sensors, with a possible VCC input range of 2.7 up to 18 V. Two other pins (A and B) are responsible for outputting the quadrature digital signals which may either be driven low (0 V) or pulled up to VCC through 10 kΩ pull-up resistors, depending on the applied magnetic field. The sensors' comparators have built-in hysteresis, allowing the prevention of spurious signals in cases where a motor stops near a transition point.

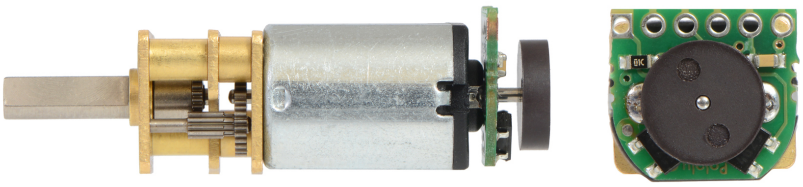

Figure 4.4: 12 CPR magnetic encoder installed in a micro metal gearmotor [71].

4.2.2 Suspension Components

The built suspension system can be divided into three main parts: the shock absorbers (which include the suspension dampers and springs), the shock towers (structures that support the shock absorbers and perform the link to the vehicle's chassis) and the suspension arms, responsible for linking the wheels, suspension and also the chassis. These last two will be in depth discussed in the 3D modelling Section 4.4.

Regarding the shock absorbers, a kit developed by a large radio control parts store named *HobbyKing* was used. This kit, *Blaze 1/10 Aluminium Shock Absorber Set 124000*, shown in Figure 4.5, offers quality dampers and springs for 1:10 scale cars, being our prototype composed by four units (one per wheel).

Figure 4.5: Blaze 1/10 Aluminium Shock Absorber Set 124000 by *HobbyKing*.

Each shock absorber has the dimensions of 19x12x48.5 mm and each spring has a length of approximately 22 mm, achieving an absolute percent deviation of 38.89 %. Although this value is higher than what would be a perfect scenario, this suspension seemed to have the overall best characteristics between all the possibilities available in the market within the same price range.

These suspensions allow the possibility of tunning the ride by compressing the springs and, consequently, applying small changes to the height of the vehicle. For the purposes of this dissertation, the compression of the springs will stay standard and no tune will be performed.

4.2.3 Steering System

The hardware used in the steering system boils down to a digital servo motor. Several tests such as the ones done in the Illinois Roadway Simulator in [72] show the importance of choosing a servo actuator with the right characteristics, having an important role in the overall behaviour of the vehicle. Also in [53], it is stated that a slow servo motor is a major limitation of the dynamic control in a scale model.

The chosen servo is a *Turnigy™TGY-EX5252MG*, as seen in Figure 4.6. This digital micro servo appeared to be a reliable solution with an amazing power capability for its diminutive size.

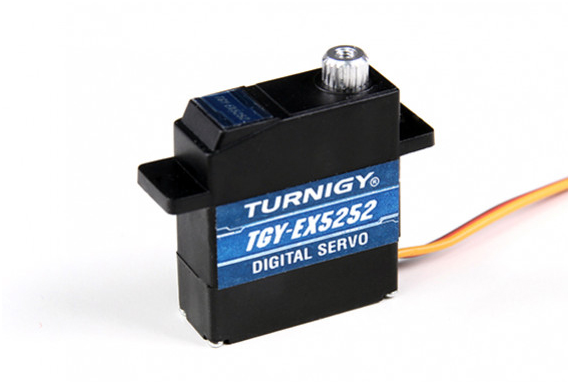

Figure 4.6: Micro servo *Turnigy™TGY-EX5252MG*.

The *TGY-EX5252MG* is a high speed servo with an operation voltage of 4.8 up to 6 V and with a no-load speed of 0.10 Sec/60 ° at 6 V of power supply. With this supply, it is capable of generating 2.8 kg-cm of torque. It allows a controlled rotation of an axle within 180 ° in both directions. All this, only weighing 12.4 g (including the lead and the plug). The servo will be controlled by signals generated by a micro-controller that will be introduced in the next subsection.

4.2.4 Micro-Controller and Motor-Shield Controller

The use of a micro-controller capable of analysing and processing all the data generated by the hardware modules used in this project was essential. This micro-controller had to be wisely chosen in order to fulfil the needs imposed by the physical size limitations available in the scale model, to have a good operating frequency, enough digital I/O and analog input ports and a user-friendly programming interface.

With all the requirements mentioned above in mind and as suggested in [55], it was decided to use the *Arduino Mega 2560 REV3*, a micro-controller board based on the ATmega2560 (Figure 4.7). The ATmega2560 has a clock speed of 16 MHz, a Flash Memory of 256 KB (of which 8 KB are used by the bootloader), 54 digital I/O pins (of which 15 are able to provide PWM output), 16 analog input pins, an operating voltage of 5 V, low weight, small overall dimensions and an open-source platform with lots of tutorials and communities willing to help online.

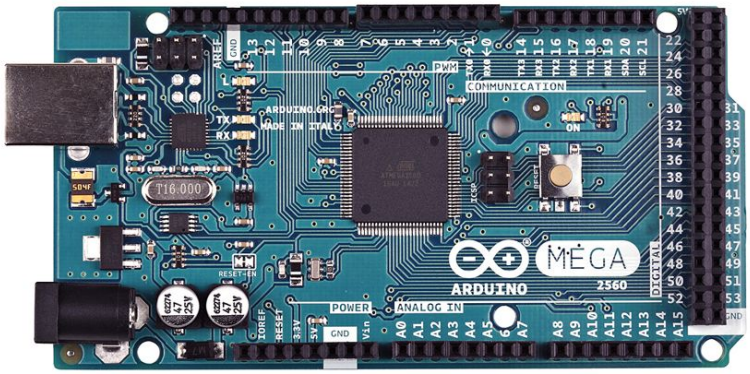

Figure 4.7: *Arduino Mega 2560 REV3* development kit.

Another aspect which helped on choosing the Arduino as the development platform was the possibility of using the *Adafruit Motorshield kit*, also known as *Adafruit Motor/Stepper/Servo Shield for Arduino v2 Kit - v2.3*, as seen in Figure 4.8 [73]. This shield enables the possibility of driving up to 4 DC motors with individual 8-bit speed selection (about 0.5 % resolution), meeting the exact requirements of this project. It also includes 2 connections for 5 V servos connected to the Arduino's high-resolution dedicated timer, reducing or even fully avoiding jitter. Its TB6612 chipset provides 1.2 A per bridge (enabling 3 A for brief 20 ms peaks) with thermal shutdown protection and internal kickback protection diodes.

Instead of using a latch and the Arduino's PWM pins, the *Adafruit Motorshield* has a fully-dedicated PWM driver chip onboard, responsible for handling all the motor and speed controls over I2C.

Since the chosen in-wheel DC gearmotors allow a maximum current of 1.6 A, and both the motors and the steering servo will operate at the voltage of 5 V, this shield represented the right fit for the development of the prototypes.

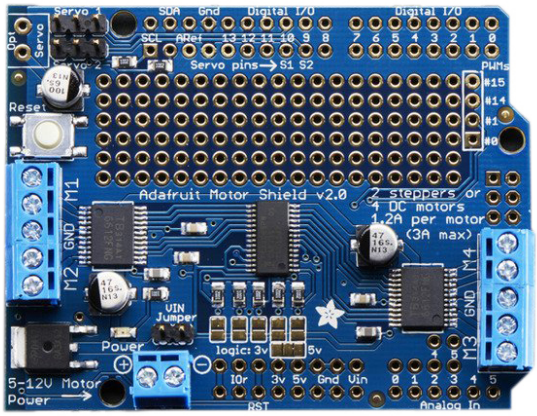

Figure 4.8: Motor-controller shield - *Adafruit Motor/Stepper/Servo Shield for Arduino v2 Kit*.

4.2.5 Sensorial Data Acquiring and Recording

In order to perform the desired control, the prototypes under development had to feature several sensors to acquire live data of what is happening while driving and performing manoeuvres. It is obvious that the previously mentioned speed sensor encoders have an important role on this topic, transmitting data to the micro-controller, such as wheel speed. But another type of sensores implemented in the project are the accelerometer and the gyroscope.

An accelerometer is known as a device capable of measuring the rate of change of velocity, also known as proper acceleration. On the other hand, a gyroscope is used for measuring or maintaining orientation and angular velocity.

The *DFROBOT 6 DOF Sensor - MPU6050*, as seen in Figure 4.9, was the elected module to assemble in the vehicle. This device combines a 3-axis gyroscope and a 3-axis accelerometer. It uses I2C digital outputs to communicate with the Arduino and is capable of easily gather information regarding pitch, roll and yaw motions.

Its tri-axis accelerometer has a programmable full scale range of ± 2, ± 4, ± 8 and $\pm 16\,g$ and its tri-axis angular rate sensor (gyroscope) has a sensitivity of up to 131 LSBs/dps and a full-scale range of ± 250, ± 500, ± 1000, and $\pm 2000\,°/s$.

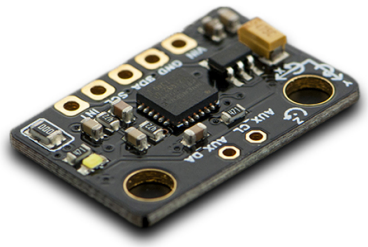

Figure 4.9: *DFROBOT 6 DOF Sensor - MPU6050* accelerometer and gyroscope module.

To later analyse and process the gathered information provided by the sensors, a Real-Time Clock (RTC) was used. A RTC is nothing more than a computer clock powered by an external battery that has the function of keeping track of the current time. This allows having an accurate timing perspective, essential for post-processing and analysing the sensorial data.

The module used was a *DS3231 RTC*, a real time clock based on the DS3231 chip, with a small size, low-cost and an extremely high accurate I2C bus real-time clock, Figure 4.10.

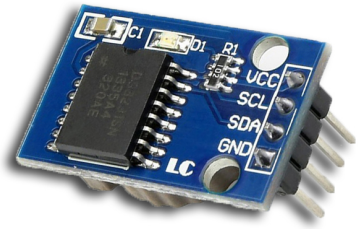

Figure 4.10: *DS3231 RTC* module.

Finally, with the purpose of storing all the information needed, the use of a MicroSD card module was almost mandatory. This enables the consultation of the logged data at any time and works like the black boxes found in airplanes, working as a data logger and facilitating the investigation of the behaviours of the car. The use of this module greatly expands the capabilities an Arduino can perform with its poor limited memory. The module used can be seen in Figure 4.11.

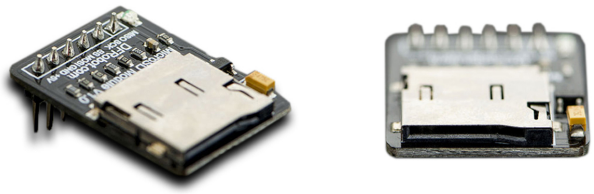

Figure 4.11: MicroSD card reader module.

4.2.6 Power Supply and Batteries

Battery concerns are still one of the most discussed topics in this new age of vehicle electrification. With this in mind, aspects like the range and charging time were taken in considerations when choosing the right power supply and batteries responsible for feeding the prototypes.

The implemented energetic system is composed by an adjustable DC-DC step-down power regulator module and three lithium-ion rechargeable batteries, connected in series, and originating what can be seen as a single 3-cell battery.

The used voltage regulator, as seen in Figure 4.12, is based on a LM2596 step down power regulator. It allows an input voltage range of 4 up to 40 V and an output voltage range of 1.25 up to 37 V. Its maximum output current is 3 A and its normal operating current is around 2 A. It features an internal oscillation frequency of 150 KHz, low power consumption and a high overall efficiency.

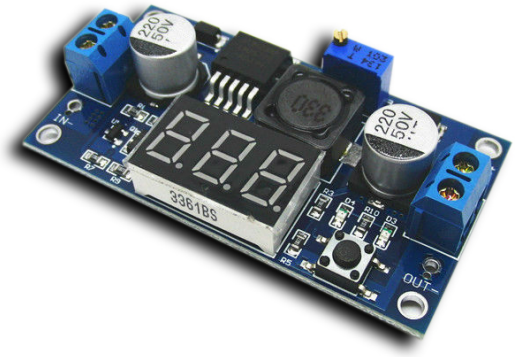

Figure 4.12: LM2596 DC-DC voltage regulator adjustable power supply module w/ display.

The embedded display in the voltage regulator unit operates as a voltmeter and allows a real-time control of both input and output voltages, giving to the user an accurate feedback about the batteries' state for a better management of the vehicle's operating time between charges.

As mentioned, the whole battery system is composed by three batteries in series. The chosen batteries are *Samsung INR18650-25R*, which, as said in its data-sheet [74], have a nominal discharge capacity of 2 500 mAh, a maximum charge of 4.20 V, a minimum discharge voltage of 2.5 V and a nominal voltage of 3.6 V. They are able of rapid charging at 4 A to 4.20 $\pm$ 0.05 V. While in rapid charge (and at 25 °C conditions), it is stated that these batteries are able of fully charging in 60 minutes, while in standard charge (at 1.25 A) it will take nothing more than 180 minutes.

Since the batteries will be in a series fashion, the expected operating voltage range of the set is between 7.5 and 12.6 V. A *Samsung INR18650-25R* battery can be seen in Figure 4.13.

Figure 4.13: *Samsung INR18650-25R* battery.

4.2.7 Bluetooth Communications

With the necessity of implementing a communication system which enables the user of the developed scale model vehicle to control the car, bluetooth was the chosen wireless technology. At a first stage, wifi was also considered, however, after reading and debating about both technologies, bluetooth was elected due to its easier protocol implementation and signal range needed.

The used module is a *HC-06 Bluetooth to serial*, as seen in Figure 4.14. This device has a 2.4 GHz digital wireless transceiver with a built-in antenna and an external 8 Mb flash memory. Its low power consumption, high-performance and low cost were also factors that turned the *HC-06* into the right choice for this project.

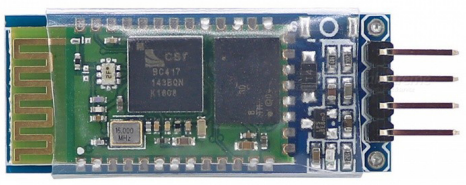

Figure 4.14: *HC-06 Bluetooth to serial* module.

4.3 Electronic Circuits and Assembly

The modules introduced in the previous section needed to be connected to the microcontroller in order to work properly. In this brief section, the interconnections and designed circuits will be explained.

In Figure 4.15 it is possible to see all the connections between the modules and the Arduino Mega board.

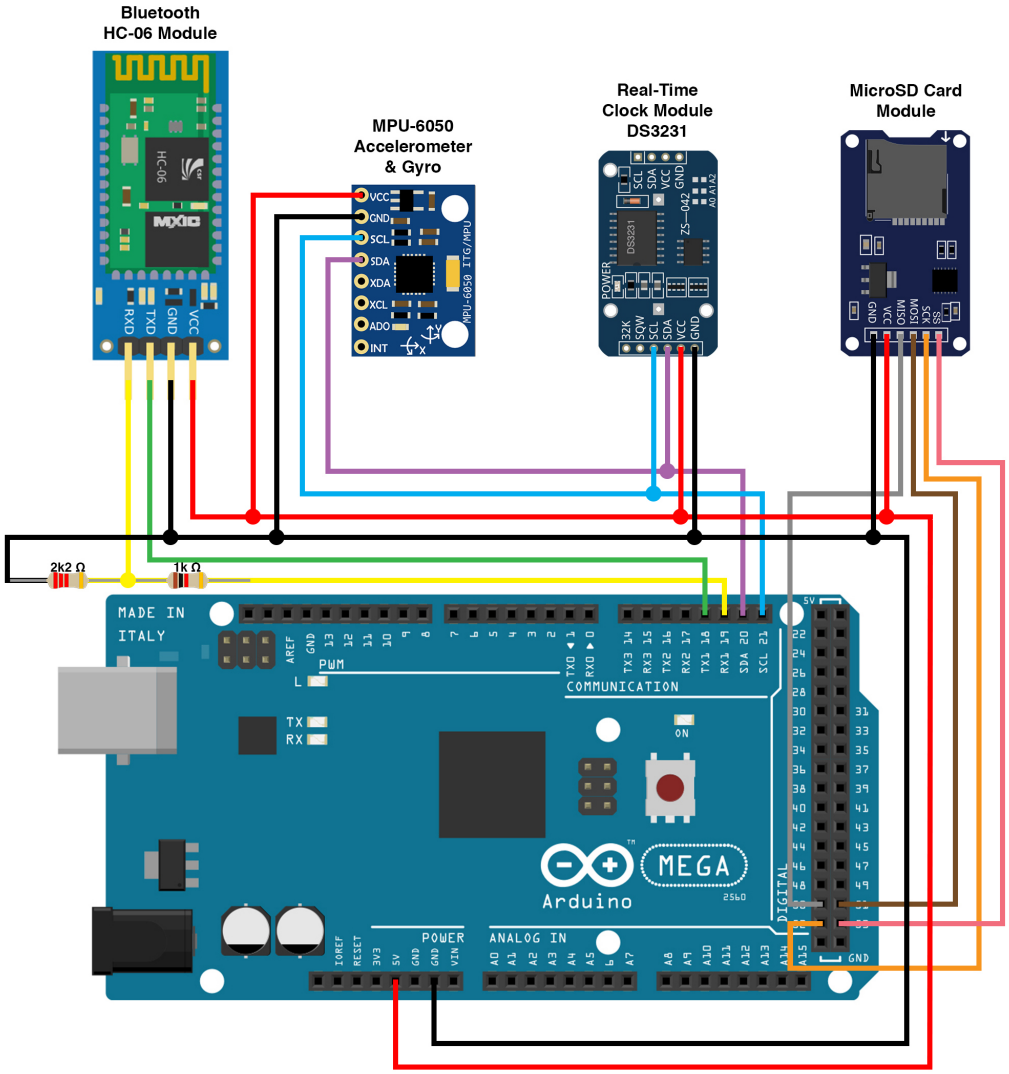

Figure 4.15: Connections between modules and the Arduino Mega board.

Starting with the bluetooth module HC-06, it is important to state that this module uses 0 - 3.3 V logic level, opposite to the 0 - 5 V used by the Arduino. The two resistors seen in the circuit have the function of working as a voltage divider, taking the 5 V high level and creating a voltage at the RX pin of around 3.3 Volts. Since the Arduino is able to read a 3.3 V logic level correctly, nothing needs to be done to the HC-06 output. Besides this, the connections are simple: the RX pin from the module is connected to pin 19 on the board and the TX to pin 18. These pins use the UART/Serial 1 available in the Arduino Mega and are endowed with the ability of having interrupts attached, useful in the communication algorithm and control of the vehicle. VCC is connected to the Arduino +5 V pin and GND to the Arduino's ground pin.

Next up with the accelerometer and gyro module (MPU-6050), the data communication is performed via I2C. Meaning that a connection is made between the SCL pin in the module and the SCL pin in the Arduino, and the same thing with SDA pins. Like in the HC-06, VCC is connected to the Arduino +5 V pin and GND to the Arduino's ground.

The Real-Time Clock module (DS3231) shares the I2C protocol with the MPU-6050. This said, SCL and SDA pins from both modules share the same circuit nodes and Arduino pins (to read more on the basics of I2C communication read in [75]). The module is also powered with the +5 V and GND pins. It was noticed that both modules were using 0x68 as the default I2C communication address. Fortunately, the MPU-6050 module has a jumper that, when removed, changes the address to 0x69, avoiding interferences with the RTC.

The MicroSD card module has six pins, two for powering the module, (+5 V VCC and GND), and four more pins for the SPI communication (SS, SCK, MOSI and MISO). These communication pins are directly connected to the respective pins in the development board (pins 53, 52, 51 and 50, respectively).

All these circuit connections were assembled in the bottom side of the Adafruit motor shield in a protoboard devoted area, as seen in Figure 4.16. This approach made it possible to hide all the wiring and to give a cleaner look to the final product.

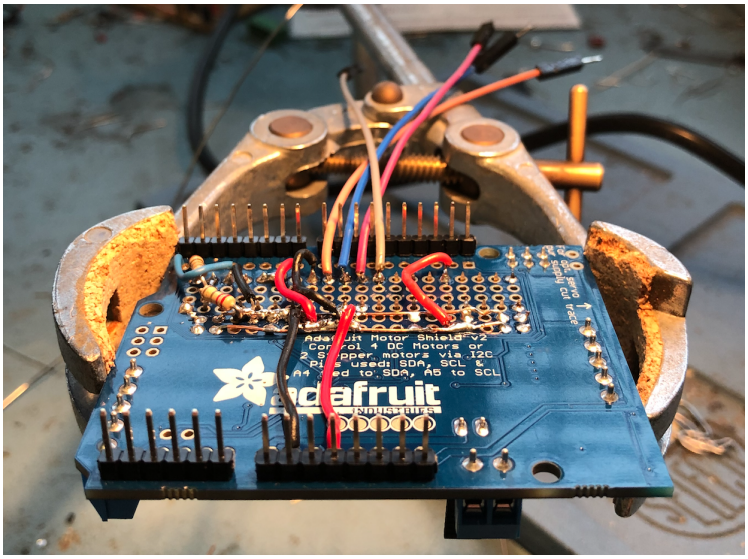

Figure 4.16: Soldering the circuits in a Adafruit shield stage.

Each of the four DC motors is directly driven up by connectors available in the shield, with M1 port connected to the front-left motor, M2 to the rear-left motor, M3 to the rear-right and M4 to the front-right one. The A pins of both front wheel encoders are connected to pins 2 and 3 (which enable the use of interrupts). Since there were no more interrupt pins available, B pins, as well as the rear encoders, are connected to normal digital pins. The encoders are also directly powered by the Arduino board's 5 V and GND pins.

The three lithium-ion rechargeable batteries are connected to the voltage regulator module in the back of the vehicle which is set to give an output of 5 Volts. This output voltage is responsible for powering the motor shield and, consequently, the four DC motors. Also from the battery case, a cable with a DC barrel jack directly supplies the Arduino. Between both, an ON/OFF switch was included in order to power the system.

Before finding out the need to separate the two DC power supplies as mentioned above, several tests were performed with a single supply, powering both the Arduino board, attached modules and motors via the output of the voltage regulator. A critical problem was found while controlling the vehicle because the bluetooth tended to break the connectivity with the device it was being controlled with. After proper examination, it was discovered that the servo motor, which was supplied by the Arduino's 5 V, was introducing a lot of noise in the power supplied signal, as seen in Figure 4.17. This signal was measured in the 2-terminal power block of the shield. The peak-to-peak signal observed was achieving values of up to 1.92 V, representing around 38.4 % of the total voltage being supplied.

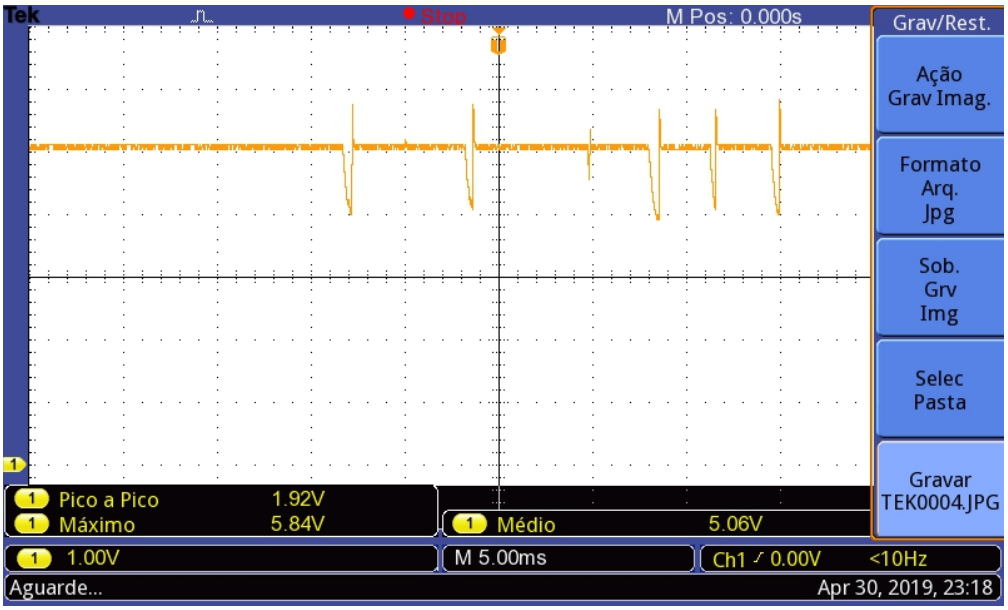

Figure 4.17: Input voltage signal measured in the shield with noise peaks caused by the servo.

In order to circumvent this problem, the double supply solution was found and the VCC cable from the servo, which was previously connected to the Arduino supply, was attached to the 5 V signal supplied to the Adafruit motor shield, creating a source for the digital signals and another to power the electronics that demanded higher current consumptions. This connection was made assuring a common ground between the Arduino and the shield.

4.4 3D CAD Modelling

In this section it will be presented all the necessary CAD modelling done to produce the scale prototypes. In order to execute this part of the project, there was a mandatory need to investigate and learn how to work with a tool like *Solidworks*. What ended up to be a great personal challenge and a way to learn about other areas.

Another important aspect that is worth mentioning is due to the fact that, although there are lots of CAD vehicle examples available online, the particularity of this being a four wheel drive car with in-wheel motors, made it impossible to make use of parts from other designs. Increasing the need of doing something from scratch.

The fact that a motor is directly attached to the wheel, also increased the challenge of developing a fully functional suspension and steering system, since the available space was limited.

In the following subsections several aspects related to the development and design of each dynamic system will be discussed.

4.4.1 Chassis Design

As said in Section 4.1, the chassis was based in a 1:10 scale vehicle. The chassis format was drawn in an entirely arbitrary fashion, while trying to take all the scale dimensional relations in consideration.

Several different schematics were performed before achieving the final chassis, shown in Figures 4.18 to 4.20.

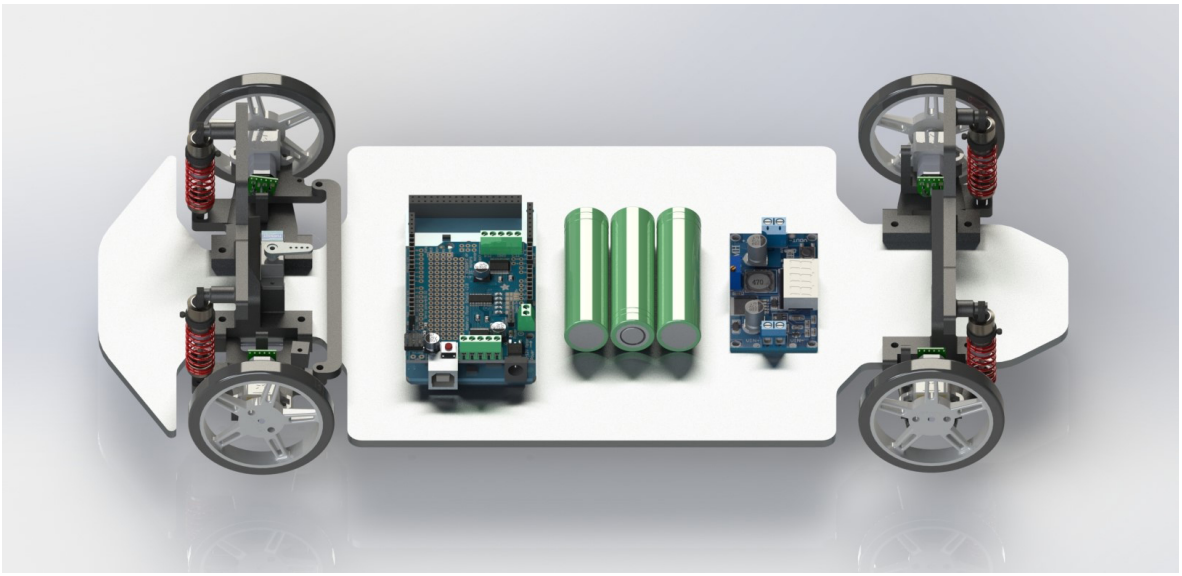

Figure 4.18: 3D CAD render of the scale model assembly made in *Solidworks*.

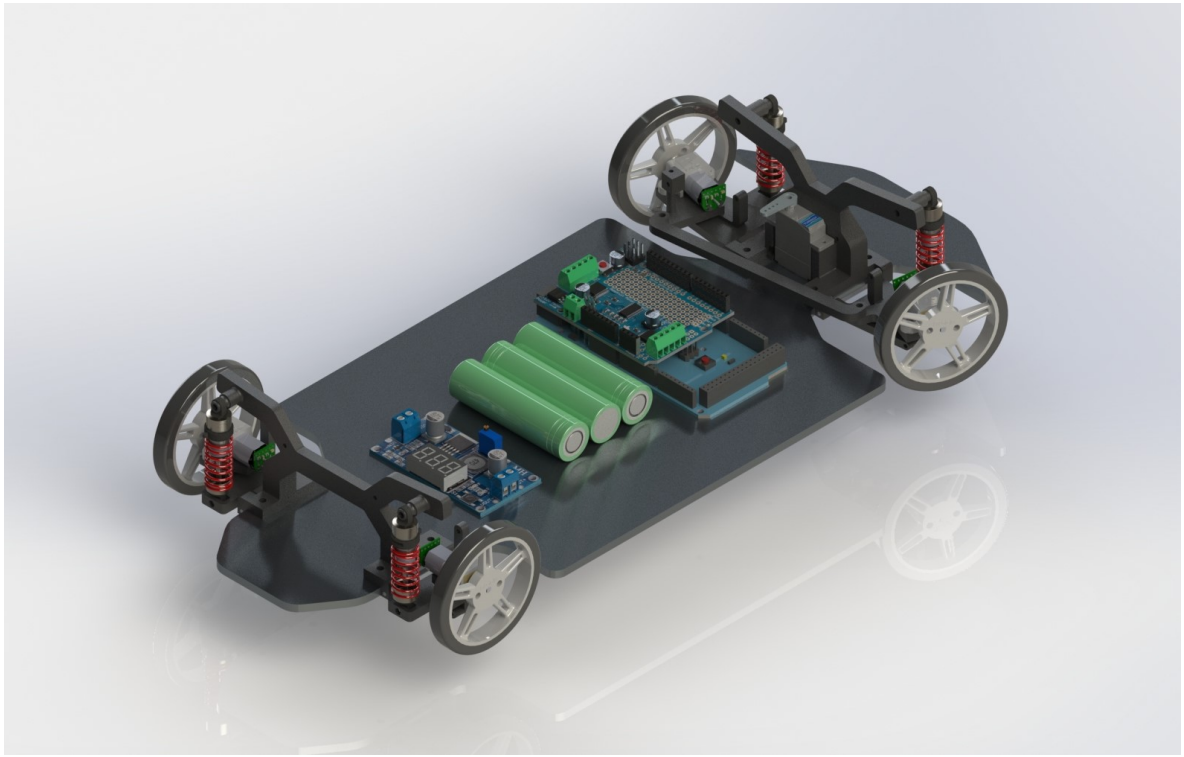

Figure 4.19: 3D CAD render of the scale model assembly made in *Solidworks*.

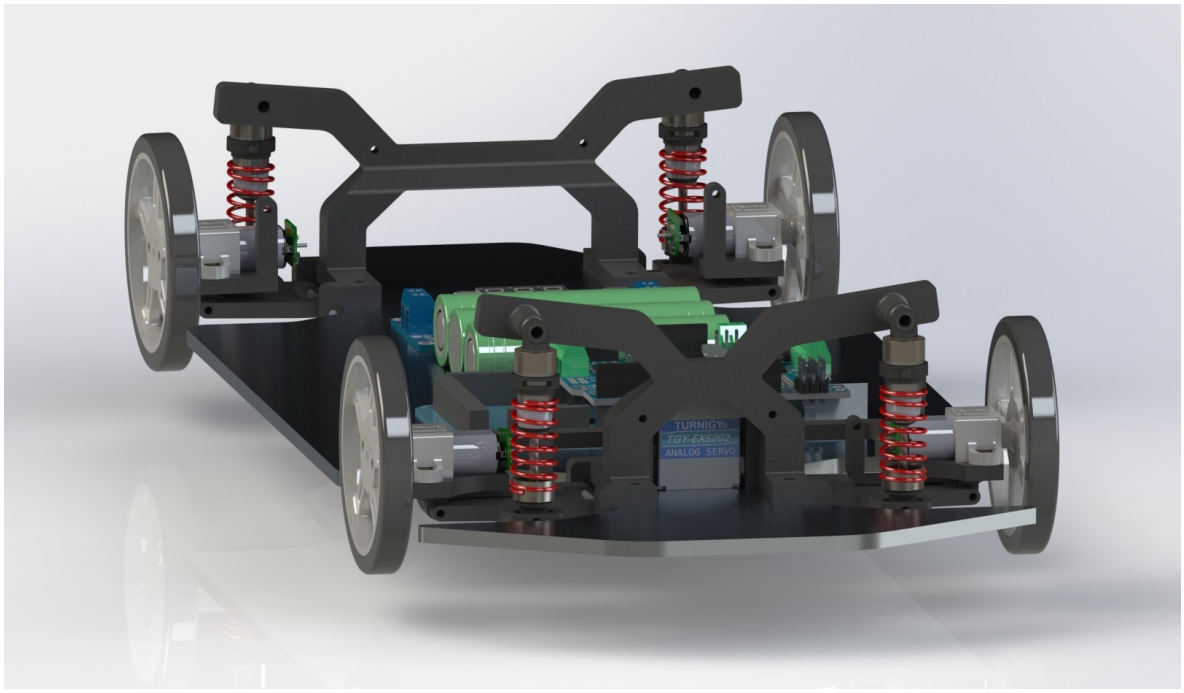

Figure 4.20: 3D CAD render of the scale model assembly made in *Solidworks*.

The chassis were designed with a thickness of 4 mm. In order to make them lighter, despite the chosen material (subject discussed in Section 4.5), a version with several extrude cuts in the center of the vehicle was tested (Figure 4.21). When evaluating the mass properties of both chassis (with and without the weight reduction cuts), with an aluminium alloy from series 6000, the observed diferences were between 549.05 g versus 435.41 g. Although being 20 % lighter, this solution was not used because it demanded an unnecessary production cost increase due to the complexity added in the machining process.

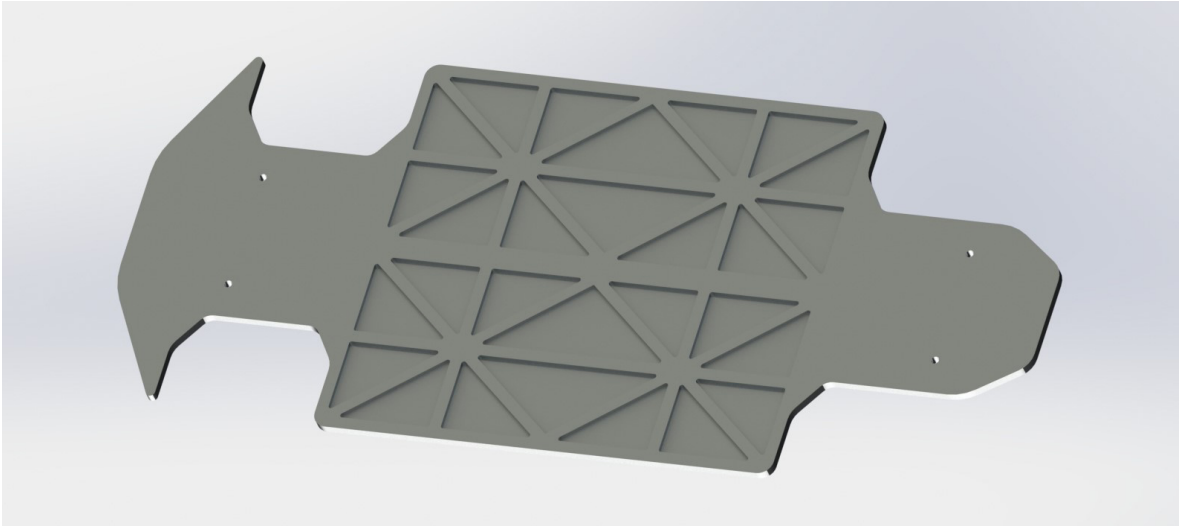

Figure 4.21: Attempt of reducing the weight of the chassis by making cuts on it.

4.4.2 Suspension Design

Although the shock absorbers were availed from a radio control 1:10 car, all the structures to support them and to physically move with them needed to be developed.

The first decision to follow was that the suspension would only work vertically - *i.e.*, the movement of the shock absorbers would be performed in a right angle relatively to ground. This choice made it easier to design the whole surrounding system.

As a starting point, the first pieces of the system to be designed were the structures which are attached to the chassis and that are responsible for supporting all the forces provided by the shocks, the front and rear shock towers. The front one is slightly different as it is possible to see in Figure 4.22, based on the need of having all the componentes of the steering system attached to the front wheels of the vehicle.

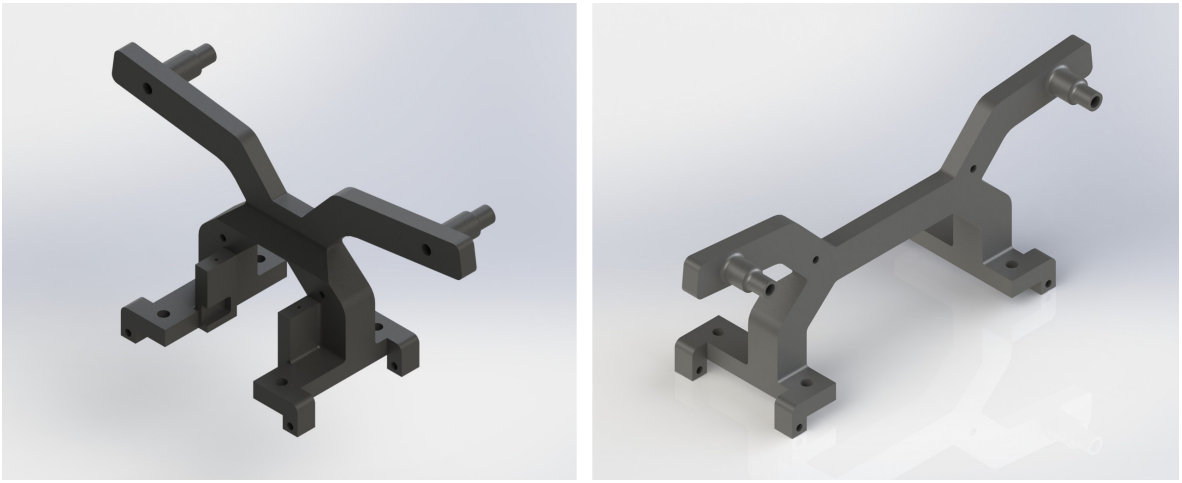

Figure 4.22: Front suspension shock tower (on the left) and rear shock tower (on the right).

Several DOF were needed to be taken into account in order to maintain the wheels with a neutral camber (the angle between the vertical axis of the wheels and the vertical axis of the vehicle when viewed from the front or rear) whenever the wheels needed to go up and down, to keep up with the work of the suspension. So, control arms, also known as A-arms (due to its format) were developed, as well as hubs where the motors and wheels are attached to. To make sure the hubs stayed parallel to the ground, holes were made in both shock towers, allowing a wire to link these two pieces and restricting the freedom of the wheels. Once again, the front and rear systems needed to be slightly different, also because of the extra complexity of the directional wheels. In Figure 4.23 it is possible to see a hub attached to an A-arm with arrows indicating where and how these parts move whenever the suspension is used.

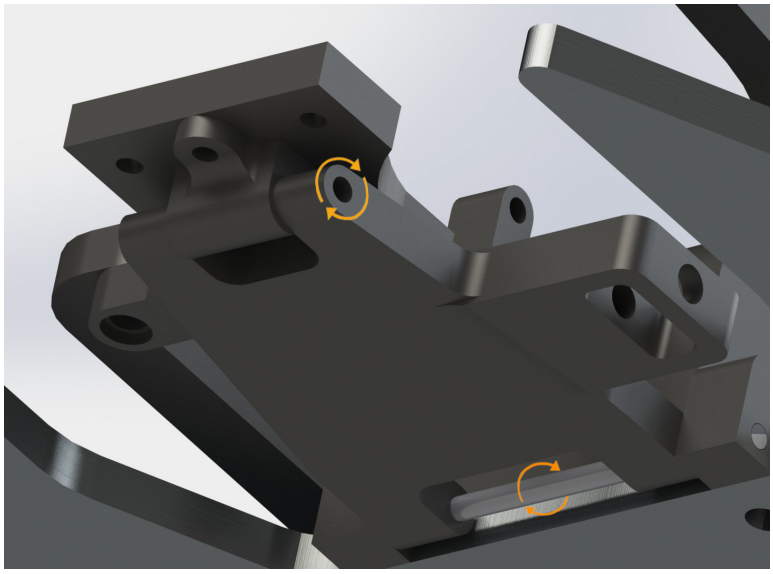

Figure 4.23: A-arm and hub parts attached with arrows indicating the movement executed by these parts.

In Figure 4.24 it is possible to observe a render of the suspension components of the rear part of the vehicle with a DC motor attached to the respective hub and a shock-absorber linked to the A-arm.

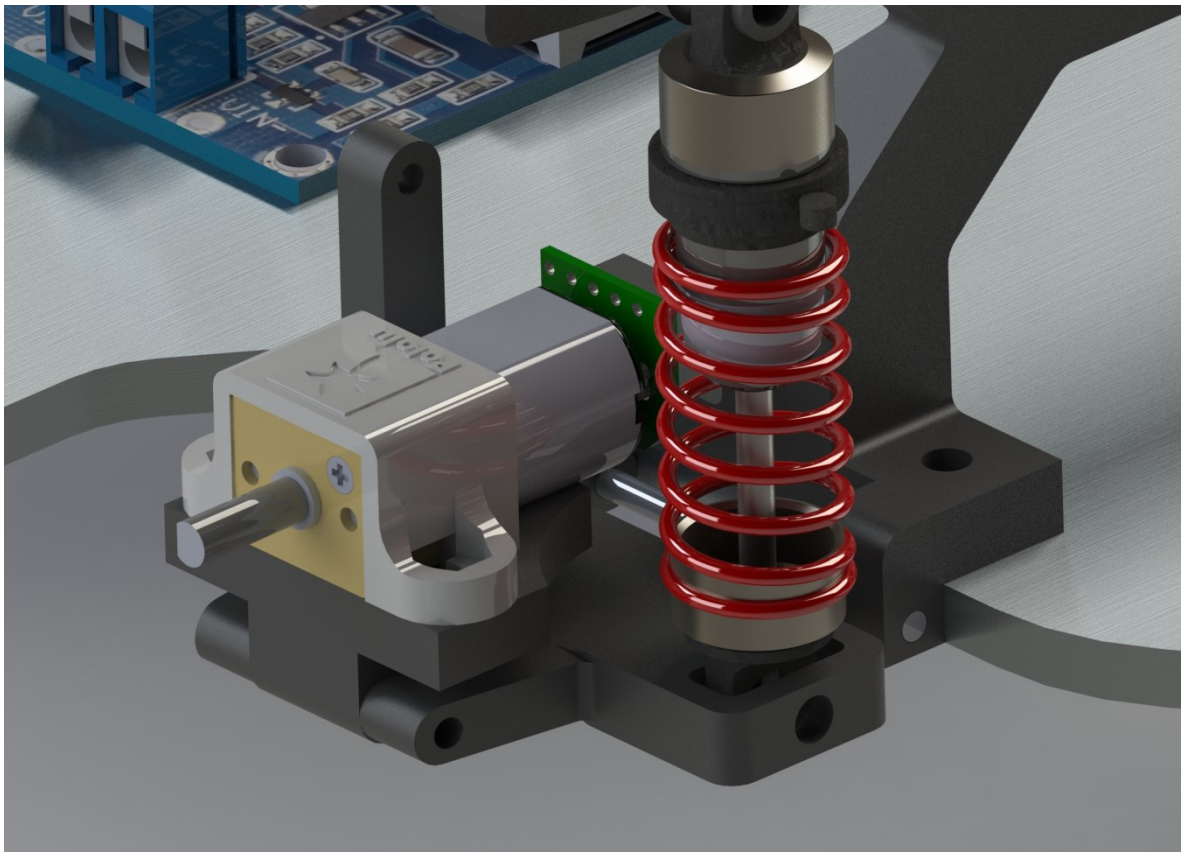

Figure 4.24: Rear suspension components with a DC motor and shock-absorber attached to.

4.4.3 Steering Design

Regarding the steering system, it was needed to find a way to attach the servo to the vehicle and a mechanism to make the wheels move according to the commands of the user. The front shock tower was designed with proper fittings in order to fasten the servo motor to the chassis structure (Figure 4.25).

The front hubs were designed in such a way that allowed the wheels to steer. This was possible since a screw located under the motors goes through both the suspension and steering hubs and the A-arms, acting as an axle and allowing the system to have the necessary DOF.

Since the design of all these parts were thought to be 3D printed, in order to make it simpler, it was tried to avoid ball joints linking the parts. This decision was hard to take since it would possibly compromise several degrees of freedom but it ended up not to be a problem.

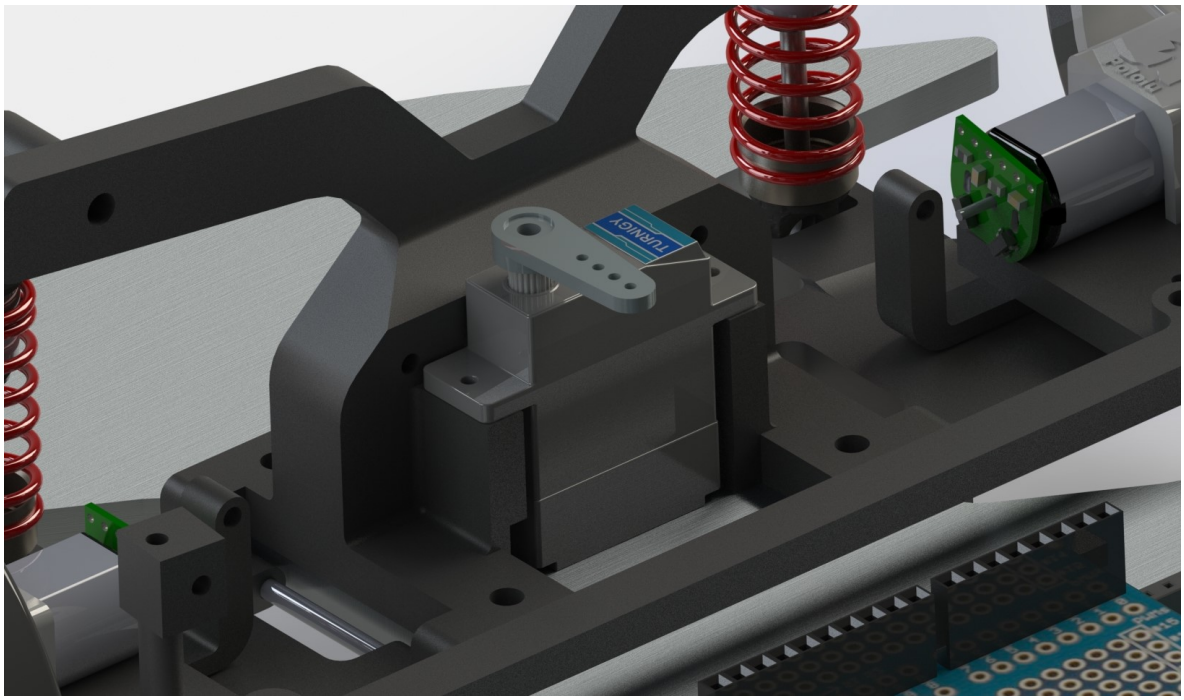

Figure 4.25: Servo fitting in the front shock tower.

The servo arm is linked by a wire to a part which serves almost exactly as a ball-joint and that makes the connection between the servo and the hub where the motors are attached to (Figure 4.26). A hole goes through this piece from down to top and a screw, again serving as a shaft, allows it to rotate within the Z axle. Another hole was drilled on this part's head, in a horizontal way, in which a wire perforates by, allowing this part to rotate over its axle when force is applied by the servo motor.

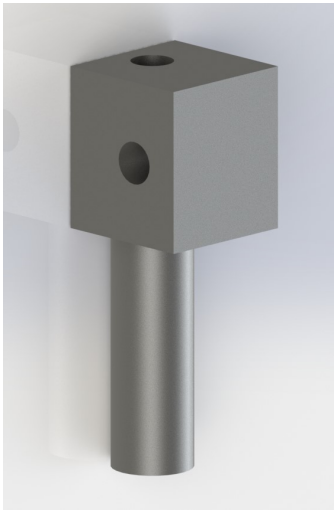

Figure 4.26: Ball-joint replacement part.

Between the left and the right hub, a steering linkage is attached (Figure 4.27) and is responsible for allowing both wheels to turn simultaneously. The interconnections between this linkage and the hubs were one of the points where ball joints could have been useful, since it was expected that with the opted approach, whenever one of the wheels tended to go up with the suspension, the force applied over the linkage would cause the other wheel to go up as a consequence. But again, after having everything assembled and as it will be seen ahead, it turned out not to have a major influence in the behaviour of the models.

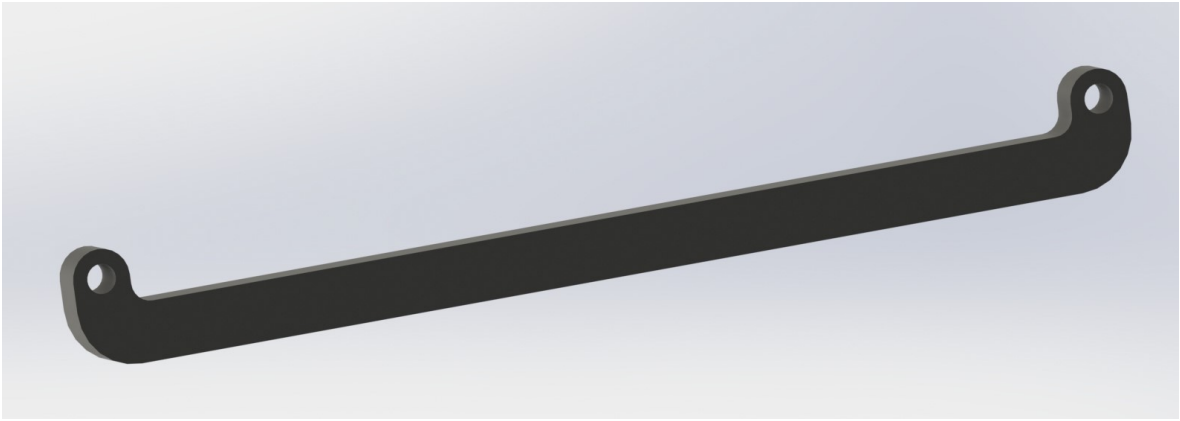

Figure 4.27: Steering linkage arm.

4.5 Prototype Build and Assembly

After modelling the vehicle, it was time to turn every piece into physical objects. In this section it will be described how everything was built. Choices taken regarding the used materials will also be discussed.

To start with the chassis, which should be seen as the support basis of the entire scale model, it was necessary to choose a material resistant enough that would be capable of supporting all the electronics, batteries and components responsible for the steering and suspension systems. Not only the resistance of the material but also weight, costs and ease on producing and obtaining the products were factors that were taken into account when choosing the right compromise between materials.

Due to the lack of knowledge in this field, a search for people in the area that would be capable of adding value to the right choices of both technique and material was needed. Several opinions were taken into consideration, from Mechanical Engineering professors of the *Universidade de Aveiro* up to technicians in the field of materials machining, and the major indecision was set between choosing polyester or aluminium. After analysing both pros and cons of each possibility, it was found that although being a lighter solution, polyester was also more expensive to shape, not as resistant and with a greater bending probability when compared with the aluminum. Thus, aluminium was the chosen material to produce the chassis of both models.

The next step was to contact companies and entities capable of producing the desired pieces, either with CNC machining or water jet cutting technologies. Six Portuguese and two Spanish companies were contacted and the project was explained in detail with the aim of possibly establishing a partnership and finding the best price for the job. The best deal was found with a Portuguese company based in Ovar, *Poly Lanema*® [76]. They offered a prompt response, the lowest prices and a fast delivery. Since the chassis is a planar object, meaning that it would not need complex machining, the job was performed with water jet cutting technology.

Poly Lanema® took two working days to deliver the proposed job, but after receiving both chassis, it was found that no finish treatment had been applied to these products, as visible in Figure 4.28.

Figure 4.28: Chassis part of the model vehicle before the polish treatment.

Unhappy with the result and in order to give a cleaner look to these pieces, it was decided to apply a polish treatment to the aluminium. This treatment consisted in using an emery machine with a polishing wheel basted with an abrasive soap, which, by causing friction over the aluminium, is capable of delivering the desired polished look. Figure 4.29 shows a picture of one of the chassis in the middle stage of the treatment and the final result, already with the Arduino Mega and voltage regulator attached to. This step was obviously not mandatory nor will add any functionality to the prototypes but was made as a matter of personal preference.

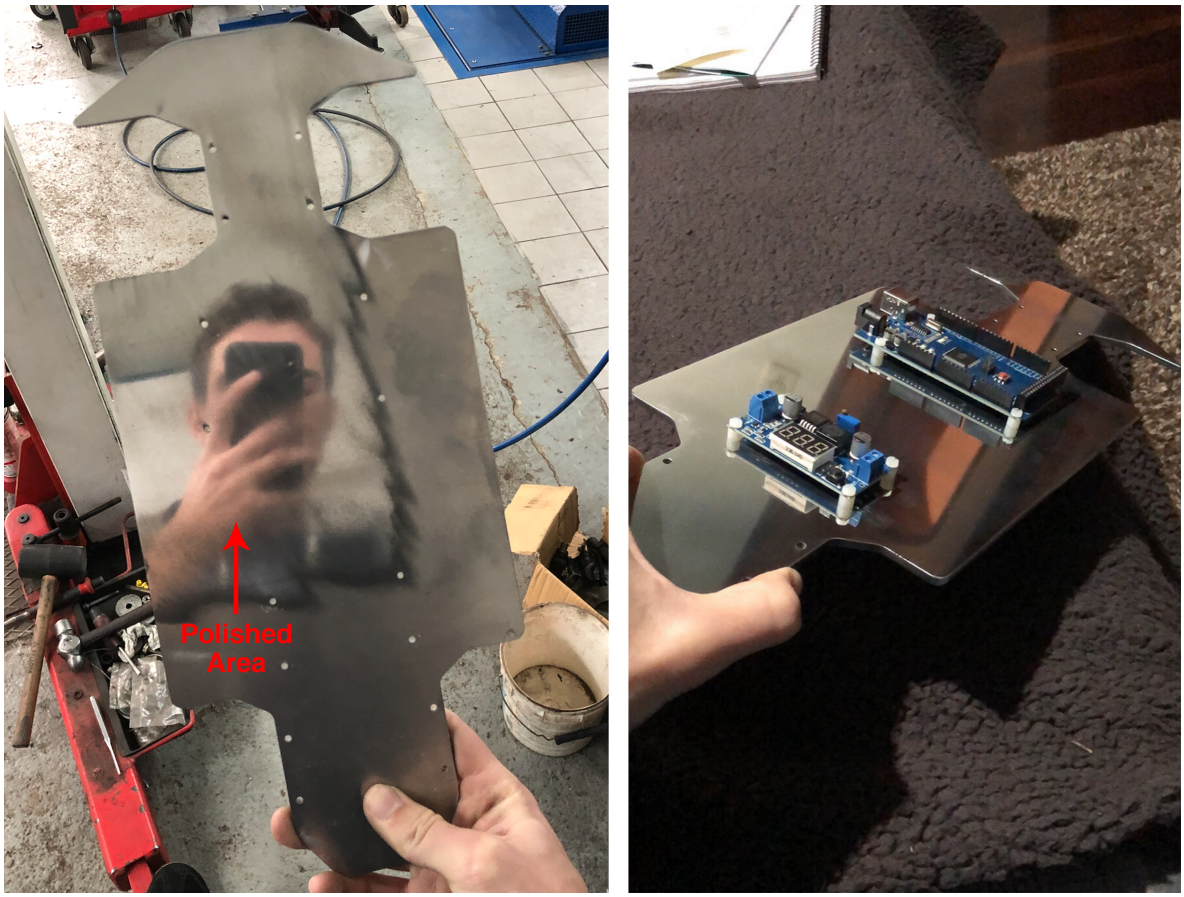

Figure 4.29: Chassis of the model vehicle in the middle of the polish treatment (on the left) and after (on the right).

The following step consisted in 3D printing all the parts that would be responsible for the steering and suspension mechanisms, as designed and introduced in Section 4.4. The printing process was performed by *MINILAB 3D* [77], a small company located in Covilhã, Portugal, specialised in high quality printing services at affordable costs. Once again the choice of the material was a matter of study with options diverging between PLA and ABS. Although being more expensive, standard ABS was the chosen material, offering good mechanical properties and with an impact strength superior to PLA.

Layer height was another characteristic taken into account in the printing process. By layer height it is meant the distance between layers of filament produced by 3D printers. Thinner layers will mean that less space is left between each filament, resulting in smother prints, while higher layers will result in stronger parts. With this in mind, a layer height of 100 μm was used in bigger parts, producing more detailed results and better curved walls, while 200 μm layers were used in thiner and moving mechanical parts, like the hubs and A-arms, were resistance was a critical factor. In Figure 4.30 it is possible to see all the designed parts already printed.

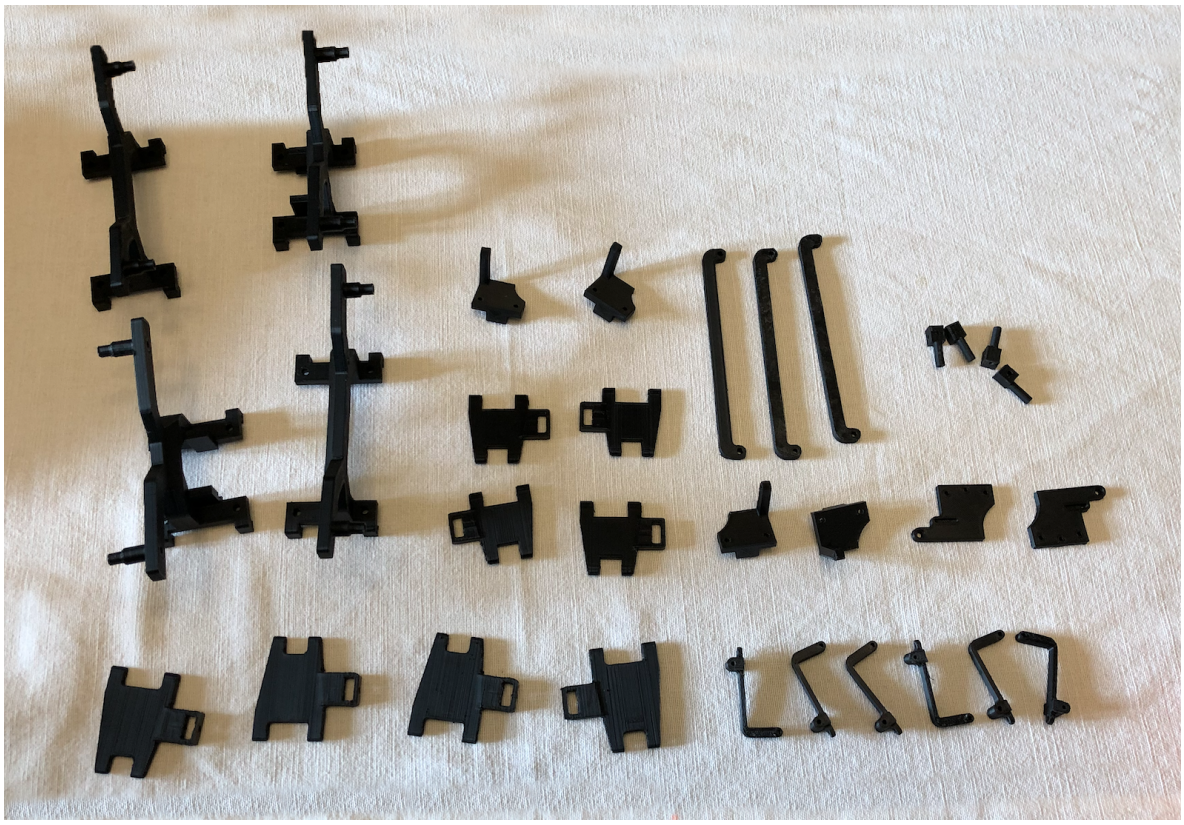

Figure 4.30: All the 3D printed parts used for building the two prototypes.

After having all the separate parts, it was time to start assembling everything together. The Arduino and voltage regulator were attached to the chassis with nylon standoff screws in order to avoid any short circuits with the aluminium of the chassis and allowing cables to be fitted underneath them. The first parts to be assembled to the chassis were the suspension towers, shocks, A-arms and hubs (Figures 4.31 and 4.32). The A-arms were fitted into the shock towers with 2 mm diameter wire pieces serving as axles. At this stage it was already possible to test the functionality of the suspensions by applying force over the arms and observing the reaction of the shock absorbers, validating the design of these componentes. The servo was also fitted into place and the *Adafruit Motorshield kit* mounted in the Arduino, since it was there where the servo cables would be connected.

Assembling the steering system was the following stage of the process. In addiction to the designed mechanism, a second setup where a different method to steer the wheels and connect the servo arm to both steering hubs was tested. In this approach, two wires were connected from the servo arm to a ball-joint replacement piece located in each steer hub. This method intended to substitute the steer linkage and was built in one of the prototypes to compare its performance against the original system. This was one of the main objectives and advantages of building two model cars, *i.e.*, being able to test different approaches and finding the solution which best fulfilled the initial requirements.

Figure 4.31: All the 3D printed parts used for building the two prototypes.

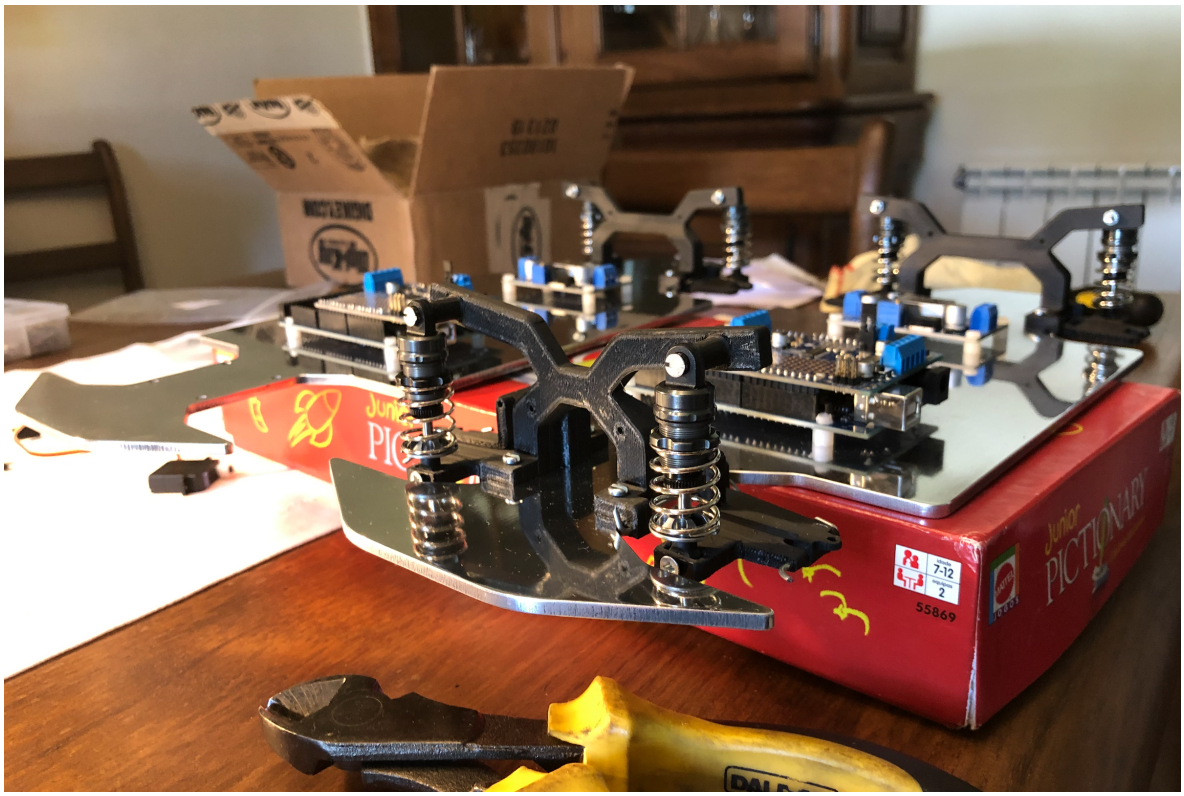

Figure 4.32: All the 3D printed parts used for building the two prototypes.

After testing both prototypes, it was clearly seen that the second setup was not as resistant as the original, since the wires tended to jump out of the servo arm after driving the car for a short period of time. The first approach also appeared to give more stability to the wheel hubs and, consequently, to the driving experience, offered by the rigidity of the steering linkage. Both configurations can be seen in Figure 4.33, with the temporary setup in the left prototype and the steer linkage original approach on the right. After this experiment, the linkage system was equally assembled in both models.

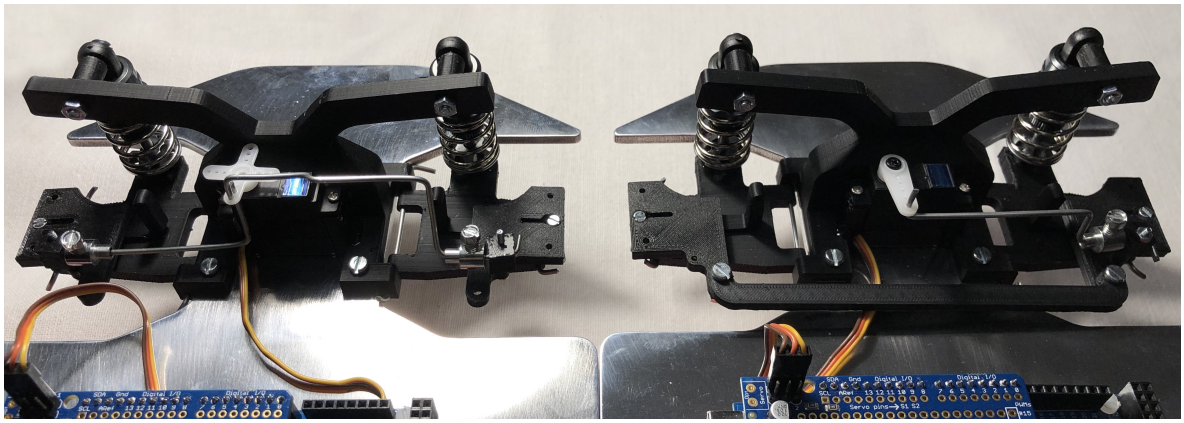

Figure 4.33: Steering setups tested: by wire (on the left) and with steer linkage (on the right).

Having both suspension and steering systems in place, it was time to start soldering the speed encoders to the DC motors and to perform its connections with the Arduino and shield. Then, the motors were attached to the wheels and fixed into the hubs with the corresponding *Pololu* mounting brackets. The remaining electronics was connected to the shield as in Figure 4.15 and the prototype assembly phase was set as complete. The final looks of the prototypes can be seen in Figures 4.34 to 4.37.

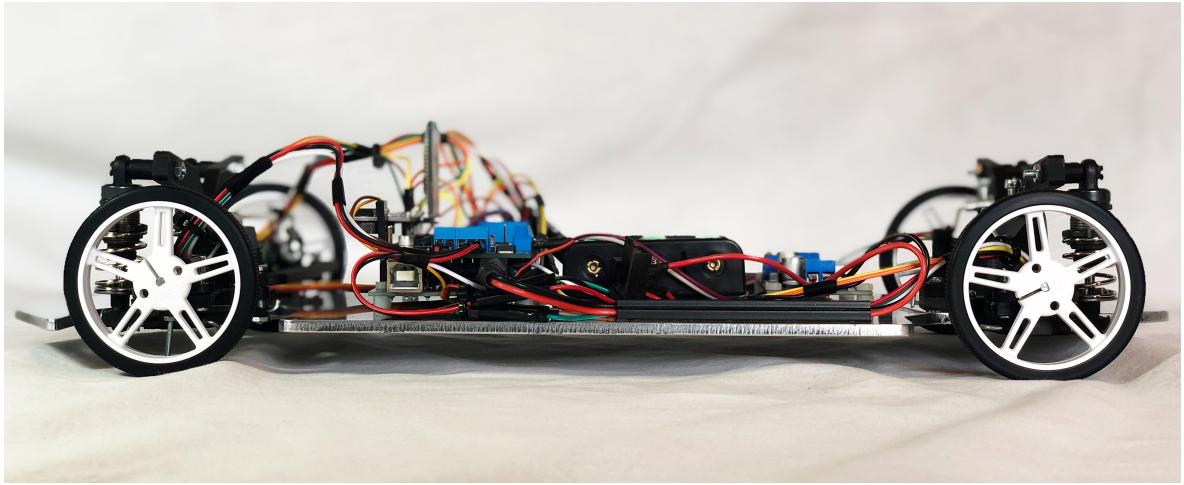

Figure 4.34: Perspective view of the final prototype.

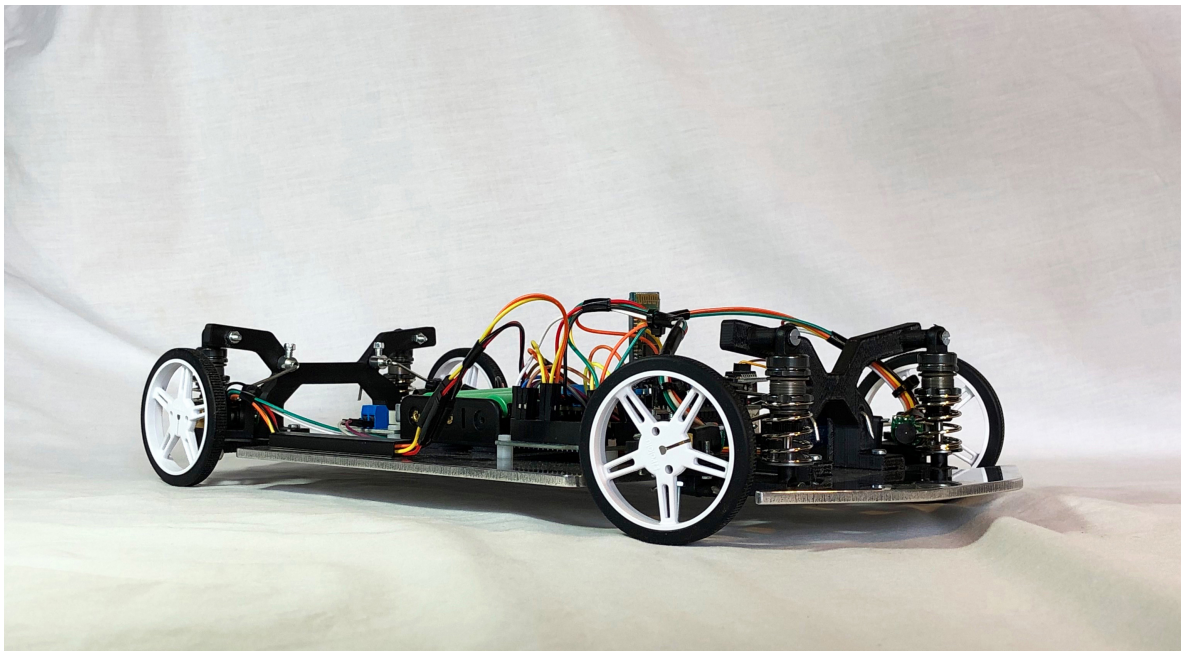

Figure 4.35: Perspective view of the final prototype.

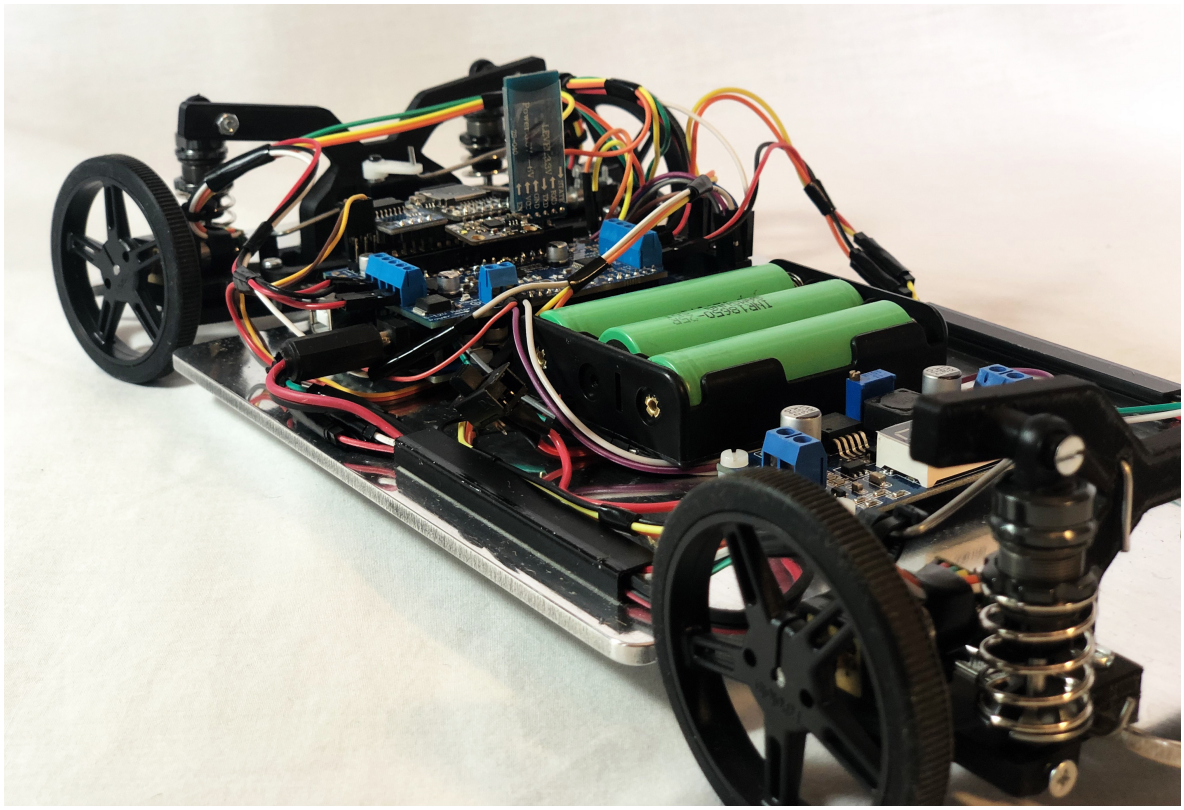

Figure 4.36: Perspective view of the final prototype.

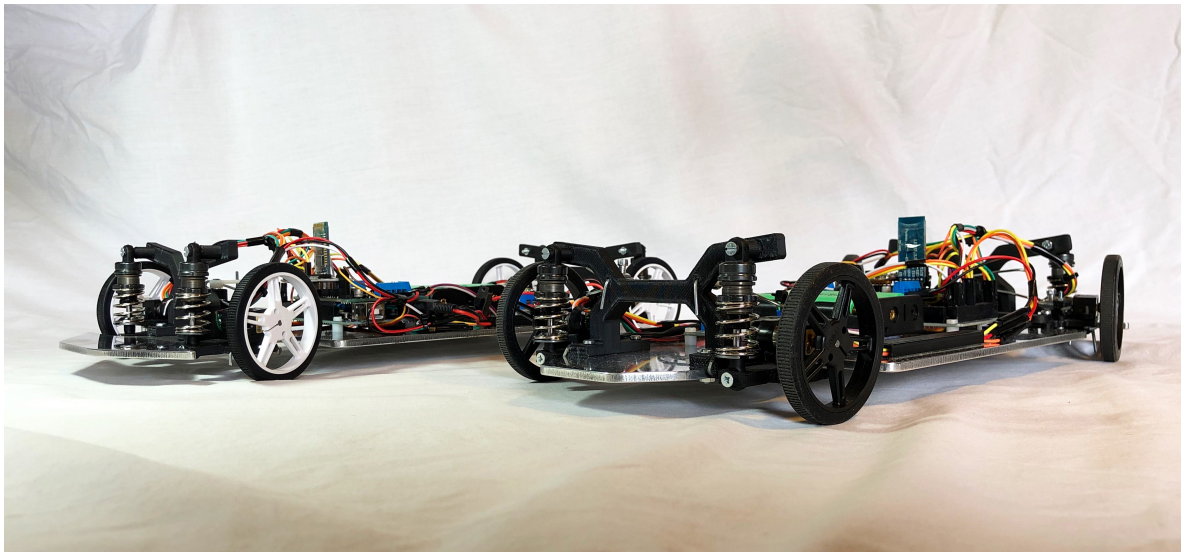

Figure 4.37: Perspective view of the two final prototypes.

4.6 Vehicle Control Implementation

In this section it will be discussed the approach used for the user of each prototype to control it, as well as to gather and analyse the provided information. Although until this part of the project almost everything was related to the construction of the models, it is relevant to notice that the main objective of this dissertation was to build a platform capable of processing relevant data for future implementation of driving aid systems. With this in mind, the application that controls the cars had to be explored as a powerful research tool and not only as a mere radio-control unit.

Since the communication technology being used is bluetooth, the followed approach was to use an Android application as the controller, allowing portability and a user-friendly interface. Fortunately, after exploring a few alternatives available, an application called *Bluetooth Electronics*, made by Keuwlsoft [78], was found. This application allows an easy control over electronic projects based on Android devices, having a large selection of controls available including buttons, switches, sliders, pads, lights, gauges, terminals, accelerometers and graphs. Even though the application has these pre-built controls, all the coding had to be customised in order to work properly with the Arduino program developed.

As it is seen in Figure 4.38, in order to control the car, a simple analog pad is responsible for sending X and Y coordinates which are later translated into throttle and steer responses in the Arduino code and consequently on the behaviour of the prototypes. The data from the pad is sent every 50 ms. A speedometer shows the instant speed in km/h, which is updated every 100 ms. As a matter of controls, the user is also able to act over an ON/OFF switch that is able to change the traction system of the car between AWD and RWD. This is again another advantage of having an independent four-motor setup, allowing the test of a wide range of different configurations with a single vehicle. Another switch gives the user the ability of starting or stopping the logging of the gathered information over the MicroSD card. This is a useful tool, allowing a controlled and timed start of every new experience. Also related

with the log, a button allows the possibility of deleting the data file found in the MicroSD.

A terminal monitor shows every command sent, useful for debugging. It is also possible to send custom commands to the Arduino via a *"Send commands"* window.

In terms of the information gathered by the sensorial modules included in the cars, there are presented two rolling graphs with raw data from both the accelerometer and gyroscope. The accelerometer data, which is in the range of $\pm 2\,g$ shows its X, Y and Z axis measurements as a function of the elapsed time in milliseconds. The same thing occurs with the gyroscope data, within a range of $\pm 250\,^{\circ}/s$, and also as a function of time.

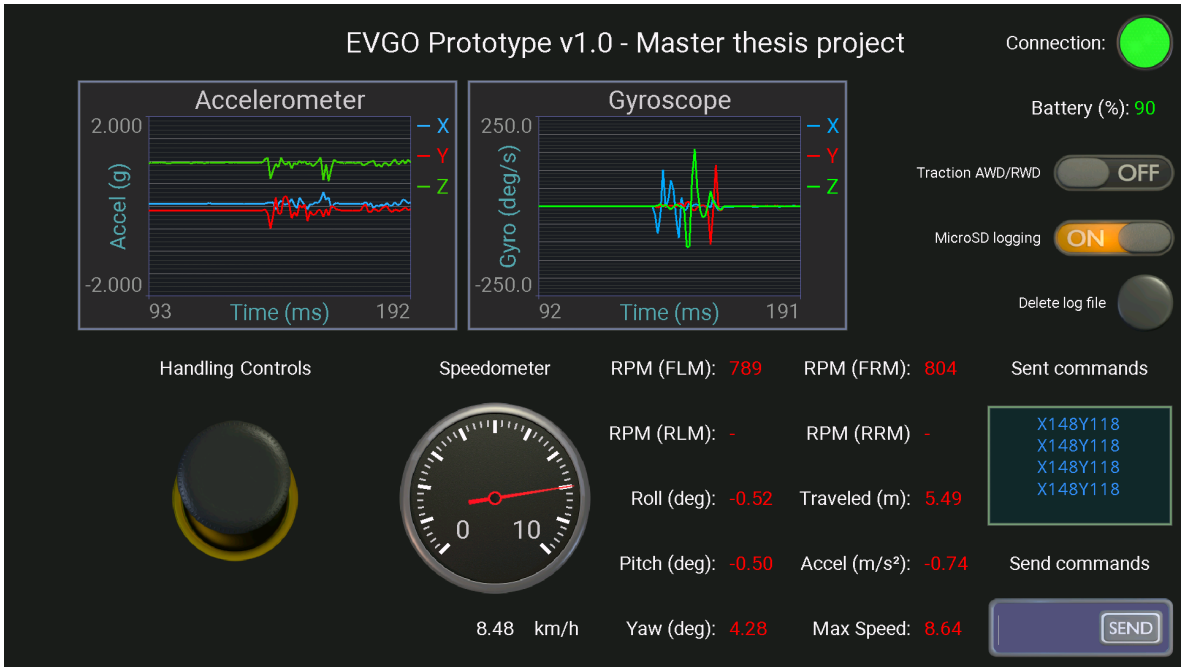

Figure 4.38: Screenshot of the application for controlling the prototypes and analysing the sensorial data.

A data analysis dedicated area provides informations, such as the individual RPM of every motor, the vehicle roll, pitch and yaw angles in degrees, the traveled distance in meters, the instant acceleration measured by the accelerometer's Y axle (which is positively faced to the front of the vehicle) in m/s^2 and the top speed achieved in the ongoing experience, in km/h. Besides this, a connection indicator light is placed on the top right side of the screen, indicating whether the connection is established (green) or if there is a problem (red). The vehicle's battery information is also provided bellow the connection indicator, as a percentage.

As it is possible to see in the Arduino code provided in Appendix B, a calibration of the MPU-6050 is executed every time the Arduino is reseted. So, in order to reset the values being provided to the app, it is important to lay the car in a flat surface and press the reset button located on the shield, whenever there is the need of gathering new sensorial information.

Chapter 5

Prototype Testing and Validation

At this stage of the document, the reader should already be familiarised with the motivations to develop this work, a brief theoretical knowledge over some of the information being analysed, that will be useful for later development of driving aid systems, as well as with the design and build process of the two proposed prototypes and their control mechanism. Therefore, this chapter is intended to serve as a final analysis of several testing scenarios that will help validating the usability of these models for future investigations.

Both vehicles were subjected to a wide range of test routines were several different manoeuvres were executed. All the sensorial information was gathered, later analysed and the results will be provided in the next few sections bellow. It is important to mention that the test runs were performed ensuring that the electric motors were being supplied with a maximum voltage value of 5 V.

In order to distinguish both cars in the following sections, let's refer to each one by the only visual difference between the two: the color of the wheels. The prototype with black wheels will be mentioned as *P1*, standing for *Prototype 1*, while the one with white wheels will be referred to as *P2*, or *Prototype 2*.

5.1 Gathered Data Analysis

The information being logged in the MicroSD card is saved in a *DATA.txt* file, as it is possible to see in Figure 5.1.

The information is updated and logged every 100 ms. The file starts by showing the data provided by the Real-Time Clock with the correct hour, minute and second when the experiment was executed. Next, it is possible to see the traction setup being used, whether it is AWD or RWD. Following, there is information on the throttle and steer values sent by the Android application. The throttle values are presented in a range of -100 to 100, where 0 corresponds to releasing the controls, positive values to a move forward command and negative values to a backwards moving order. Steer is also in the same range, with negative values corresponding to the intention of turning the wheels to the left, whereas positive ones to the right. Succeeding it is found information on the instant speed, measured in km/h, which is calculated by the mean rotation values of both front wheels. It is also found information

about acceleration, in m/s^2, measured by the accelerometer's Y axle, as explained in Section 4.6. It is specified the traveled distance, in meters, since the car was reseted. Next, it is possible to see the RPM values provided by both front wheel encoders, the vehicle's roll, pitch and yaw angles, in degrees, and both gyro and accelerometer raw data of every axle (X, Y and Z). Finally, there is also information regarding the battery life percentage.

DATA.TXT

EVGO Prototype v1.0 Black Wheels – Master thesis project
Date: 2019/6/5

Time	Traction	Throttle	Steer	Speed (km/h)	Accel (m/s^2)	Distance (m)	RPM (FLM)	RPM (FRM)	Roll (deg)	Pitch (deg)	Yaw (deg)	Gyro (deg/s)	Accel (g)	Battery (%)
17:31:47	AWD	40	12	0.00	-0.80	0.00	0	0	-0.29	-0.48	0.08	X = 0.08 Y = 0.09 Z = 0.18	X = 0.0 Y = -0.08 Z = 0.98	93
17:31:48	AWD	100	6	0.31	-0.82	0.01	28	28	-0.62	-0.28	0.34	X = -0.00 Y = 2.61 Z = 2.61	X = 0.07 Y = -0.23 Z = 0.98	93
17:31:48	AWD	100	-2	1.08	-2.22	0.04	100	100	-0.95	-0.57	0.53	X = 1.48 Y = -6.14 Z = 1.89	X = -0.05 Y = -0.39 Z = 0.84	93
17:31:48	AWD	100	-2	2.11	-3.84	0.10	195	200	-2.23	-1.25	1.15	X = -12.19 Y = -3.91 Z = 6.24	X = 0.07 Y = -0.44 Z = 0.84	93
17:31:48	AWD	100	-2	3.11	-4.28	0.18	286	290	-1.51	-1.05	1.93	X = 3.89 Y = 0.67 Z = 7.75	X = 0.01 Y = -0.28 Z = 0.82	93
17:31:48	AWD	100	0	4.04	-2.76	0.29	371	376	-2.57	-1.72	2.89	X = -4.78 Y = -1.76 Z = 9.58	X = 0.20 Y = -0.47 Z = 0.67	93
17:31:48	AWD	100	0	4.58	-4.62	0.42	419	429	-2.40	-1.56	3.81	X = -4.36 Y = -4.43 Z = 9.28	X = -0.02 Y = -0.36 Z = 1.03	93
17:31:48	AWD	100	-16	5.30	-3.54	0.57	486	495	-3.35	-2.24	5.07	X = -7.09 Y = -4.65 Z = 12.55	X = 0.17 Y = -0.28 Z = 0.62	93
17:31:48	AWD	100	-20	5.92	-2.78	0.73	543	552	-1.20	-1.50	6.24	X = 8.30 Y = 4.36 Z = 11.71	X = 0.06 Y = 0.10 Z = 0.57	93
17:31:48	AWD	100	-20	6.33	0.97	0.91	581	591	-3.40	-1.69	6.75	X = -8.02 Y = -2.73 Z = 5.06	X = 0.08 Y = -0.45 Z = 0.93	93
17:31:48	AWD	100	-20	6.33	-4.44	1.09	586	586	-2.03	-0.91	6.92	X = -1.28 Y = 3.29 Z = 1.77	X = -0.09 Y = 0.14 Z = 0.67	93
17:31:49	AWD	100	-20	6.92	1.34	1.28	643	643	-2.36	-0.95	7.02	X = 6.40 Y = 2.90 Z = 0.98	X = 0.02 Y = -0.23 Z = 1.04	92
17:31:49	AWD	100	-20	7.21	-2.23	1.48	672	667	-0.93	-1.23	6.91	X = 2.30 Y = 1.64 Z = -1.10	X = 0.19 Y = 0.29 Z = 0.88	92
17:31:49	AWD	100	-18	7.08	2.84	1.67	657	657	-2.77	-0.58	6.58	X = -2.50 Y = 2.01 Z = -3.31	X = 0.01 Y = -0.40 Z = 0.97	92
17:31:49	AWD	100	-14	7.62	-3.88	1.89	714	705	-2.98	-1.19	6.18	X = -5.56 Y = -4.08 Z = -4.01	X = 0.11 Y = -0.26 Z = 1.04	92
17:31:49	AWD	100	-12	7.80	-2.55	2.10	724	719	-1.45	-0.91	5.73	X = 14.70 Y = 5.36 Z = -4.46	X = 0.11 Y = -0.11 Z = 0.54	92
17:31:49	AWD	100	-12	7.93	-1.06	2.32	738	734	-1.87	-1.37	5.33	X = -3.07 Y = -9.14 Z = -4.03	X = 0.03 Y = -0.35 Z = 1.37	92
17:31:49	AWD	100	-6	7.85	-3.43	2.54	729	724	-0.74	-0.57	5.24	X = -3.86 Y = 8.80 Z = -0.91	X = 0.03 Y = 0.27 Z = 0.61	92
17:31:49	AWD	100	-4	8.34	2.60	2.77	776	767	-0.83	-0.38	5.00	X = 6.25 Y = 5.77 Z = -2.41	X = 0.13 Y = 0.07 Z = 0.65	92
17:31:49	AWD	100	-4	8.31	0.69	3.00	776	767	-1.28	-1.41	4.66	X = -2.14 Y = -14.81 Z = -3.35	X = 0.02 Y = -0.00 Z = 0.78	92
17:31:49	AWD	100	-4	8.19	-0.03	3.23	762	753	-2.05	-1.89	4.37	X = -5.82 Y = -4.23 Z = -2.89	X = 0.05 Y = -0.08 Z = 0.89	92
17:31:50	AWD	100	-4	8.57	-0.83	3.47	800	791	-1.59	-1.72	4.43	X = 2.84 Y = 5.16 Z = 0.60	X = 0.17 Y = -0.01 Z = 0.84	92
17:31:50	AWD	100	-4	8.49	-0.10	3.71	791	791	-2.09	-0.23	4.48	X = -3.07 Y = 11.06 Z = 0.44	X = 0.01 Y = -0.09 Z = 0.85	92
17:31:50	AWD	100	-4	8.67	-0.89	3.95	805	805	-1.76	-0.75	4.25	X = 3.97 Y = -4.64 Z = -2.27	X = 0.04 Y = -0.13 Z = 0.99	92
17:31:50	AWD	100	-4	8.37	-1.25	4.18	781	772	-1.62	-1.63	3.87	X = -2.39 Y = -6.03 Z = -3.78	X = 0.14 Y = 0.03 Z = 0.81	92
17:31:50	AWD	100	-6	8.55	0.20	4.42	796	791	-1.84	-1.01	3.84	X = 0.70 Y = 2.69 Z = -0.30	X = 0.02 Y = -0.09 Z = 0.99	92
17:31:50	AWD	100	-6	8.60	-0.89	4.65	796	796	-1.85	-0.68	3.66	X = -0.99 Y = 2.85 Z = -1.75	X = -0.01 Y = -0.06 Z = 1.04	92
17:31:50	AWD	100	-8	8.26	-0.56	4.88	767	762	-1.92	-1.00	3.59	X = 1.16 Y = 3.07 Z = -0.71	X = 0.25 Y = -0.13 Z = 0.91	92
17:31:50	AWD	100	-8	8.26	-1.25	5.11	772	762	-1.64	-1.45	3.45	X = 2.41 Y = -8.10 Z = -1.42	X = 0.12 Y = -0.12 Z = 1.03	92
17:31:50	AWD	100	-8	8.21	-1.18	5.34	767	757	-0.91	-0.88	3.33	X = 9.30 Y = -0.17 Z = -1.17	X = -0.13 Y = -0.17 Z = 0.90	92
17:31:50	AWD	100	-8	8.31	-1.70	5.57	772	767	-1.09	-0.43	2.98	X = -3.92 Y = 7.80 Z = -3.31	X = 0.00 Y = -0.07 Z = 0.72	92
17:31:51	AWD	0	0	7.88	-0.69	5.79	734	724	-1.72	-0.59	2.92	X = -4.80 Y = -2.01 Z = -0.64	X = -0.01 Y = -0.22 Z = 1.30	92
17:31:51	AWD	12	16	8.21	-2.15	6.02	762	762	-1.47	-1.23	3.04	X = 2.59 Y = -1.68 Z = 1.09	X = 0.17 Y = -0.15 Z = 0.86	92
17:31:51	AWD	2	20	6.59	-1.50	6.20	595	624	-0.90	-1.09	4.17	X = 1.01 Y = -4.36 Z = 11.31	X = -0.06 Y = 0.04 Z = 1.15	92
17:31:51	AWD	-16	26	5.15	0.35	6.34	462	495	0.23	-1.37	6.23	X = -0.69 Y = 0.32 Z = 20.28	X = 0.07 Y = 0.47 Z = 0.75	92
17:31:51	AWD	-26	28	3.35	4.57	6.44	276	343	-1.18	-1.40	8.12	X = 1.46 Y = -3.48 Z = 19.07	X = -0.06 Y = -0.15 Z = 1.25	92
17:31:51	AWD	-30	28	2.27	-1.50	6.50	181	238	0.04	-1.69	9.38	X = -1.04 Y = 1.43 Z = 12.31	X = 0.14 Y = 0.43 Z = 0.86	92
17:31:51	AWD	0	0	1.03	4.20	6.53	90	100	-0.62	-1.51	9.63	X = 0.56 Y = -2.18 Z = 2.51	X = -0.03 Y = 0.16 Z = 1.09	92
17:31:51	AWD	0	0	0.21	1.57	6.54	19	19	-0.96	-1.85	9.63	X = 1.20 Y = -1.94 Z = 0.05	X = 0.04 Y = -0.05 Z = 1.03	92
17:31:51	AWD	0	0	0.00	-0.53	6.54	0	0	-1.13	-1.93	9.66	X = -0.41 Y = -0.29 Z = 0.30	X = 0.07 Y = -0.11 Z = 1.01	92
17:31:51	AWD	0	0	0.00	-1.11	6.54	0	0	-1.09	-1.92	9.65	X = 0.06 Y = -0.10 Z = -0.08	X = 0.05 Y = -0.10 Z = 0.97	92
17:31:52	AWD	89	0	8.19	-0.03	3.23	762	753	-2.05	-1.89	4.37	X = -5.82 Y = -4.23 Z = -2.89	X = 0.05 Y = -0.08 Z = 0.89	92
17:31:53	AWD	100	0	8.57	-0.83	3.47	800	791	-1.59	-1.72	4.43	X = 2.84 Y = 5.16 Z = 0.60	X = 0.17 Y = -0.01 Z = 0.84	92
17:31:54	AWD	100	0	8.49	-0.10	3.71	791	791	-2.09	-0.23	4.48	X = -3.07 Y = 11.06 Z = 0.44	X = 0.01 Y = -0.09 Z = 0.85	92
17:31:55	AWD	100	0	8.67	-0.89	3.95	805	805	-1.76	-0.75	4.25	X = 3.97 Y = -4.64 Z = -2.27	X = 0.04 Y = -0.13 Z = 0.99	92
17:31:56	AWD	100	0	8.37	-1.25	4.18	781	772	-1.62	-1.63	3.87	X = -2.39 Y = -6.03 Z = -3.78	X = 0.14 Y = 0.03 Z = 0.81	92
17:31:57	AWD	100	0	8.55	0.29	4.42	796	791	-1.84	-1.01	3.84	X = 0.70 Y = 2.69 Z = -0.30	X = 0.02 Y = -0.09 Z = 0.99	92
17:31:58	AWD	56	0	8.60	-0.89	4.65	796	796	-1.85	-0.68	3.66	X = -0.99 Y = 2.85 Z = -1.75	X = -0.01 Y = -0.06 Z = 1.04	92
17:31:59	AWD	32	0	8.26	-0.56	4.88	767	762	-1.92	-1.00	3.59	X = 1.16 Y = 3.07 Z = -0.71	X = 0.25 Y = -0.13 Z = 0.91	92
17:32:00	AWD	10	0	8.26	-1.25	5.11	772	762	-1.64	-1.45	3.45	X = 2.41 Y = -8.10 Z = -1.42	X = 0.12 Y = -0.12 Z = 1.03	92
17:31:01	AWD	0	0	1.03	4.20	6.53	90	100	-0.62	-1.51	9.63	X = 0.56 Y = -2.18 Z = 2.51	X = -0.03 Y = 0.16 Z = 1.09	92
17:31:02	AWD	0	0	0.21	1.57	6.54	19	19	-0.96	-1.85	9.63	X = 1.20 Y = -1.94 Z = 0.05	X = 0.04 Y = -0.05 Z = 1.03	92
17:31:03	AWD	0	0	0.00	-0.53	6.54	0	0	-1.13	-1.93	9.66	X = -0.41 Y = -0.29 Z = 0.30	X = 0.07 Y = -0.11 Z = 1.01	92
17:31:04	AWD	0	0	0.00	-1.11	6.54	0	0	-1.09	-1.92	9.65	X = 0.06 Y = -0.10 Z = -0.08	X = 0.05 Y = -0.10 Z = 0.97	92

Figure 5.1: DATA.txt file with the logged information of an example manoeuvre.

All this data is really useful for analysing the behaviour of the car, and is easily treated in a processing environment like Matlab®. The following sections will show the executed testing routines where data such as in the example of Figure 5.1 will be interpreted in detail.

5.2 Maximum Speed

The first test routines were performed with the aim of observing performance differences over the maximum speeds achieved with AWD versus RWD traction. Each experiment was repeated three times, under the same testing conditions and on both prototypes. The results were obtained by positioning the cars at a starting mark, applying the maximum throttle signal and letting them travel for around 15 meters, in a straight line and on a plane surface.

Figure 5.2 shows the obtained results based on the speeds provided by the encoders while using AWD traction. It is also presented a curve which is achieved by applying a five degree polynomial fit to the mean values of the three experiments, which is intended to represent an approximate behaviour of the speed evolution.

The peak speed value obtained with *P1* prototype was 11.24 km/h, against 11.10 km/h achieved by *P2*. These results are pretty optimistic and show that, using AWD, the motors are able to run at around 1000 RPM, a value that would theoretically only be achieved with a 6 V supply, as shown in the performance graph of Figure 4.3, in Section 4.2.1.

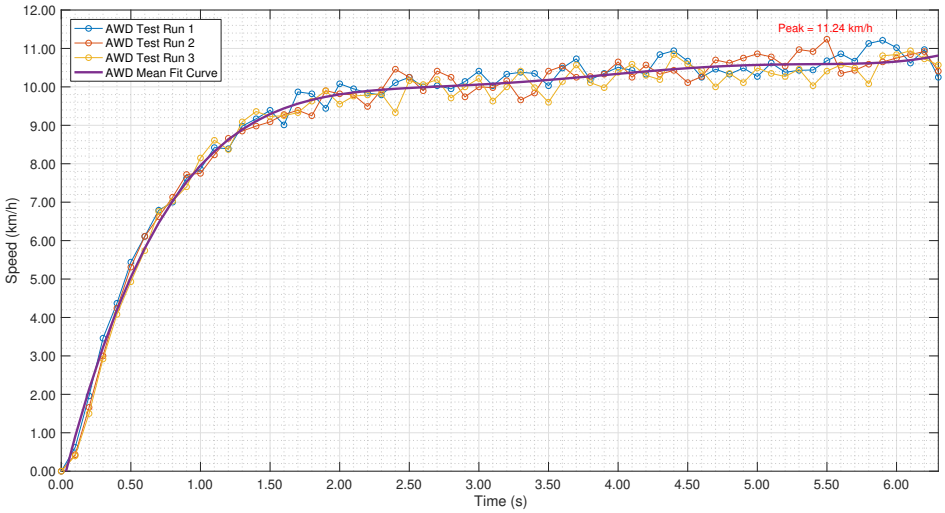

(a)

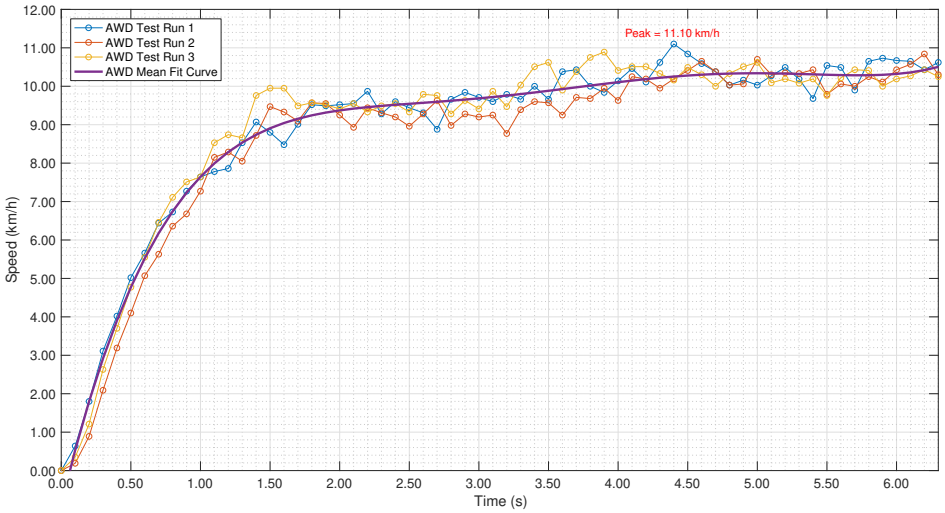

(b)

Figure 5.2: All-Wheel Drive (AWD) maximum speed test runs data. Graph (a) corresponds to the *P1* prototype and (b) to the *P2*.

In Figure 5.3 it is now presented the same test as above but with the vehicles being propelled by the rear motors only, *i.e.*, with RWD traction. This time, the *P1* vehicle achieved 8.61 km/h, while the *P2* went up to a maximum of 8.93 km/h. Values that are 23.40 % and 19.55 % respectively lower than the results obtained with AWD.

It was already expected that these values would be lower than the ones achieved with AWD, since theoretically the cars are outputting half of the power they would produce in the first scenario. It is also important to mention that although the front motors are not being used, they are not completely free spinning, since their stator magnets and armature are still producing a friction force that is opposite to the direction of the movement of the wheels.

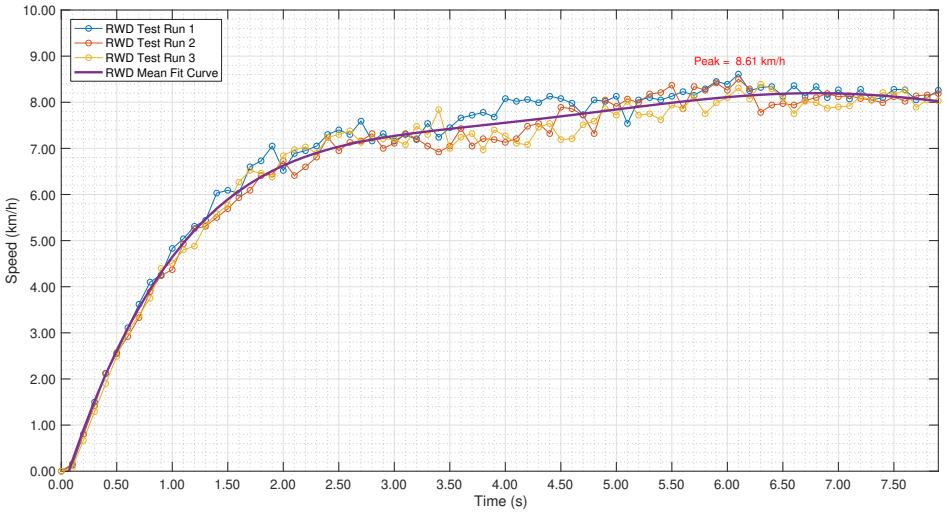

(a)

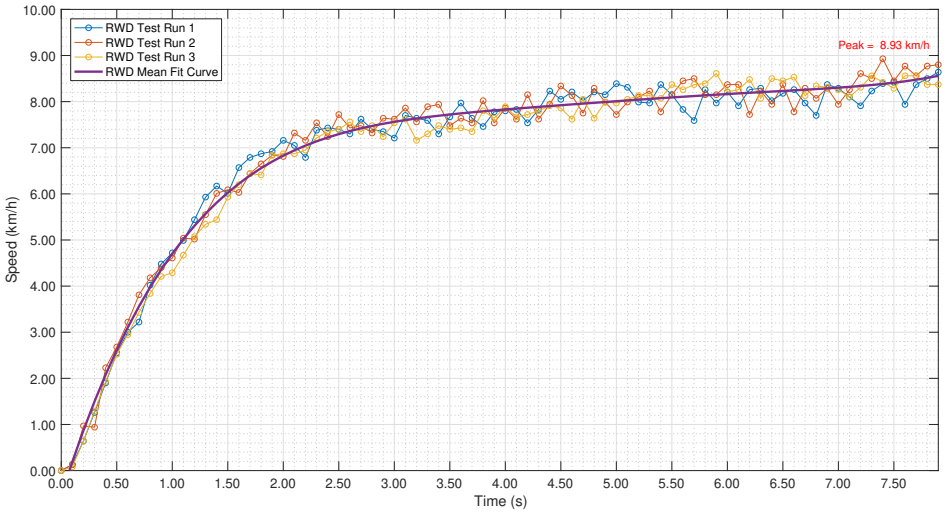

(b)

Figure 5.3: Rear-Wheel Drive (RWD) maximum speed test runs data. Graph (a) corresponds to the *P1* prototype and (b) to the *P2*.

It is also possible to verify light oscillations in the final region of each polynomial fit curve, contrary to the constant lines that would be expected in optimum testing conditions. These may be a result of small irregularities on the pavement, which are consequently translated in speed variations. However, the obtained results are able to validate the capability of processing the encoder readings, as well as the expected behaviour of the models with respect to their maximum speeds.

5.3 Maximum Acceleration

The maximum acceleration experiment consisted in processing the experimental results obtained in Section 5.2 and calculating the average acceleration curves, which are intended to represent the rate at which velocity changes.

Figure 5.4 represents the acceleration curves of both prototypes using AWD and RWD.

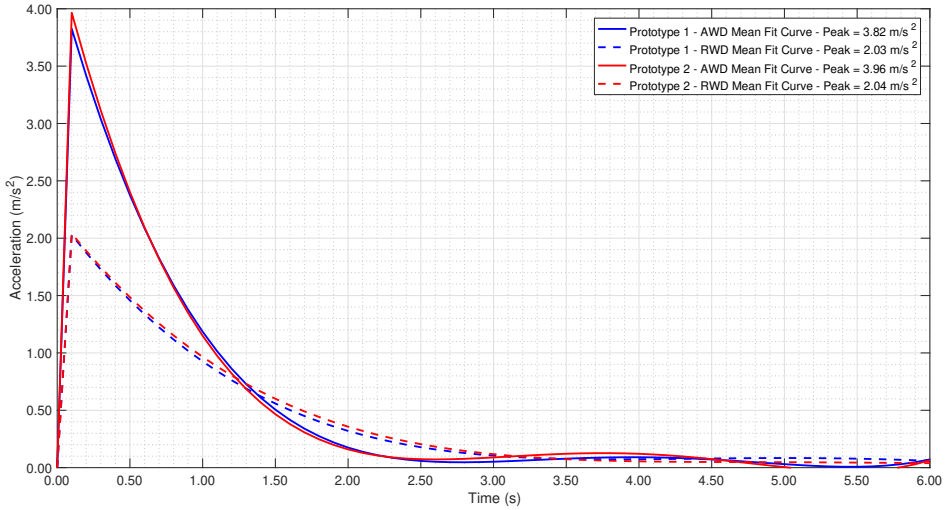

Figure 5.4: Maximum acceleration test runs with AWD versus RWD traction, over both prototypes.

It is noticeable that using four motors, the acceleration peaks are about twice the values achieved when using only two. There is not a huge variation between both cars. *P1* achieved 3.82 m/s^2 and 2.03 m/s^2, while *P2* obtained 3.96 m/s^2 and 2.04 m/s^2, for AWD and RWD respectively.

Using AWD it is seen that the acceleration curves tend to decay at a higher rate when compared to RWD. This is justified by the fact that in the first situation, the maximum speed is obtained sooner. The small oscillations at the end of the curves are also justifiable by the irregularities on the pavement as experienced in the maximum speed runs.

The accelerometer module is also able of gathering instant acceleration measurements. At the instants of the peaks seen in Figure 5.4, values of 5.00 $\pm$ 1.00 m/s^2 for AWD and 3.00 $\pm$ 1.00 m/s^2 for RWD. However, the results obtained tend to present severe oscillations between consecutive measurements, probably caused by small vibrations which are responsible for introducing noise over the results.

The highest values are obtained at the first measuring instants and support the fact that the electric motors are able to deliver high torque values to the wheels from standing still situations. As said in [79], and as an example, a 2008 Aston Martin DBS is capable of achieving accelerations of 6.5 m/s^2, which considering scale factors, reinforce the substantial performance capabilities of an electric vehicle with these configurations.

5.4 Braking Performance

In order to evaluate the braking capabilities of the models, several tests were conducted where the vehicles had to perform emergency braking while travelling for 3 consecutive seconds, at a controlled speed between 7.00 and 8.00 km/h. The tests were set as complete as soon as the vehicles were immobilised, and were executed with the aim of discovering differences between braking with four motors against braking with the two rear motors only.

As it is possible to see in Figure 5.5, the final results were obtained by the mean values of three consecutive runs on each car and performed under the same testing conditions.

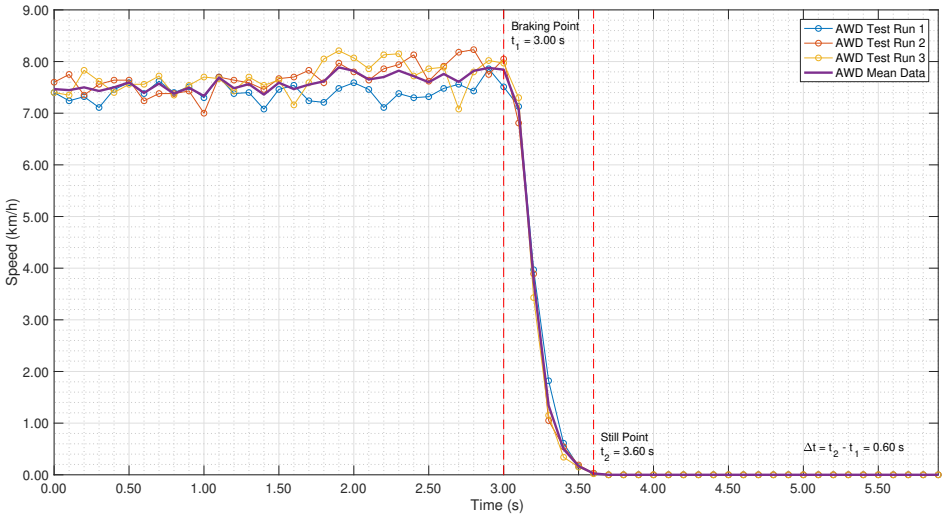

(a)

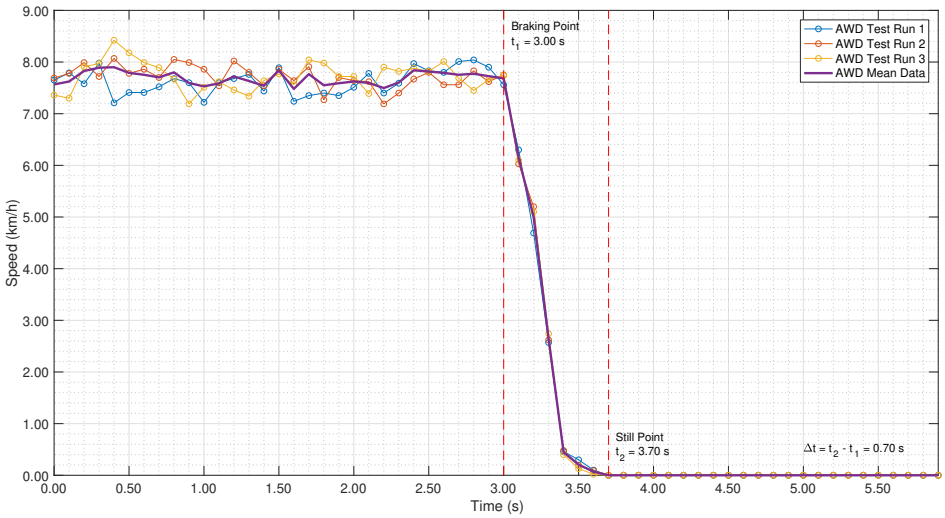

(b)

Figure 5.5: All-Wheel Drive (AWD) braking performance test runs data. Graph (a) corresponds to the *P1* prototype and (b) to the *P2*.

In the AWD test, *P1* only took 0.60 seconds to get immobilised, while the *P2* achieved an average stopping time of 0.70 seconds. This 0.10 second difference is not considerable and is believed to be related with unsystematic errors in the experiments.

Figure 5.6 represents the same test as above but this time considering that the only motors which were braking were the rear ones. And results show that *P1* took on average 1.10 seconds to stop, while *P2* did it in 1.00 second.

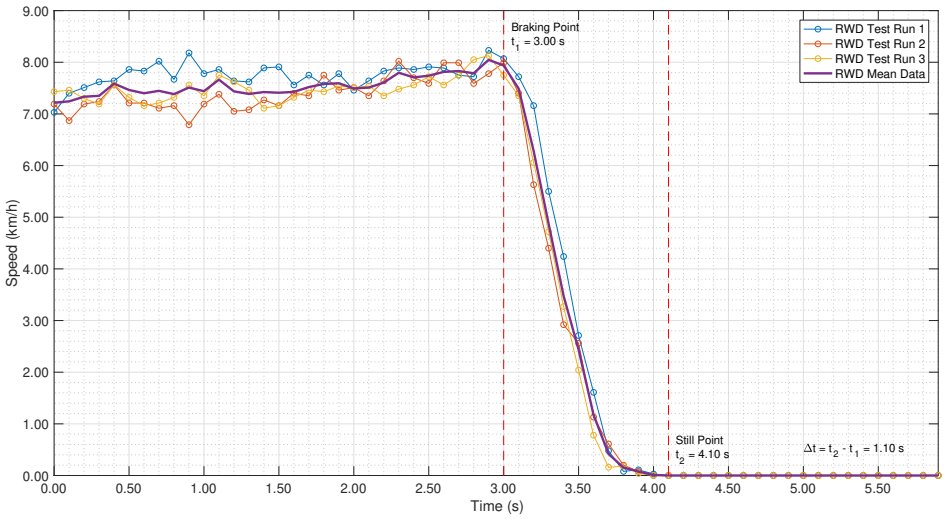

(a)

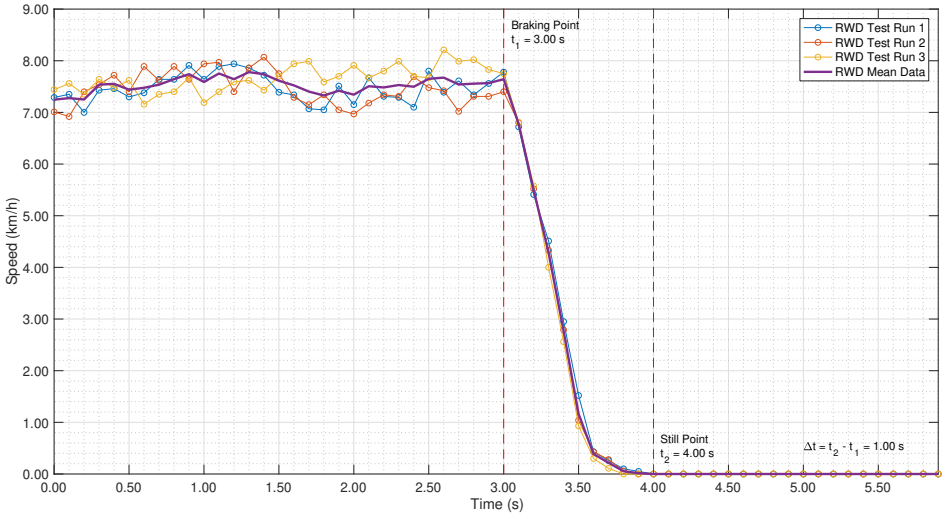

(b)

Figure 5.6: Rear-Wheel Drive (RWD) braking performance test runs data. Graph (a) corresponds to the *P1* prototype and (b) to the *P2*.

RWD took around 83 % more time immobilising the cars than AWD. The braking behaviours of the models meet what was initially expected. It is also important to make reference to the fact that when braking with the rear motors, the friction force produced by the front ones, contrary to what was mentioned in Section 5.2, is now helping the cars to stop.

5.4.1 Slip Detection

There are several ways to detect unwanted wheel slip. This subsection is intended to validate the idea that it is possible to observe uncommon behaviours which are typically an indication of slipping. This is one important factor to help triggering traction and braking aid systems.

For this experiment, the four wheels of *P1* were covered with adhesive tape in order to simulate a slippery surface. The prototype was driven up to the same speed range as in the braking performance tests above and, with traction set to AWD, an emergency brake was done at the 3 seconds mark. The tests were also repeated for three times and the shown results are based on the mean values of these three runs.

Figure 5.7 shows a comparison between the obtained results from Figure 5.5a (representing the *Traction Run*) and the run where the wheels had not enough traction to stop the vehicle in safety.

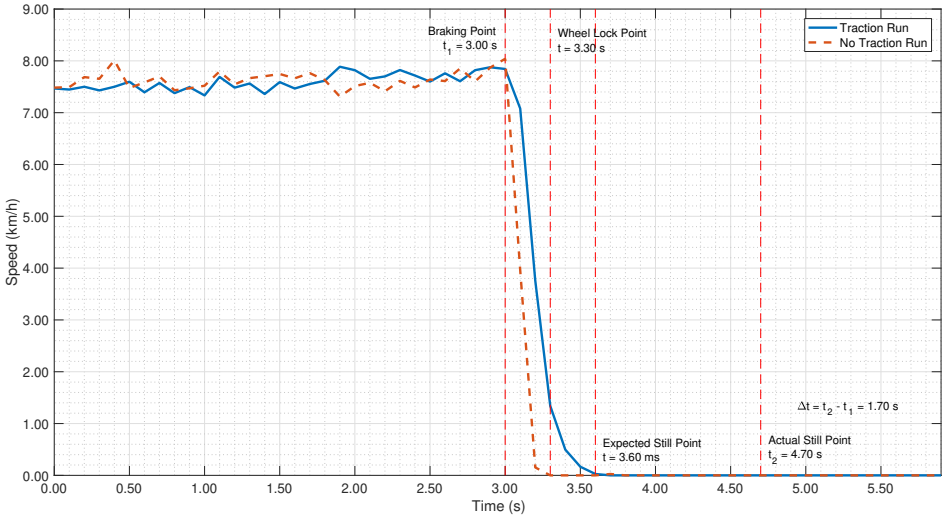

Figure 5.7: Braking slip detection test run.

When the brake command is applied, the wheels lock almost immediately. And since the speed of the vehicles is being calculated in both front wheels, the speed graph suggests that the vehicle has already stopped when in fact, it is not. The car keeps sliding and both braking distance and time are increased.

Analysing the results in Figure 5.7, it is possible to see that the wheels took around 0.30 seconds to lock. At second 3.60, *i.e.*, 0.60 seconds later, it was expected that, in good traction conditions, the vehicle would have stopped. However, the actual still point was obtained 1.70 seconds later from the moment the brake command was applied. The actual braking point was measured based on the instant that the acceleration values measured by the accelerometer had stabilised.

These results validate the fact that the data provided by the sensorial modules applied to the prototypes, when compared to standard behavioural patterns, are able to predict unsafe and also danger scenarios, where triggering systems like the ABS or TCS would probably avoid fatal crashes and save lives.

5.5 Steering Performance

In this section, the steering capabilities of the prototypes are subjected to several tests. It is important to validate this specific system since it was one of the most challenging parts of the design stage of this work. Not only the design but also the sensorial modules, which are able to provide information regarding steering, were tested and the results are shown bellow.

5.5.1 Yaw Validation

The yaw angle provided by the gyroscope is one of the most useful measurements for analysing steering related experiments. Thus, it is important to validate the output values of the MPU-6050.

To begin, the prototypes were placed at a starting position and the gyroscope values were calibrated. Twenty circular laps, corresponding to a total of 7200 °, were then executed to the left, ensuring that the vehicles stopped at the exact same position as they started. Then, the test was repeated but this time turning to the right. The final yaw angles were retrieved and the errors calculated.

Table 5.1 presents the results obtained in each of the experiments. It is shown the absolute values of the final yaw angles, the deviation degrees per lap, as well as the average lap error percentage.

	Yaw Angle (|°|)	**Deviation per Lap ($\pm$ 0.01 °/lap)**	**Average Lap Error Percentage ($\pm$ 0.01 %)**
Prototype 1 - Left Turn	7131.37	3.43	0.95
Prototype 1 - Right Turn	7124.62	3.77	1.05
Prototype 2 - Left Turn	7094.52	5.27	1.47
Prototype 2 - Right Turn	7075.80	6.21	1.73

Table 5.1: Yaw validation test results after 20 consecutive laps for each side.

It is possible to verify that the obtained deviations per lap are not huge and would fit a vast list of safety testing scenarios. However, these measurements would require improvements depending on the level of precision demanded in each specific application.

In [80] it is proved that the gyroscope data tend to accumulate error with time. So, a second validation test was performed and consisted in letting the prototypes measuring yaw variations while being completely immobilised.

After one hour, the results were analysed and it was verified that the yaw angles had evolved at a rate of 196 ± 1 °/h in *P1* and 179 ± 1 °/h in *P2*.

These said, the yaw angle measuring is still possible to be validated, mainly if the experiments being executed do not require large testing periods. In these particular cases, the error values should be taken into consideration.

5.5.2 Turning Manoeuvre for Ackermann Criteria Validation

The turning manoeuvre test was performed with the aim of validating the Ackermann steering kinematics presented in Chapter 3. This was possible by finding the minimum turning radius each prototype was capable of achieving, as well as the respective angles that the inner and outer steering wheels were doing with respect to a centre curvature point.

To perform this experiment, each vehicle was placed in a starting position, reseted to ensure correct measurements and began doing twenty consecutive laps for each side, at constant throttle and ensuring that no wheel-slip was happening.

When analysing the gathered data, the mean distance traveled to performe each of those twenty laps was used to represent the circumference perimeter and the curvature radius was extrapolated from:

$$Turning\ Radius = \frac{Circumference\ Perimeter}{2 \cdot \pi} \tag{5.1}$$

Table 5.2 presents the results obtained. It is seen that the biggest difference between the turning radius is of around 0.01 m, which is considered to be a really small deviation for the total distance covered in this experiment.

	Circumference Perimeter ($\pm$ 0.0001 m)	**Turning Radius ($\pm$ 0.0001 m)**
Prototype 1 - Left Turn	6.1755	0.9829
Prototype 1 - Right Turn	6.1120	0.9728
Prototype 2 - Left Turn	6.2003	0.9868
Prototype 2 - Right Turn	6.1580	0.9801

Table 5.2: Turning manoeuvre results for circumference perimeter and turning radius.

It is now possible to compare the practical results with what was supposed to be obtained if perfect Ackermann criteria were achieved. Looking at Equations 3.15 and 3.16 it is extrapolated the inner and outer angles, (θ_i and θ_o), that the cars are capable of executing for both sides. Since the yaw angle is calculated by the gyroscope, that is positioned in the middle of the models, half of the wheel-track value is subtracted from each of the previous radius to calculate c_i, and added to calculate c_o. Manipulating the equations mentioned above we get:

$$\theta_i = \arctan\left(\frac{l}{radius - \frac{b}{2}}\right), \quad radius - \frac{b}{2} = c_i \tag{5.2}$$

$$\theta_o = \arctan\left(\frac{l}{radius + \frac{b}{2}}\right), \quad radius + \frac{b}{2} = c_o \tag{5.3}$$

The obtained results are expressed in the following table:

	Inner Wheel Angle ($\theta_i \pm 0.01\,°$)	**Outer Wheel Angle** ($\theta_o \pm 0.01\,°$)
Prototype 1 - Left Turn	16.67	14.24
Prototype 1 - Right Turn	16.84	14.37
Prototype 2 - Left Turn	16.60	14.19
Prototype 2 - Right Turn	16.71	14.28

Table 5.3: Inner and outer experimental turning angles.

The Ackermann criteria was not completely achieved due to the complexity associated with the design of the steering system. Figure 5.8 shows both the ideal (coloured in green) and the designed geometry (coloured in red) of the steering linkages. It is also possible to see that the two imaginary lines, as explained in Section 3.1, do not meet in the centre of the rear axle, which would theoretically increase the probability of unwanted slipping. However, with normal traction conditions, no slip was detected.

Considering that the exact criteria was fulfilled, ψ would be 61.69 °, contrarily to the ψ_p obtained of 37.09 °. A value that is around 39.89 % away from what was expected.

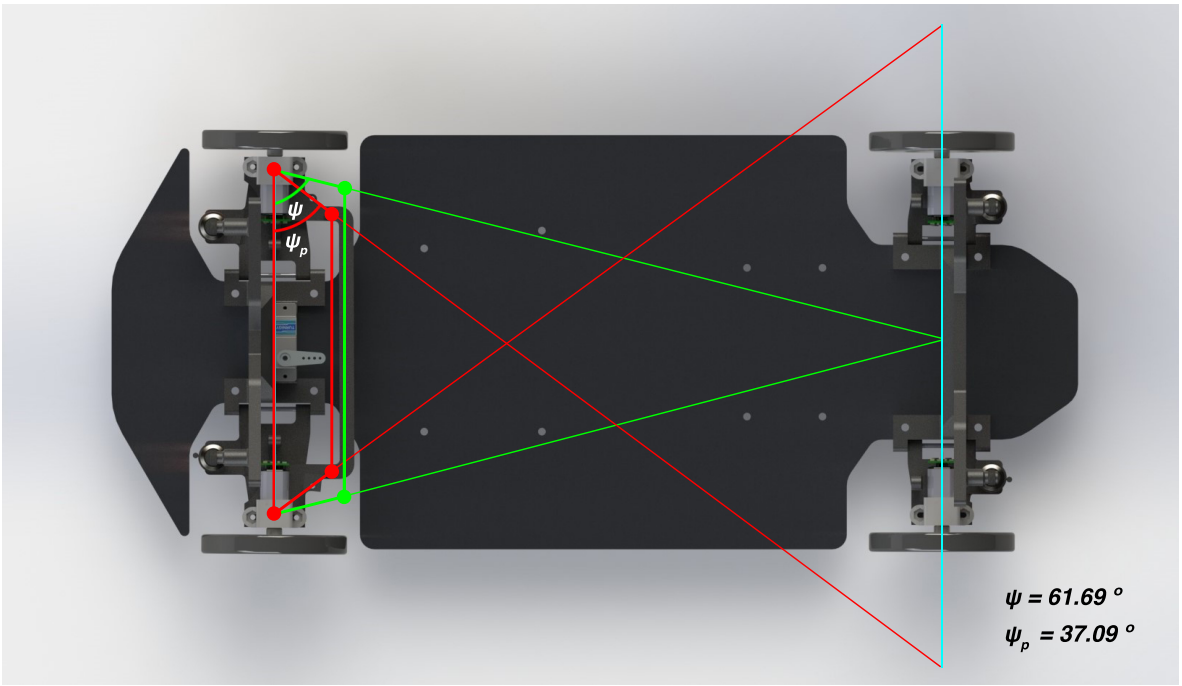

Figure 5.8: Prototype render with lines representing the ideal and the obtained steering linkage geometries (in green and red, respectively) and angles.

Evaluating the turning radius mentioned above, as well as the yaw angles obtained during the twenty testing laps performed, the data was converted into cartesian coordinates and approximations of the vehicles trajectories are presented in Figure 5.9.

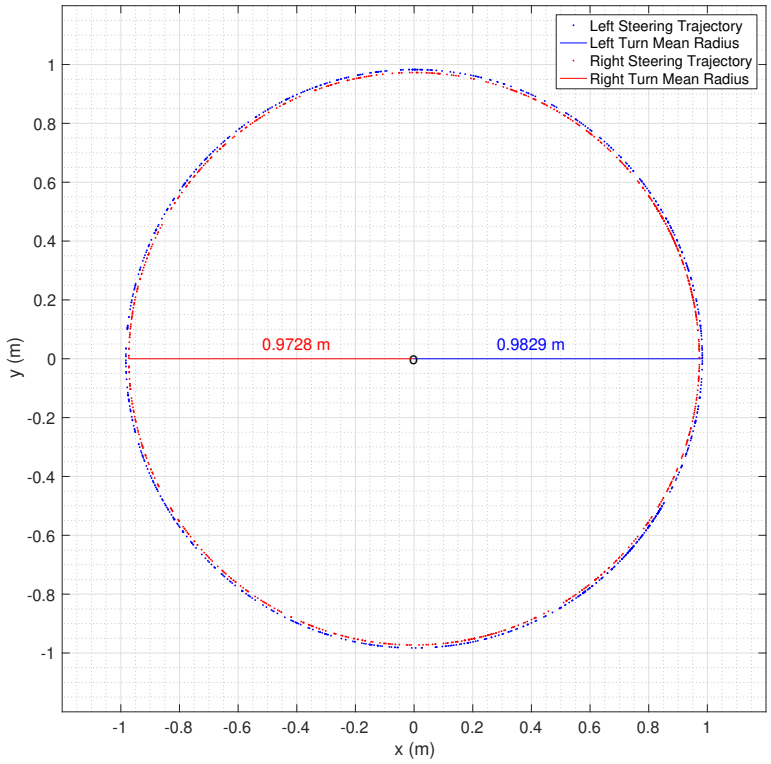

(a)

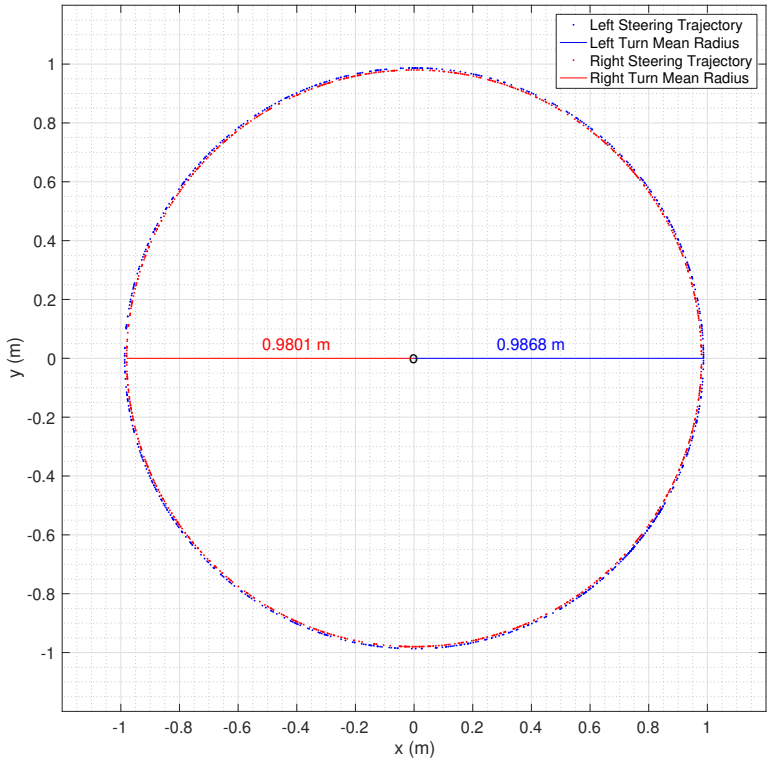

(b)

Figure 5.9: Turning manoeuvre trajectory representation to the right and left side. Figure (a) corresponds to the *P1* and (b) to *P2*.

5.5.3 Spin Detection

Just like slip detection is the key for triggering ABS and TCS systems, figuring out when a spin is about to happen is massively important to engage ESC or TV safety systems. With this in mind, a simple test was performed with the aim of evaluating if the sensors of the prototypes were able to predict a spin situation.

With adhesive tape covering the wheels of a prototype in order to simulate a low traction surface, a steer command was sent and the vehicle started performing a circular manoeuvre. At a certain point the car lost traction and uncontrolledly executed a spin. At this same exact moment, both steer and throttle commands were released.

Figure 5.10 shows the evolution of the yaw angle and the moment the steer command was released.

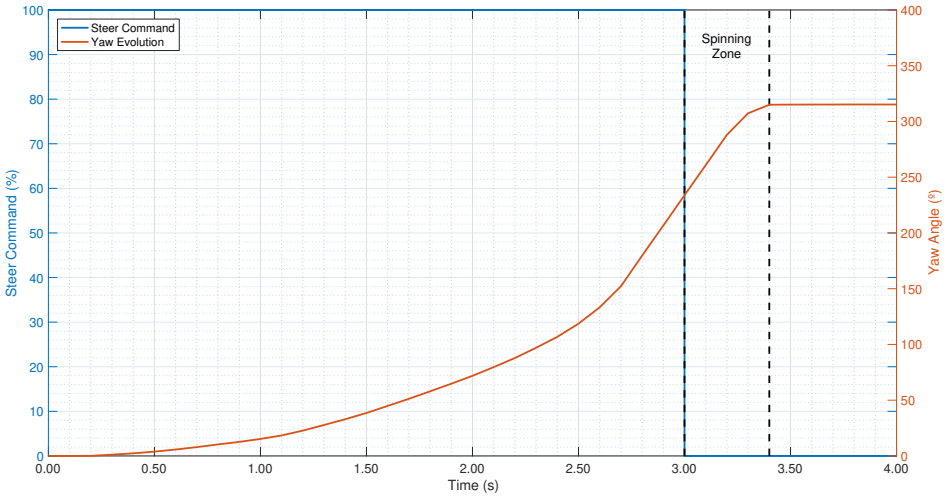

Figure 5.10: Yaw angle and steer command evolution analysis for unwanted spin detection.

As seen, at second 3.0 the steer command was released. A null input steering command makes the servo ensure that the wheels are facing forward with the car. Although, it is possible to verify that the yaw angle is still evolving for another 0.40 seconds. This incoherence is enough to verify that the model started spinning and validates the idea that it is possible to predict these unwanted driving behaviours.

5.6 Road Bump Effect

As a way of validating the suspension system of the car and to see if the accelerometer was capable of correctly representing pitch variations while going through a bump on the road, a 6.00 mm-high bump was built on the ground.

The prototype was then commanded to go over the object and it was verified that no matter the speed with which the vehicle was going over the bump, the suspension system was well absorbing its impact, almost being unnoticed and not affecting the controls of the user.

Figure 5.11 represents the evolution of the pitch angle with respect to time. The bump was gone over between second 1.0 and second 2.0. Small vibrations captured on the way to the bump area are responsible for creating the noise observed in the remaining time period (before jumping and also after the suspension had fully recovered its original state).

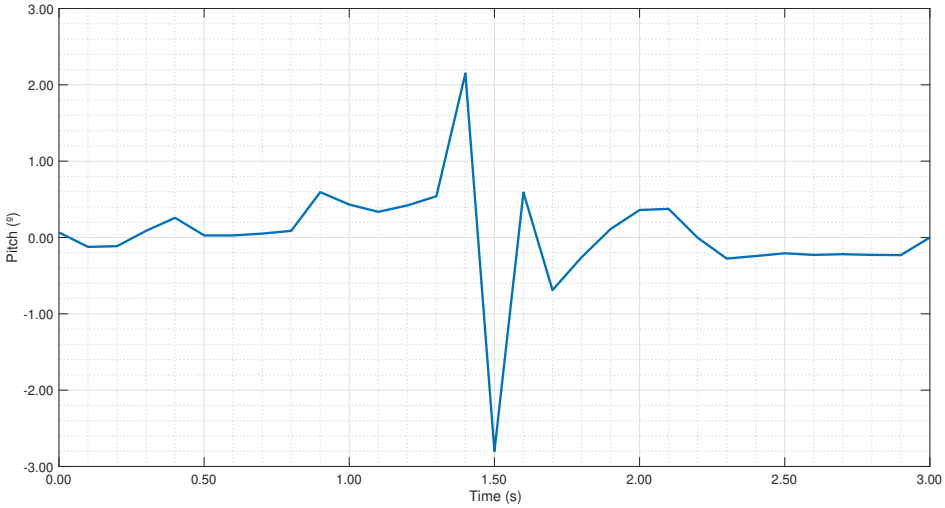

Figure 5.11: Pitch angle evolution when going over a bump on the road.

As expected, between the mention time slot, the pitch angle starts by increasing its value, meaning that the nose of the vehicle is facing upwards. Then, after passing the bump, the angle goes negative and the oscillations are rapidly absorbed by the suspension.

It is further interesting to note the similarities between the obtained pitch angle curve and what was simulated in Chapter 3 for the step response behaviour of the suspension. Serving both as a validation of the accelerometer pitch measurement behaviour and of the physical suspension system of the prototypes.

In this particular testing, it would be interesting to log the data at a greater sampling frequency to observe the pitch evolution with higher detail and precision. Therefore, a dynamic logging sampling frequency implementation will be proposed as future work.

5.7 Bluetooth Communication Range

The range the cars are able to communicate with the controller is an important factor to evaluate testing conditions such as the available area.

HC-06 bluetooth module data-sheets do not make any reference to the distance these are capable of communicating. A more in depth search allowed finding, in [81], that these components are used for communications of less than 100 meters.

In order to validate this reference value, a test was conducted that consisted in controlling the car around a defined safety perimeter while increasing the distance between the car and the controller. This experiment was performed in an open road as shown in Figure 5.12. Surprisingly, the connection remained stable for 130 meters, validating the theoretical value.

It is important to have in mind that this results were obtained in an open-environment with no obstacles between the car and the controller. Meaning that in other circumstances the results could have been different. So, for safety reasons, it is not advised to get the prototypes out-of-sight.

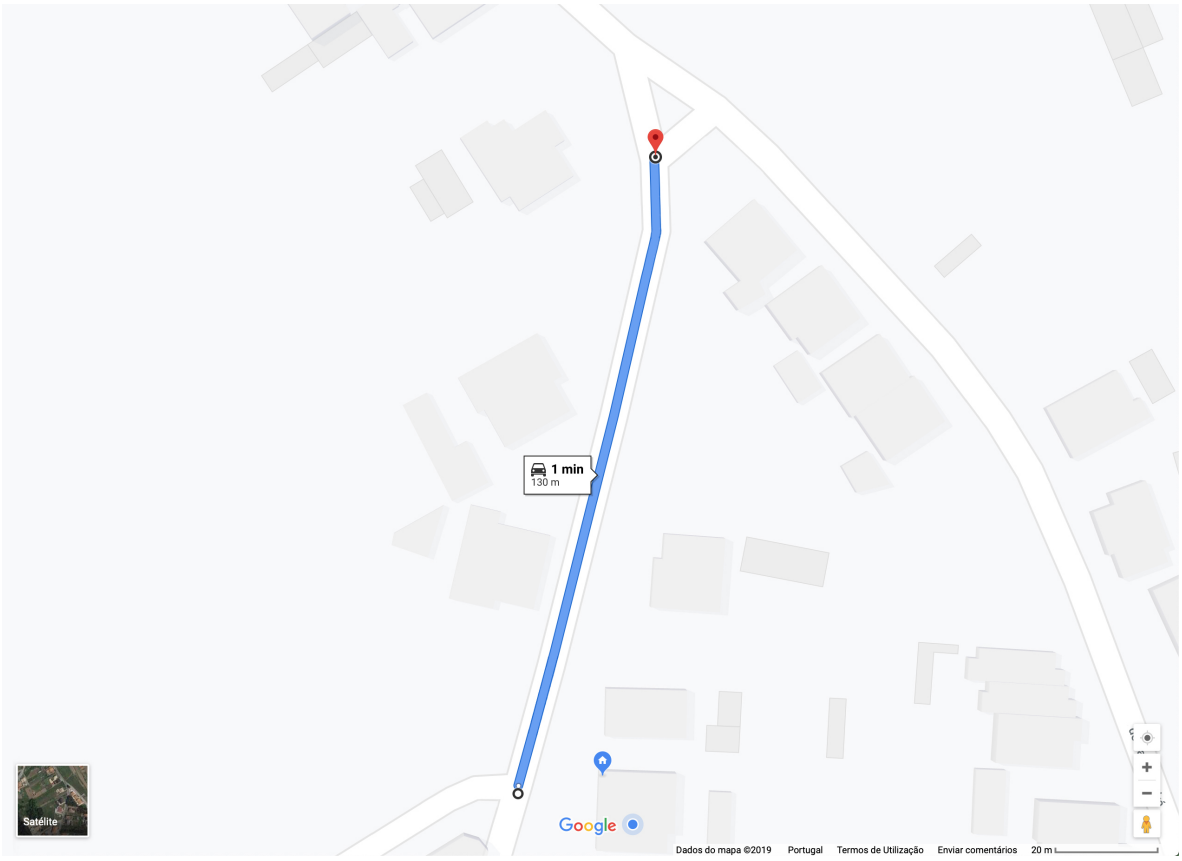

Figure 5.12: Bluetooth range test distance, adapted from Google Maps [82].

5.8 Power Consumption and Battery Testing

Battery range concerns are still one of the biggest drawbacks in the evolution of mentalities regarding the changes from ICEVs to EVs. So, a final test was conducted with the aim of finding the power consumptions that the developed prototypes require while performing several different tests.

Six different scenarios were experimented. To begin with, the prototypes were let in standby mode, *i.e.*, with everything powered on and connected but without receiving any moving command. Using an ammeter, the current flowing on the output of the battery was measured. This approach was then repeated while constantly sending a steering command to verify the battery consumption required by the servo motor.

The following four tests consisted in sending full-throttle commands to the cars and verifying the differences between the behaviour of each traction setup when in a no load situation

(with the wheels in the air) and when in stall (with the wheels blocked). This way, the best and the worst scenarios related to the autonomy and range of the batteries were studied.

Table 5.4 shows information on the measured current consumption, autonomy time and an estimate on how long the Li-ion batteries would let the cars travale while continuously performing each of the tests mentioned.

Test Type	**Current Consumption ($\pm$ 10 mA)**	**Autonomy Time ($\pm$ 1 min.)**	**Distance Range ($\pm$ 0.01 km)**
Standby	165	909	-
Turning the Wheels	370	405	-
Full-Throttle RWD (No Load)	260	577	84.33
Full-Throttle AWD (No Load)	310	484	90.11
Full-Throttle RWD (Stall)	1085	138	20.17
Full-Throttle AWD (Stall)	2140	70	13.03

Table 5.4: Battery consumption testing results.

Autonomy time was directly calculated considering the batteries nominal discharge capacity of 2500 mAh. Distance range was obtained considering the mean value of the maximum speeds of both prototypes in each traction configuration (8.77 km/h for RWD and 11.17 km/h for AWD).

It is seen that even at stall conditions, a fully charged battery pack would last for more than one-hour, considering full-throttle and with the car being propelled by its four electric motors. A result that is good enough to satisfy most of the testing needed to study with the developed vehicles, serving as a validation of the chosen batteries.

Chapter 6

Conclusions and Future Work

6.1 Conclusions

Beginning with the analysis of the results presented in the previous chapter, it is admitted that the developed prototypes can be validated as testing platforms capable of retrieving sensorial data needed for future implementation of driving aid systems.

Although the exact scale of every parameter was not achieved during the design stage, as seen in Table 4.1, the fundamental relations between the real car and the 1:10 prototypes were maintained, such as length and width, not compromising any of the initially stipulated objectives. This process was challenging mainly due to the need of creating a system capable of including both suspension and steering mechanisms while considering the extra amount of space required to incorporate the in-wheel motors into place. Likewise, being an uncommon setup for the current industry, no examples or guidelines of similar vehicles were used when developing the prototypes, fortifying the need of creating almost everything from scratch.

All the chosen electronics were useful to validate the idea that these cars are able to accomplish the data acquisition needed to implement driving assistance technologies like the ones introduced in Chapter 2. The only major drawback found in the hardware was the fact that the Arduino Mega is limited to six interrupt pins, of which two are assigned to I2C communications and other two to Serial Port 1, remaining two free pins and consequently imposing limitations to the correct use of the all four wheel encoders assembled in the cars. An easy solution for this would be its replacement with an Arduino Due, since all its pins are usable for interrupts and since the Adafruit motorshield is also drop-in compatible with it. Even though the prototypes are not monitoring their rear wheels, everything has been ensured to be ready to work if the Arduinos are changed.

It is proved that electric vehicles are a future bet to maintain and reinforce in the years to come. This particular configuration, although feasible and believed to be one of the most beneficial approaches regarding the implementation of better safety systems, should not be the most common to see in the few next years due to the high costs of having four motors in a real car. For this to happen, it would be necessary to further improve the technology of the in-wheel motors and to force a paradigm shift in the mentality of manufacturers.

Embracing this project was a great challenge to put into practice some of the many competences acquired during this Master in Electronics and Telecommunication Engineering, as well as to develop new skills such as being able to work with CAD tools like *SolidWorks*. Being capable of projecting something in my head, drawing it in a paper, going through all the design stages, turning those thoughts into real physical pieces, putting everything together and validating all the work done is one of the most grateful sensations I have felt during my academic career. Since all the objectives were successfully achieved, it is secure to evaluate this dissertation as complete.

6.2 Future work

The work developed during this dissertation constitutes the beginning of the implementation of driving aid technologies applied to vehicles with four independent electric motors. This is an investigation with a long way to go and that deserves to be continued. The construction of test platforms such as the ones built here require a lot of study, dedication and time, which unfortunately is limited to the period devoted to perform a thesis. Therefore, a set of suggestions are proposed next, with the aim of proceeding with this dissertation's work.

At the level of construction of the prototypes, there is not much to change. So, the next main objective would be to develop active driving aid systems, such as ABS, TV, TCS and ESC, applying them to several testing conditions and comparing the results with the simulations performed in [6], which would also require some adjustments since they were studied considering planar dynamics, *i.e.*, ignoring the effects of the suspension system.

Although there were not felt any major consequences over the tests performed, there is a small discrepancy between the RPM of every motor. Thus, it is suggested the development of a speed controller based on PID, Pole Placement (also known as RST) or other control technique to avoid small deviations from the trajectory of the prototypes and also to increase the reliability of the driving aids to be executed.

As mentioned in Section 5.6, it would be interesting to improve the logging algorithms in order for the sampling frequencies to be dynamic, *i.e.,* to record data at a higher rate, for example, whenever a certain interesting activity was sensed by the accelerometer, as a matter of capturing data with greater precision.

Implementing a measuring mechanism in every suspension, capable of calculating the displacement suffered by both spring and shock while going through irregularities on the road, or even while performing turns at higher speeds or on heavy loads, would be an interesting case study. This would allow investigating how weight transfers affect the behaviour of the car and would possible be a good starting point to develop an active suspension system.

A lot of other sensorial electronics can be added to the cars as a measure of maximising the countless capabilities related to the use of ADAS. An intelligent vision system based on ultrasounds, LIDAR technology or even on image processing for object avoidance or autonomous driving would also be a great improvement to what has been done.

Lastly, it is important to recall that several other test routines, different from the ones performed in Chapter 5, may be executed as a result of the flexibility the prototypes are able to deliver.

Bibliography

[1] Erik Eckermann. The first automobile. In *World History of the Automobile*. 2001.

[2] Tariq Muneer and Irene Illescas García. *The automobile*. 2017.

[3] Routley Nick. Visualizing Electric Vehicle Sales Around the World. `https://www.visualcapitalist.com/electric-vehicle-sales/`, 2019. (Accessed in 2019-05-27).

[4] Wannasuphoprasit Witaya, Wattananukulchai Parinya, and Chundang Krissada. Scaled vehicle for interactive dynamic simulation (SIS). *2008 IEEE International Conference on Robotics and Biomimetics, ROBIO 2008*, (December):554–559, 2008.

[5] Padeanu Adrian. Rimac C_Two Arrives In Geneva With Attractive Livery. `https://www.motor1.com/news/307746/rimac-c-two-galactic-white/`, 2019. (Accessed in 2019-05-28).

[6] Bruno Grego. Segurança Automóvel: Sistemas de Apoio à Condução. *Dissertação de Mestrado, Universidade de Aveiro*, 2016.

[7] Sérgio Ivo Marques Ferreira. Desenvolvimento de um veículo elétrico em escala reduzida. *Dissertação de Mestrado, Universidade de Aveiro*, 2018.

[8] History of Car Safety - Crash Test. `https://www.crashtest.org/history-car-safety/`. (Accessed in 2019-02-14).

[9] Where does Volvo's reputation for safety come from? `https://wyantgroup.com/where-does-volvos-reputation-for-safety-come-from/`. (Accessed in 2019-02-14).

[10] The evolution of car safety: a history — Auto Express. `https://www.autoexpress.co.uk/car-news/90221/the-evolution-of-car-safety-a-history`. (Accessed in 2019-02-14).

[11] T. Denton. *Automobile Electrical and Electronic Systems, third edition*. 2004.

[12] What is Euro NCAP? Car safety, star ratings and dual rating crash test scores — Auto Express. `https://www.autoexpress.co.uk/car-news/94398/what-is-euro-ncap-car-safety-star-ratings-and-dual-rating-crash-test-scores`. (Accessed in 2019-02-15).

[13] Autopilot — Tesla. `https://www.tesla.com/autopilot?redirect=no`. (Accessed in 2019-05-30).

[14] W Harris. How Car Suspensions Works. http://auto.howstuffworks.com/car-suspension.htm/printable, 2008. (Accessed in 2019-02-13).

[15] B. T. Fijalkowski. Automotive Mechatronics: Operational and Practical Issues. *Automotive Mechatronics: Operational and Practical Issues*, pages 255–279, 2011.

[16] Special Issue and Issn Online. Conference Special Issue March 2016 Stress Analysis of Multi Leaf Spring by Using Experimental Method. 2(1):1–5, 2016.

[17] Stephen Mraz. What Are the Differences Between Sprung and Unsprung Weight? https://www.machinedesign.com/springs/what-are-differences-between-sprung-and-unsprung-weight, 2016. (Accessed in 2019-02-21).

[18] Cătălin Alexandru and Petre Alexandru. Passive & Active use. *International Journal Of Mechanics*, 2011.

[19] Trends in suspension systems. https://www.automotive-iq.com/chassis-systems/articles/trends-suspension-systems. (Accessed in 2019-02-21).

[20] Scott Collie. Audi eROT suspension harvests energy as it rides the bumps. https://newatlas.com/audi-erot-electrical-suspension/44848/, 2016. (Accessed in 2019-02-21).

[21] Alasdair Morton. Volvo XC40 to feature electronic suspension — Vehicle Dynamics International. https://www.vehicledynamicsinternational.com/news/ride-comfort/volvo-xc40-to-feature-electronic-suspension.html, 2018. (Accessed in 2019-02-21).

[22] Karim Nice. How Differentials Work — HowStuffWorks. https://auto.howstuffworks.com/differential.htm, 2000. (Accessed in 2019-02-24).

[23] Differential Introduction - Mechanical Engineering. http://mechanicalmania.blogspot.com/2011/07/differential-introduction.html. (Accessed in 2019-02-25).

[24] Sahil Jitesh. Antilock Braking System. *International Journal of Mechanical Engineering and Robotics Research*, 2014.

[25] Wu Jian Ye Yifan, Zhao Jian, Zhao Yang. Research and Test on Traction Control System of Distributed Driving Electric Vehicles. *IEEE 3rd International Conference on Control Science and Systems Engineering*, 2017.

[26] Top 10 Car Technologies You Should Definitely Know About - All About Selling Used Cars - CARS24 BLOG. https://www.cars24.com/blog/top-10-car-technologies-that-you-should-definitely-know-about/. (Accessed in 2019-02-25).

[27] European Patent Office. Anton van Zanten (The Netherlands, Germany). https://www.epo.org/learning-events/european-inventor/finalists/2016/vanzanten.html, 2016. (Accessed in 2019-02-25).

[28] Prateek Khurana, Rajat Arora, and Manoj Kr Khurana. Implementation of electronic stability control and adaptive front lighting system for automobiles. *2014 International Conference on Power, Control and Embedded Systems, ICPCES*, 2014.

[29] The Differences Between Understeer & Oversteer And How To Combat Them - YouTube. https://www.youtube.com/watch?v=EwmDdMzzDjY, 2017. (Accessed in 2019-02-26).

[30] Martin Mondek. *Active torque vectoring systems for electric drive vehicles*. PhD thesis, Czech Technical University in Prague, 2018.

[31] Jake Whitehead, Robin Smit, and Simon Washington. Where are we heading with electric vehicles? *Air Quality and Climate Change*, 2018.

[32] Pedro Danilo Godinho Abrantes Coimbra e Costa. Environmental and Economical Competitiveness of Battery Electric Vehicles in the Portuguese Market : exploring the potential economical advantages of a Vehicle. 2012.

[33] Worldwide Sales of Toyota Hybrids Surpass 10 Million Units. https://newsroom.toyota.eu/global-sales-of-toyota-hybrids-reach-10-million/, 2017. (Accessed in 2019-02-28).

[34] Fundo Ambiental, Ministério do Ambiente. www.fundoambiental.pt/avisos-2019/incentivo-pela-introducao-no-consumo-de-veiculos-de-baixas-emissoes-2019.aspx, 2019. (Accessed in 2019-02-28).

[35] Incentivos para veículos — Tesla. https://www.tesla.com/pt_PT/support/incentives. (Accessed in 2019-02-28).

[36] Nora Manthey. All-electric car market share on the rise worldwide - electrive.com. https://www.electrive.com/2018/12/13/all-electric-car-market-share-on-the-rise-worldwide/, 2018. (Accessed in 2019-03-01).

[37] Ying Tian. China Is About to Shake Up the World of Electric Cars: QuickTake - Bloomberg. https://www.bloomberg.com/news/articles/2018-11-14/china-is-about-to-shake-up-the-world-of-electric-cars-quicktake, 2018. (Accessed in 2019-03-01).

[38] Tesla Model 3. https://www.tesla.com/model3. (Accessed in 2019-03-01).

[39] Energy, Ergon. Types Of Electric Cars. https://www.ergon.com.au/network/smarter-energy/electric-vehicles/types-of-electric-vehicles, 2015. (Accessed in 2019-02-14).

[40] Chris Riley. Dispelling The Disadvantages Of An Electric Car. https://autowise.com/top-7-disadvantages-of-electric-cars/, 2019. (Accessed in 2019-03-02).

[41] João Delfim Tomé. Piech Automotive estreia-se em Genebra com um elétrico que carrega em 4 minutos. https://www.razaoautomovel.com/2019/03/piech-automotive-apresentacao-genebra, 2019. (Accessed in 2019-03-06).

[42] Tesla Roadster. https://www.tesla.com/pt_PT/roadster?redirect=no, 2019. (Accessed in 2019-03-04).

[43] Swaraj Ravindra Jape and Archana Thosar. Comparison of Electric Motors for Electric Vehicle Application. *International Journal of Research in Engineering and Technology*, 06(09):12–17, 2017.

[44] Peter Campbell. How Mate Rimac is supercharging electric cars - Financial Times. https://www.ft.com/content/26441146-de02-11e8-b173-ebef6ab1374a, 2018. (Accessed in 2019-03-06).

[45] Jim Gorzelany. The Coolest New 2019-2020 Electric Cars Worth Waiting For. https://www.forbes.com/sites/jimgorzelany/2019/01/22/the-coolest-new-2019-2020-electric-cars-worth-waiting-for/#2976986446a3, 2019. (Accessed in 2019-03-06).

[46] Sam Davis. In-Wheel Motor Systems Will Propel EV Performance. https://www.powerelectronics.com/automotive/wheel-motor-systems-will-propel-ev-performance, 2018. (Accessed in 2019-03-07).

[47] Christopher DeMorro. Protean To Begin In-Wheel Electric Motor Production In 2014 - Gas 2. https://gas2.org/2013/04/17/protean-to-begin-in-wheel-electric-motor-production-in-2014/, 2013. (Accessed in 2019-03-07).

[48] Andrew Whitehead and Chris Hilton. Protean Electric's In-Wheel Motors Could Make EVs More Efficient - IEEE Spectrum. https://spectrum.ieee.org/transportation/advanced-cars/protean-electrics-inwheel-motors-could-make-evs-more-efficient, 2018. (Accessed in 2019-03-07).

[49] Thornton John. in-Wheel Motors. *Electric and Hybrid Vehicle Technology International*, pages 50–56, 2013.

[50] Protean Electric. Protean Drive - Test Sheet. Technical Report May, 2018.

[51] ProteanDrive - Protean. https://www.proteanelectric.com/protean-drive/#overview. (Accessed in 2019-03-07).

[52] Richard T O Brien and Joyce E Shade. Scale-model Vehicle Analysis For The Design Of A Steering by Certification of Advisers Approval Acceptance for the Trident Scholar Committee. 309, 2003.

[53] Sean N Brennan. Modeling And Control Issues Associated With Scaled Vehicles. *University of Illinois at Urbana-Champaign*, 1999.

[54] S. Lapapong, V. Gupta, E. Callejas, and S. Brennan. Fidelity of using scaled vehicles for chassis dynamic studies. *Vehicle System Dynamics*, 47(11):1401–1437, 2009.

[55] Andrew Liburdi. Development of a Scale Vehicle Dynamics Test Bed. *University of Windsor*, 2010.

[56] Goegoes Dwi Nusantoro and Gigih Priyandoko. PID State Feedback Controller of a Quarter Car Active Suspension System. *Journal of Basic and Applied Scientific Research 1*, 1(11):2304–2309, 2011.

[57] P. Sathishkumar, J. Jancirani, D. John, and S. Manikandan. Mathematical modelling and simulation quarter car vehicle suspension. *IOSR Journal of Mechanical and Civil Engineering (IOSR-JMCE)*, (1):1280–1283, 2014.

[58] R N Jazar. *Vehicle Dynamics: Theory and Application*. Engineering (Springer-11647; ZDB-2-ENG). Springer, Melbourne, Australia, third edit edition, 2008.

[59] Control Tutorials for MATLAB and Simulink - Suspension: System Modeling. `http://ctms.engin.umich.edu/CTMS/index.php?example=Suspension&section=SystemModeling`. (Accessed in 2019-05-15).

[60] Aissms Coe. Determination of Damping Coefficient of Automotive Hydraulic Damper Using Sinusoidal. *Technical Research Organisation India*, (7):4–13, 2016.

[61] Jing Shan Zhao, Xiang Liu, Zhi Jing Feng, and Jian S. Dai. Design of an Ackermann-type steering mechanism. *Proceedings of the Institution of Mechanical Engineers, Part C: Journal of Mechanical Engineering Science*, 227(11):2549–2562, 2013.

[62] Engineering Explained. Ackerman Steering - Explained - YouTube. `https://www.youtube.com/watch?v=oYMMdjbmQXc`, 2012. (Accessed in 2019-05-12).

[63] SK8215. Ackreman Steering Geometry and Anti Ackreman - YouTube. `https://www.youtube.com/watch?v=YVisLuiU-Oo&frags=pl%2Cwn`, 2018. (Accessed in 2019-05-12).

[64] Fundamentals of car science : Pitch, roll and yaw - cars explained. `https://carsexplained.wordpress.com/2017/02/21/fundamentals-of-car-science-pitch-and-roll`, 2017. (Accessed in 2019-06-12).

[65] P. Hoblet, R. T. O'Brien, and J. A. Piepmeier. Scale-model vehicle analysis for the design of a steering controller. *Proceedings of the Annual Southeastern Symposium on System Theory*, 2003-Janua(309):201–205, 2003.

[66] Renault Megane I Maxi (1996) - Racing Cars. `http://tech-racingcars.wikidot.com/renault-megane-i-maxi`. (Accessed in 2019-04-12).

[67] Jon Zamboni. How to Calculate Percent Deviation — Sciencing. `https://sciencing.com/calculate-percent-deviation-6192580.html`, 2018. (Accessed in 2019-04-12).

[68] Pololu Robotics and Electronics. `https://www.pololu.com/`. (Accessed in 2019-04-12).

[69] Pololu. Micro Metal Gearmotors Datasheet - Pololu. (February), 2019.

[70] ElectronicsTutorials. Hall Effect Sensor and How Magnets Make It WorksBasic Electronics Tutorials. `https://www.electronics-tutorials.ws/electromagnetism/hall-effect.html`, 2018. (Accessed in 2019-04-17).

[71] Pololu - Magnetic Encoder Pair Kit for Micro Metal Gearmotors, 12 CPR, 2.7-18V (HPCB compatible). `https://www.pololu.com/product/3081`. (Accessed in 2019-04-16).

[72] S. Brennan, A. Alleyne, and M. DePoorter. The Illinois roadway simulator - A hardware-in-the-loop testbed for vehicle dynamics and control. *Proceedings of the American Control Conference*, 1:493–497, 1998.

[73] Adafruit Motor/Stepper/Servo Shield for Arduino v2 Kit [v2.3] : Adafruit Industries, Unique & fun DIY electronics and kits. https://www.adafruit.com/product/1438. (Accessed in 2019-04-18).

[74] Samsung SDI Co. Lithium-ion rechargeable cell for power tools - Datasheet. *INR18650-25R datasheet*, (1):0–16, 2014.

[75] Dejan. How I2C Communication Works & How To Use It with Arduino. https://howtomechatronics.com/tutorials/arduino/how-i2c-communication-works-and-how-to-use-it-with-arduino/. (Accessed in 2019-05-06).

[76] Who we are — Poly Lanema. https://www.polylanema.pt/en/who-we-are/. (Accessed in 2019-05-08).

[77] MINILAB 3D – CAD Design e Impressão 3D. https://minilab3d.pt/. (Accessed in 2019-05-19).

[78] Keuwl bluetooth electronics development. http://keuwl.com/index.html. (Accessed in 2019-06-05).

[79] Acceleration of a car - the physics factbook, meredith barricella, 2001. https://hypertextbook.com/facts/2001/MeredithBarricella.shtml. (Accessed in 2019-06-19).

[80] Radoslaw Cechowicz. Bias Drift Estimation for MEMS Gyroscope Used in Inertial Navigation. *Lublin University of Technology*, 2017.

[81] Hc-06 bluetooth module - components101. https://components101.com/wireless/hc-06-bluetooth-module-pinout-datasheet. (Accessed in 2019-06-07).

[82] Google maps. www.google.com/maps. (Accessed in 2019-06-07).

Appendix A

Production Costs

Product Description	Manufacturer	Retailer	Unit Price (€)	Qty.	Extended Price (€)
Motor/Stepper/Servo Shield for Arduino v2 Kit - v2.3	Adafruit Industries LLC	Digi-Key	17.45	1	17.45
MicroSD Card Module - DFR0229	DFRobot	Digi-Key	4.69	1	4.69
6 DOF Sensor - MPU6050	DFRobot	Digi-Key	8.92	1	8.92
Magnetic Encoder Pair Kit for Micro Metal Gearmotors 12 CPR 2.7-18V	Pololu Robotics & Electronics	PTRobotics	9.53	2	19.06
Micro Metal Gearmotor Bracket Pair	Pololu Robotics & Electronics	PTRobotics	5.35	2	10.70
LM2596 DC-DC Voltage Regulator Adjustable Power Supply Module w/ Display	-	PTRobotics	6.40	1	6.40
Bluetooth Module HC-06	-	PTRobotics	8.24	1	8.24
DS3231 RTC Module	-	PTRobotics	4.92	1	4.92
Wheel 60x8mm Pair	Pololu Robotics & Electronics	PTRobotics	8.49	2	16.98
CR1220 Coin Cell Battery 3V 38mAh	-	PTRobotics	1.60	1	1.60
30:1 Micro Metal Gearmotor HP w/ Extended Motor Shaft	Pololu Robotics & Electronics	Electan	16.14	4	64.56
Arduino Mega board 2560 R3 ATmega2560	Makershop.de	eBay	9.95	1	9.95
Aluminium Shock Absorber Set 124000 1/10	Blaze Spare Parts	HobbyKing	8.43	2	16.86
Digital Micro Servo 2.8 kg / 0.10sec / 12.4 g - TGY-EX5252MG	Turnigy™	HobbyKing	9.05	1	9.05
Water Jet Cut in AW6082-T651 4 mm Aluminium Sheet	PolyLanema®	PolyLanema®	61.50	1	61.50
3D Printed Parts (16 pcs.)	MiniLab3D	MiniLab3D	35.13	1	35.13
MicroSD Card - 2.0 GB	SanDisk	-	3.60	1	3.60
Li-Ion Batteries INR18650-25R 3.6V, 2.5Ah	Samsung	-	11.35	3	34.05
Series 3.7V Flat Tip Battery Holder Case for 3x18650 Batteries	-	eBay	1.11	1	1.11
Dupont Jump Wires (100 pcs.)	-	-	6.40	1	6.40
Miscellaneous (Bolts, Nuts,...)	-	-	20.00	1	20.00
				Total:	**361.17 €**

Table A.1: Detailed list of products and costs needed for building one prototype vehicle (the prices do not include postage costs and were consulted in June, 2019).

Appendix B

Arduino Code

```
/*
Goncalo Marques | 76390 | MIEET - Universidade de Aveiro
EVGO Prototype v1.0 - Master thesis project */

#include <Wire.h>
#include <Adafruit_MotorShield.h>
#include <Servo.h>
#include "Timer.h"
#include <SPI.h>
#include <SD.h>
#include <RTClib.h>

/* SD Card */
const int chipSelect = 53;
File myLog;
volatile int start_log = 0;

/* Real-Time Clock */
RTC_DS3231 rtc;

/* MPU-6050 Accelerometer & Gyro */
const int MPU = 0x69; // MPU6050 I2C address = 1101001 (AD0 = 1)
float AccX, AccY, AccZ;
float GyroX, GyroY, GyroZ;
float accAngleX, accAngleY, gyroAngleX, gyroAngleY, gyroAngleZ;
float roll, pitch, yaw;
float AccErrorX, AccErrorY, GyroErrorX, GyroErrorY, GyroErrorZ;
float elapsedTime, currentTime, previousTime;
int c = 0;

/* Motors, servo, encoders and shield */
// Create the motor shield object with the default I2C address
Adafruit_MotorShield AFMS = Adafruit_MotorShield();
// Create the servo object
Servo servo;
// Attach each motor to a 'port'
Adafruit_DCMotor *FLM = AFMS.getMotor(1); // Front Left  Motor
Adafruit_DCMotor *RLM = AFMS.getMotor(2); // Rear  Left  Motor
Adafruit_DCMotor *RRM = AFMS.getMotor(3); // Rear  Right Motor
Adafruit_DCMotor *FRM = AFMS.getMotor(4); // Front Right Motor
```

```
41
42 #define encoder1PinA  3  // Front Left  Wheel Encoder - Pin A
43 #define encoder1PinB  22 // Front Left  Wheel Encoder - Pin B
44 #define encoder2PinA  2  // Front Right Wheel Encoder - Pin A
45 #define encoder2PinB  23 // Front Right Wheel Encoder - Pin B
46
47 volatile unsigned int encoder1Pos = 0;
48 volatile unsigned int encoder2Pos = 0;
49
50 volatile double speed_val = 0;
51 volatile double max_speed_val = 0;
52 volatile double acceleration = 0;
53 volatile double distance = 0;
54 volatile int RPM_FLM = 0;
55 volatile int RPM_FRM = 0;
56 volatile uint32_t rev_FLM = 0;
57 volatile uint32_t rev_FRM = 0;
58 volatile int throttle = 0, steer = 0;
59 volatile double m_factor = 1.17;
60 volatile int traction_setup = 1; // 1 = AWD, 2 = RWD
61
62 /* Battery readings */
63 int battery_pin = A15; // Analog pin used for measuring battery
64 uint32_t battery_val = 100, battery_read = 100;
65
66 /* Communication readings */
67 int count_X = 0, count_Y = 0;
68 volatile int count = 0;
69 boolean wr_X = false, wr_Y = false;
70 String X = "", Y = "";
71
72 /* Interrupt pins */
73 const byte BT_RX = 19; // Serial Port 1 - RX pin connected to the BT
       module
74
75 /* Timers */
76 Timer t;
77 volatile int tick = 0;
78 volatile int sub_tick = 0;
79 uint32_t time_count = 0;
80
81
82 void setup() {
83
84   /* Initialization */
85   delay(2000); // Wait 2000 ms to ensure power stability
86   Serial.begin(115200); // USB serial communication
87   Serial1.begin(9600); // Bluetooth module communication
88   Serial.println("EVGO Prototype v1.0 - Master thesis project");
89   Serial1.print("*CR0G255B0*"); // Set app connectivity light as 'green'
90
91   /* MPU-6050 initialization and calibration */
92   Wire.begin(MPU);
93   setupMPU();
94   Serial.println("Initializing MPU calibration...");
95   resetMPU(); // Calibrates the MPU values - Vehicle should be placed in a
       flat surface
```

```
96    delay(20);
97
98    AFMS.begin(); // AdaFruit Motor Shield begin
99    servo.attach(10); // Attaches the servo on pin 10 to the servo
100   servo.write(90);
101
102   pinMode(encoder1PinA, INPUT); // Sets Encoder 1 - Pin A as input (3)
103   pinMode(encoder1PinB, INPUT); // Sets Encoder 1 - Pin B as input (22)
104   pinMode(encoder2PinA, INPUT); // Sets Encoder 2 - Pin A as input (2)
105   pinMode(encoder2PinB, INPUT); // Sets Encoder 2 - Pin B as input (23)
106
107   /* Interrupts */
108   attachInterrupt(digitalPinToInterrupt(BT_RX), receive, FALLING); //
        Bluetooth RX pin - Generates an interrupt to receive data
109   attachInterrupt(0, int2_callback, CHANGE); // Encoder pin on interrupt 0
        - Pin 2
110   attachInterrupt(1, int3_callback, CHANGE); // Encoder pin on interrupt 1
        - Pin 3
111
112   /* Timers */
113   t.every(100, timer_tick); // Timer w/ 100 ms sampling period
114
115   /* RTC module setup - Uncomment to reset the RTC data & time */
116   // rtc.adjust(DateTime(F(__DATE__), F(__TIME__))); // Sets the RTC to
        the date & time this sketch was compiled
117
118   /* SD Card module setup */
119   Serial.print("Initializing SD card...");
120   if(!SD.begin(chipSelect)) {
121     Serial.println("initialization failed!");
122     return;
123   }
124   Serial.println("initialization done.");
125
126   myLog = SD.open("DATA.txt", FILE_WRITE); // Opening file
127   // If the file opened ok, write to it:
128   if (myLog) {
129     Serial.println("File opened ok");
130     // Print the headings for our data
131     DateTime now = rtc.now();
132     myLog.println("EVGO Prototype v1.0 Black Wheels - Master thesis
        project");
133     myLog.print("Date: ");
134     myLog.print(now.year(), DEC);
135     myLog.print('/');
136     myLog.print(now.month(), DEC);
137     myLog.print('/');
138     myLog.println(now.day(), DEC);
139     myLog.println("Time | Traction | Throttle | Steer | Speed (km/h) |
        Accel (m/s^2) | Distance (m) | RPM (FLM) | RPM (FRM) | Roll (deg) |
        Pitch (deg) | Yaw (deg) | Gyro (deg/s) X | Y | Z | Accel (g) X | Y | Z
        | Battery (%)");
140   }
141   myLog.close(); // Closing file
142
143 }
144
```

```
145 void loop() {
146
147   sub_tick++;
148
149   if((sub_tick % 1) == 0) {
150
151     speed_val = (3600.0 * m_factor * (rev_FLM+rev_FRM) / 2) / 100000; //
      Speed is given by the mean value measured in both front wheels (km/h)
152     if(speed_val > max_speed_val) { // Max speed value calculation
153       max_speed_val = speed_val;
154     }
155     distance = distance + m_factor * ((rev_FLM+rev_FRM) / 2) / 1000.0; //
      Distance is given by the mean value measured in both front wheels (m)
156     acceleration = AccY * 9.8065; // Horizontal acceleration measured by
      the Y-axis of the accelerometer that is pointing backwards relative to
      the car (m/s^2) - Gravitational acceleration = 9.8065 m/s^2
157     RPM_FLM = m_factor * (600 * rev_FLM) / 180; // Instant Front Left
      Motor RPM value
158     RPM_FRM = m_factor * (600 * rev_FRM) / 180; // Instant Front Right
      Motor RPM value
159     // Sending speed values to the app
160     Serial1.print("*S");
161     Serial1.print(speed_val);
162     Serial1.print("*");
163
164     recordMPU(); // Measuring MPU-6050 values
165
166     if(start_log){ // Checks if there is an order to log data to the SD
      Card
167       logging(); // Logging the retrieved data to the SD Card
168     }
169
170     // Reseting variables
171     speed_val = 0;
172     sub_tick = 0;
173     rev_FLM = 0;
174     rev_FRM = 0;
175    }
176
177   controls(); // Vehicle controls
178   sendLog();  // Send retrieved data to the bluetooth app
179
180   /* Timer update */
181   while(!tick) {
182     t.update();
183   }
184   tick = 0;
185
186 }
187
188 /* Pin 2 interrupt callback - Measuring the signals from the FRM encoder
      */
189 void int2_callback() {
190   rev_FRM++; // Front Right Motor Encoder pulse counter
191   if (digitalRead(encoder2PinA) == digitalRead(encoder2PinB)) { // If pinA
       and pinB are both high or both low, it is spinning forward. If they're
       different, it's going backward
```

```
192     encoder2Pos++;
193   } else {
194     encoder2Pos--;
195   }
196 }
197
198 /* Pin 3 interrupt callback - Measuring the signals from the FLM encoder
      */
199 void int3_callback() {
200   rev_FLM++; // Front Left Motor Encoder pulse counter
201   if (digitalRead(encoder1PinA) == digitalRead(encoder1PinB)) { // If pinA
       and pinB are both high or both low, it is spinning forward. If they're
       different, it's going backward
202     encoder1Pos++;
203   } else {
204     encoder1Pos--;
205   }
206 }
207
208 /* Timer */
209 void timer_tick() {
210   tick = 1;
211
212 }
213
214 /* Parses the received data */
215 void receive() {
216
217   while (Serial1.available()) {
218     char inChar = (char)Serial1.read(); // Get new byte
219
220     if (inChar == 'c') { // Clears file "DATA.txt" on the SD Card
221       SD.remove("DATA.txt");
222     }
223
224     if (inChar == 'a') { // Changes traction to AWD
225       traction_setup = 1;
226     }
227     if (inChar == 'r') { // Changes traction to RWD
228       traction_setup = 2;
229     }
230
231     if (inChar == 'L') { // Start logging order
232       start_log = 1;
233       m_factor = 1.49;
234     }
235     if (inChar == 'l') { // Stop logging order
236       start_log = 0;
237       m_factor = 1.17;
238     }
239
240     if (inChar == 'X') { // Starts parsing the steering command
241       wr_X = true;
242     }
243     else if (wr_X && count_X < 3) { // Reads the 3 numbers which follow 'X
      ' and concatenates them
244       X += inChar;
```

```
245       count_X++;
246     }
247
248     if (inChar == 'Y') { // Starts parsing the throttle command
249       wr_Y = true;
250     }
251     else if (wr_Y && count_Y < 3) { // Reads the 3 numbers which follow 'Y
      ' and concatenates them
252       Y += inChar;
253       count_Y++;
254     }
255
256     if (inChar == '\n') { // Converts the 'X' and 'Y' values from
      [100;200] to [-100;100]
257
258       throttle = (Y.toInt() - 150) * -2;
259       steer = (X.toInt() - 150) * -2;
260
261       // Reseting variables
262       wr_X = false;
263       wr_Y = false;
264       count_X = 0;
265       count_Y = 0;
266       X = "";
267       Y = "";
268     }
269   }
270
271 }
272
273 /* Controls motors and the servo */
274 void controls() {
275
276   switch (traction_setup) {
277     case 1: // AWD
278       // 'throttle' is converted to a [0 to 255] range and each motor
      speed is set
279       FLM->setSpeed(abs(throttle)*2.55);
280       FRM->setSpeed(abs(throttle)*2.55);
281       RLM->setSpeed(abs(throttle)*2.55);
282       RRM->setSpeed(abs(throttle)*2.55);
283       // If 'throttle' value is positive, the car should move forwards
284       if (throttle > 0 && throttle < 101) {
285         FLM->run(FORWARD);
286         FRM->run(FORWARD);
287         RLM->run(FORWARD);
288         RRM->run(FORWARD);
289       }
290       // If 'throttle' value is negative, the car should move backwards
291       else if (throttle < 0) {
292         FLM->run(BACKWARD);
293         FRM->run(BACKWARD);
294         RLM->run(BACKWARD);
295         RRM->run(BACKWARD);
296       }
297       // If 'throttle' is '0' or an out of range value, the motors are
      released
```

```
298       else {
299         FLM->run(RELEASE);
300         FRM->run(RELEASE);
301         RLM->run(RELEASE);
302         RRM->run(RELEASE);
303         // Battery read is updated when the motors are in release
304         battery_read = analogRead(battery_pin); // Reads the Analog Pin
      A15
305         battery_read = (battery_read - 577) * 100 /446; // 12.4 V = 100 %,
       7 V = 0 %
306         if (battery_read < battery_val) {
307           battery_val = battery_read; // Battery % is given by the lowest
      value measured in release state
308         }
309       }
310     case 2: // RWD
311       // Throttle is converted to a [0 to 255] range and each motor speed
      is set
312       RLM->setSpeed(abs(throttle)*2.55);
313       RRM->setSpeed(abs(throttle)*2.55);
314       // If 'throttle' value is positive, the car should move forwards
315       if (throttle > 0 && throttle < 101) {
316         RLM->run(FORWARD);
317         RRM->run(FORWARD);
318       }
319       // If 'throttle' value is negative, the car should move backwards
320       else if (throttle < 0) {
321         RLM->run(BACKWARD);
322         RRM->run(BACKWARD);
323       }
324       // If 'throttle' is '0' or an out of range value, the motors are
      released
325       else {
326         RLM->run(RELEASE);
327         RRM->run(RELEASE);
328         RLM->run(RELEASE);
329         RRM->run(RELEASE);
330         // Battery read is updated when the motors are in release
331         battery_read = analogRead(battery_pin); // Reads the Analog Pin
      A15
332         battery_read = (battery_read - 577) * 100 /446; // 12.4 V = 100 %,
       7 V = 0 %
333         if (battery_read < battery_val) {
334           battery_val = battery_read; // Battery % is given by the lowest
      value measured in release state
335         }
336       }
337   }
338
339   // Steering controls
340   // If 'steer' value is positive, the wheels should turn to the right
341   if(steer > 0 && steer < 101) {
342     servo.write(90 + (0.35 * steer)); // 35 degree limitation for each
      side
343   }
344   // If 'steer' value is negative, the wheels should turn to the left
345   else if(steer < 0) {
```

```
346       servo.write(90 + (0.35 * steer)); // 35 degree limitation for each
          side
347     }
348     // If 'steer' is '0' or an out of range value, the servo is set to its
          centered position (90 deg)
349     else {
350       servo.write(90);
351     }
352
353   }
354
355   /* Logs the retrieved data into the SD Card */
356   void logging() {
357
358     DateTime now = rtc.now(); // Gets time from the RTC module
359     myLog = SD.open("DATA.txt", FILE_WRITE); // Opening file
360     // If the file opened ok, write to it
361     if (myLog) {
362       myLog.print(now.hour(), DEC);
363       myLog.print(':');
364       myLog.print(now.minute(), DEC);
365       myLog.print(':');
366       myLog.print(now.second(), DEC);
367       myLog.print(" | ");
368       if(traction_setup == 1){
369         myLog.print("AWD");
370       }
371       else{
372         myLog.print("RWD");
373       }
374       myLog.print(" | ");
375       myLog.print(throttle);
376       myLog.print(" | ");
377       myLog.print(steer);
378       myLog.print(" | ");
379       myLog.print(speed_val);
380       myLog.print(" | ");
381       myLog.print(acceleration);
382       myLog.print(" | ");
383       myLog.print(distance);
384       myLog.print(" | ");
385       myLog.print(RPM_FLM);
386       myLog.print(" | ");
387       myLog.print(RPM_FRM);
388       myLog.print(" | ");
389       myLog.print(roll);
390       myLog.print(" | ");
391       myLog.print(pitch);
392       myLog.print(" | ");
393       myLog.print(yaw);
394       myLog.print(" | ");
395       myLog.print(GyroX);
396       myLog.print(" | ");
397       myLog.print(GyroY);
398       myLog.print(" | ");
399       myLog.print(GyroZ);
400       myLog.print(" | ");
```

```
401       myLog.print(AccX);
402       myLog.print(" | ");
403       myLog.print(AccY);
404       myLog.print(" | ");
405       myLog.print(AccZ);
406       myLog.print(" | ");
407       myLog.println(battery_val);
408     }
409     myLog.close(); // Closing file
410
411 }
412
413 /* Setup for the MPU-6050 scales */
414 void setupMPU(){
415
416     Wire.beginTransmission(MPU); // MPU6050 I2C address = 1101001 (AD0 = 1)
        - Note: if AD0 = 0, the address should be 1101000 (0x68)
417     Wire.write(0x6B); // Accessing the register 6B - Power Management
418     Wire.write(0b00000000); // Setting SLEEP register to 0
419     Wire.endTransmission();
420     Wire.beginTransmission(MPU); // MPU6050 I2C address = 1101001 (AD0 = 1)
421     Wire.write(0x1B); // Accessing the register 1B - Gyroscope Configuration
422     Wire.write(0x00000000); // Setting the gyro to full scale +/- 250deg./s
423     Wire.endTransmission();
424     Wire.beginTransmission(MPU); // MPU6050 I2C address = 1101001 (AD0 = 1)
425     Wire.write(0x1C); // Accessing the register 1C - Acccelerometer
        Configuration
426     Wire.write(0b00000000); // Setting the accel to +/- 2g scale
427     Wire.endTransmission();
428
429 }
430
431 /* Reads the MPU-6050 accel and gyro data */
432 void recordMPU() {
433
434     // Read the acceleromter data
435     Wire.beginTransmission(MPU);
436     Wire.write(0x3B); // Start with register 0x3B (ACCEL_XOUT_H)
437     Wire.endTransmission(false);
438     Wire.requestFrom(MPU, 6, true); // Read 6 registers total, each axis
        value is stored in 2 registers
439     // For a range of +-2g, we need to divide the raw values by 16384,
        according to the datasheet
440     AccX = (Wire.read() << 8 | Wire.read()) / 16384.0; // X-axis value
441     AccY = -(Wire.read() << 8 | Wire.read()) / 16384.0; // Y-axis value
442     AccZ = (Wire.read() << 8 | Wire.read()) / 16384.0; // Z-axis value
443     // Calculating Roll and Pitch from the accelerometer data
444     accAngleX = (atan(AccY / sqrt(pow(AccX, 2) + pow(AccZ, 2))) * 180 / PI)
        - AccErrorX;
445     accAngleY = (atan(-1 * AccX / sqrt(pow(AccY, 2) + pow(AccZ, 2))) * 180 /
        PI) - AccErrorY;
446
447     // Read the gyroscope data
448     previousTime = currentTime; // Previous time is stored before the actual
        time read
449     currentTime = millis(); // Current time read
```

```
450   elapsedTime = (currentTime - previousTime) / 1000; // Divide by 1000 to
        get seconds
451   Wire.beginTransmission(MPU);
452   Wire.write(0x43); // Gyro data first register address 0x43
453   Wire.endTransmission(false);
454   Wire.requestFrom(MPU, 6, true); // Read 6 registers total, each axis
        value is stored in 2 registers
455   // For a 250deg/s range we have to divide first the raw value by 131.0,
        according to the datasheet
456   GyroX = (Wire.read() << 8 | Wire.read()) / 131.0;
457   GyroY = (Wire.read() << 8 | Wire.read()) / 131.0;
458   GyroZ = (Wire.read() << 8 | Wire.read()) / 131.0;
459   // Correct the outputs with the calculated error/calibration values
460   GyroX = GyroX - GyroErrorX;
461   GyroY = GyroY - GyroErrorY;
462   GyroZ = GyroZ - GyroErrorZ;
463
464   // Currently the raw values are in degrees per seconds (deg/s), so we
        need to multiply by sendonds (s) to get the angle in degrees
465   gyroAngleX = gyroAngleX + GyroX * elapsedTime; // deg/s * s = deg
466   gyroAngleY = gyroAngleY + GyroY * elapsedTime;
467   yaw =  yaw + GyroZ * elapsedTime;
468
469   // Complementary filter - combine acceleromter and gyro angle values
470   pitch = (0.96 * gyroAngleX) + (0.04 * accAngleX);
471   roll = (0.96 * gyroAngleY) + (0.04 * accAngleY);
472
473 }
474
475 /* Sends logged data to the app */
476 void sendLog() {
477
478   Serial1.print("*A");
479   Serial1.print(AccX);
480   Serial1.print(",");
481   Serial1.print(AccY);
482   Serial1.print(",");
483   Serial1.print(AccZ);
484   Serial1.print("*");
485   Serial1.print("*G");
486   Serial1.print(GyroX);
487   Serial1.print(",");
488   Serial1.print(GyroY);
489   Serial1.print(",");
490   Serial1.print(GyroZ);
491   Serial1.print("*");
492   Serial1.print("*L");
493   Serial1.print(RPM_FLM);
494   Serial1.print("*");
495   Serial1.print("*R");
496   Serial1.print(RPM_FRM);
497   Serial1.print("*");
498   Serial1.print("*r");
499   Serial1.print(roll);
500   Serial1.print("*");
501   Serial1.print("*p");
502   Serial1.print(pitch);
```

```
503   Serial1.print("*");
504   Serial1.print("*y");
505   Serial1.print(yaw);
506   Serial1.print("*");
507   Serial1.print("*d");
508   Serial1.print(distance);
509   Serial1.println("*");
510   Serial1.print("*a");
511   Serial1.print(acceleration);
512   Serial1.println("*");
513   Serial1.print("*B");
514   Serial1.print(battery_val);
515   Serial1.println("*");
516   Serial1.print("*M");
517   Serial1.print(max_speed_val);
518   Serial1.print("*");
519
520 }
521
522 /* Calibrates the MPU gyro and accel error - the car should be placed in a
        flat surface */
523 void resetMPU() {
524
525   Serial.print("Calibrating MPU sensors...");
526
527   while (c < 200) { // Read accelerometer values 200 times
528     Wire.beginTransmission(MPU);
529     Wire.write(0x3B);
530     Wire.endTransmission(false);
531     Wire.requestFrom(MPU, 6, true);
532     AccX = (Wire.read() << 8 | Wire.read()) / 16384.0 ;
533     AccY = - (Wire.read() << 8 | Wire.read()) / 16384.0 ;
534     AccZ = (Wire.read() << 8 | Wire.read()) / 16384.0 ;
535     // Sum all readings
536     AccErrorX = AccErrorX + ((atan((AccY) / sqrt(pow((AccX), 2) + pow((
        AccZ), 2))) * 180 / PI));
537     AccErrorY = AccErrorY + ((atan(-1 * (AccX) / sqrt(pow((AccY), 2) + pow
        ((AccZ), 2))) * 180 / PI));
538     c++;
539   }
540   // Divide the sum by 200 to get the error value
541   AccErrorX = AccErrorX / 200;
542   AccErrorY = AccErrorY / 200;
543   c = 0;
544
545   while (c < 200) {  // Read gyro values 200 times
546     Wire.beginTransmission(MPU);
547     Wire.write(0x43);
548     Wire.endTransmission(false);
549     Wire.requestFrom(MPU, 6, true);
550     GyroX = Wire.read() << 8 | Wire.read();
551     GyroY = Wire.read() << 8 | Wire.read();
552     GyroZ = Wire.read() << 8 | Wire.read();
553     // Sum all readings
554     GyroErrorX = GyroErrorX + (GyroX / 131.0);
555     GyroErrorY = GyroErrorY + (GyroY / 131.0);
556     GyroErrorZ = GyroErrorZ + (GyroZ / 131.0);
```

```
557       c++;
558     }
559     //Divide the sum by 200 to get the error value
560     GyroErrorX = GyroErrorX / 200;
561     GyroErrorY = GyroErrorY / 200;
562     GyroErrorZ = GyroErrorZ / 200;
563
564     Serial.println("calibration success!");
565
566 }
```

Listing B.1: Arduino code implemented for controlling the prototypes.